Title
THE CONVECTIVE EVOLUTION OF LARGE AMPLITUDE ALFVEN WAVES IN THE SOLAR WIND

Author
Patterson, Blake R.

Publication Date
1971-08-01

THE CONVECTIVE EVOLUTION OF LARGE AMPLITUDE ALFVÉN WAVES IN THE SOLAR WIND

Blake R. Patterson
(Ph. D. Thesis)

August 16, 1971

AEC Contract No. W-7405-eng-48

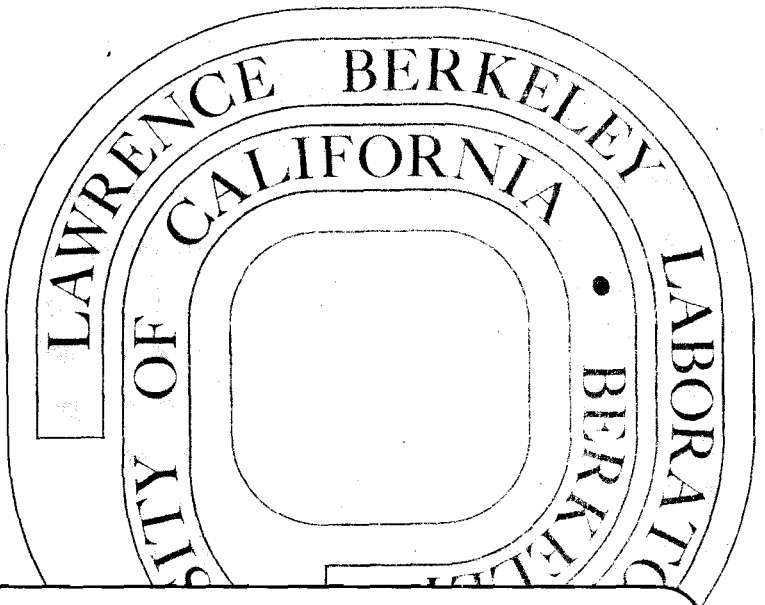

DISCLAIMER

THE CONVECTIVE EVOLUTION OF LARGE AMPLITUDE ALFVÉN WAVES IN THE SOLAR WIND

Contents

THE CONVECTIVE EVOLUTION OF LARGE AMPLITUDE ALFVÉN WAVES IN THE SOLAR WIND

Blake R. Patterson

Lawrence Berkeley Laboratory
University of California
Berkeley, California 94720

August 16, 1971

ABSTRACT

The convective evolution of large amplitude Alfvén waves propagating in a nonuniform, streaming plasma modeled after the solar wind is investigated. Observed large- and small-scale properties of the interplanetary medium which are relevant to this study are reviewed. An idealized solar wind model is developed which neglects solar rotation and has a radial magnetic field.

In preparation for the nonuniform plasma problem, Alfvén waves parallel to a uniform magnetic field B_0 in a uniform but anisotropic plasma are studied in the Chew-Goldberger-Low and guiding-center formalisms. Exact solutions are found for stable and unstable plasmas. The exact nonlinear behavior of an unstable circularly polarized Alfvén mode is obtained: growth of a finite perturbation is quenched in a finite time, and decay begins immediately. When the plasma is stable, an arbitrarily large, constant-amplitude perturbation perpendicular to the uniform field can propagate without distortion parallel to this field.

The propagation velocity, $V_A(b) = (B_0^2/4\pi\rho)^{\frac{1}{2}}[1 - 4\pi(p_{\parallel}-p_{\perp})/B^2]^{\frac{1}{2}}$, is nonlinearly dependent on the amplitude b of the wave part of the magnetic field through $B = (B_0^2 + b^2)^{\frac{1}{2}}$ and the two invariants $p_{\perp} B^{-1} \rho^{-1}$ and $p_{\parallel} B^2 \rho^{-3}$.

Experimental evidence indicates that this propagating Alfvén wave is an important low-frequency phenomenon in the solar wind. Its convective evolution in the idealized solar wind model is solved in two ways: by energetic considerations and by a detailed treatment of the wave equations in the Chew-Goldberger-Low approximation. When the radial flow velocity is large compared to the Alfvén velocity V_A, both methods produce the simple result $V_A(b/B_0)^2 = \text{constant}$, where B_0 denotes the radial magnetic field. The adiabatic plasma expansion tends to increase the effective anisotropy $(p_{\parallel} - p_{\perp})/B^2$ and thus decreases V_A. Consequently b/B_0 grows, which reduces the effective anisotropy and keeps V_A finite. Thus the wave prevents the solar wind from becoming unstable with respect to Alfvén perturbations.

CHAPTER 1

INTRODUCTION TO THE CONVECTIVE EVOLUTION OF ALFVÉN WAVES

1.1 The Driven Instability

The objective of this research is the study of a driven instability in a plasma.

Envision a situation in which some mechanism, internal or external or both, causes a plasma to become unstable with respect to some mode. The mode cannot grow indefinitely, as linear theory implies, due to the finite amount of energy available in the plasma. Hence, as the mode grows, it affects the plasma, ultimately in a manner which limits its amplitude.

With continuous application of the driving mechanism, the plasma must reach a steady state condition. This steady state may exhibit either an oscillatory behavior or a time independent asymptotic limiting configuration. The consequent balance between the applied driving mechanism and the self-limiting character of the wave constitutes a highly nonlinear problem.

Although such driven instability processes frequently occur in both laboratory and astrophysical plasmas, theorists have done little more than speculate on their properties. Both linear and quasilinear techniques are usually impotent against the severe nonlinearities which, of necessity, occur when the wave amplitude is so large that it quenches its own growth.

One driven instability problem, which has yielded to analytic methods, forms the subject of this dissertation.

1.2 Alfvén Waves in the Solar Wind

As the solar wind expands adiabatically from the sun, the double adiabatic or Chew-Goldberger-Low equations[1] predict that the particle pressures parallel and perpendicular to the local field and the magnetic pressure decrease. The parallel pressure decreases more slowly than the perpendicular and magnetic pressures that tend to stabilize the Alfvén mode. Far enough from the sun, this model predicts that the plasma becomes unstable with respect to Alfvén waves.

An Alfvén wave propagating in the solar wind near the sun finds itself in an increasingly unstable environment as the streaming plasma convects it outward. Finding itself convected into a region where unstable growth occurs, the wave must approach a large amplitude at which self-quenching effects counter the driving mechanism provided by the adiabatic expansion.

The analysis of the convective evolution of Alfvén waves in the solar wind is studied in the following chapters.

1.3 Summary of the Paper

Chapter 2 outlines the experimentally observed characteristics of the solar wind which are relevant to the study of Alfvén waves convected by it. Several excellent review articles provide additional details.[2-6]

Section 2.2 deals with large-scale characteristics of the interplanetary medium. The solar wind plasma streams radially from the sun and drags solar magnetic field lines with it. This radial flow and the sun's rotation cause the interplanetary field

lines to have the shape of Archimedes' spirals.[7] The ecliptic plane can be divided roughly into sectors along such spirals. In alternate sectors the field is predominantly toward or away from the sun, as sketched in Fig. 1. The plasma's bulk velocity also shows a sector structure consisting of slow streams and fast streams.[8-10] The fast streams tend to be hotter, with lower density and more high frequency field activity. The dominant heavy particle in the solar wind is the proton.[11] Its temperature is characteristically a few electron volts with an anisotropy of approximately 2 at 1 AU. The electron temperature there averages 13 ev with an anisotropy between 1.1 and 1.2.

Section 2.3 discusses low frequency modes observed in the solar wind. East Coast observers, Ness, Burlaga, Ogilvie, Sari, and others, emphasize the importance of tangential discontinuities in the solar wind.[12-16] Belcher, Coleman, Davis, Jones, and Smith on the West Coast view Alfvén waves as a dominant meso-scale feature of the solar wind's wave population.[17-21] Both sets of observers agree that Alfvénic perturbations occur at least 25% of the time. Figures 2 - 4 present examples of spacecraft data which indicate the presence of outward propagating Alfvén waves.[19] The plasma density remains relatively constant, and perturbations in the magnetic field components correlate well with those of the plasma velocity. It is also observed that the magnitude of the total field remains constant in time, a characteristic shared by the waves treated theoretically in Chapters 4 and 5. The waves seen in space are aperiodic and nonsinusoidal. The average

field direction is also the direction of minimum field fluctuation. The data indicate that the most pure examples of Alfvén waves occur in the high velocity streams and on their trailing edges. Amplitudes are largest in these regions as well. Belcher and Davis argue that the waves observed at 1 AU probably are remnants of turbulent structures occurring near or on the sun.[19]

In Chapter 3, an idealized model is developed for use in studying the convective evolution of large-amplitude Alfvén waves in the solar wind.

In order to obtain analytic results for the convective evolution problem, some simplifications are necessary. The spiral nature of the field is neglected, and the purely radial magnetic field which results corresponds physically to a non-rotating sun. The complication of the magnetic sector structure is also eliminated by assuming that the field is that of a magnetic monopole centered at the sun. Thus $\underset{\sim}{B}$ is everywhere outward or toward the sun in the absence of waves, as indicated in Eq. (3.1). The sector structure of the plasma streaming is also ignored for simplicity, and Eq. (3.3) specifies the bulk velocity $\underset{\sim}{u}$.

The result is a spherically symmetric idealized model in which the plasma bulk velocity and the magnetic field lines are radial everywhere. Background quantities, such as the radial streaming velocity, temperatures, density, and so forth, are assumed to depend only on the distance r from the center of the sun.

The model set of equations chosen to describe the solar wind plasma and waves is the Chew-Goldberger-Low model.[1] This set of equations allows for the pressure anisotropy which is necessary to produce instability in Alfvén perturbations. It has the disadvantage of omitting electron heat flow effects, which are important in the solar wind, and which must be included in a more complete theoretical treatment of it.

Although this paper treats highly nonlinear effects, many processes, such as coulomb collisions, wave-wave interactions, and resonant particle interactions are not included in the analysis.

Since the wavelengths of the Alfvén waves observed in space are small compared to 1 AU, the waves find themselves in a locally uniform background plasma. In Chapter 4 the behavior of large amplitude Alfvén modes in a uniform plasma immersed in a uniform magnetic field is investigated. The solutions obtained are exact solutions of both the Chew-Goldberger-Low and the guiding-center equations.[1,22,23]

Section 4.2 outlines the analysis using the Chew-Goldberger-Low formalism. The same results are obtained in Sec. 4.3 within the more general guiding-center theory. Two classes of Alfvén modes are described, both oriented parallel to the uniform field.

Sections 4.2A and 4.3A deal with a wave propagating parallel to the background field. This is characterized by a wave magnetic field component perpendicular to the uniform field

whose amplitude is constant in space and time, but whose orientation is quite general. The total field, given by Eqs. (4.9b) and (4.17), is aperiodic and nonsinusoidal, in general. In the uniform plasma it propagates at the generalized Alfvén velocity V_A given by Eq. (4.16) without change of shape. The plasma must be stable with respect to Alfvén perturbations, i.e. V_A must be real, for this solution to exist. Simple examples of this wave are illustrated in Fig. 5.

Sections 4.2B and 4.3B describe circularly polarized standing wave modes of the form shown in Fig. 6. These may occur in stable or unstable plasmas. The temporal evolution of the perpendicular signed field amplitude b of these waves is the same as the displacement of a classical particle moving in the magnetic potential ϕ, defined by Eq. (4.25). Equation (4.28) is the equivalent energy equation. When the plasma is Alfvén stable in the absence of any Alfvén mode, ϕ has the form sketched in Fig. 7(a). In this case the standing wave mode oscillates in amplitude, passing through zero twice each period. When the unperturbed plasma is unstable with respect to Alfvén waves, Fig. 7(b) indicates the shape of the magnetic potential. An infinitesimal circularly polarized Alfvén mode at first grows exponentially with time in such a plasma, and then more slowly. It ultimately reaches a quenched state, corresponding to the most extreme displacement of the associated magnetic pseudoparticle, and decays, eventually at an exponential rate, toward zero amplitude.

Some interesting properties of the propagating wave are discussed in Sec. 4.4A. This wave shares important properties with the Alfvén perturbations observed in the solar wind. Both are characterized by constant plasma density, constant total magnetic field, and nonsinusoidal behavior. The relation between magnetic field and plasma velocity given by Eq. (4.18) agrees with the correlation observed experimentally. Moreover, the exact solution of Secs. 4.2A and 4.3A is characterized by variations in the components of $\underset{\sim}{B}$ in the plane orthogonal to the propagation direction, but the parallel component of $\underset{\sim}{B}$ is constant. Belcher and Davis observe such an anisotropy: the variation in $\underset{\sim}{B}$ along $\langle \underset{\sim}{B} \rangle$ is one-fourth to one-sixth of that in the directions orthogonal to $\langle \underset{\sim}{B} \rangle$.[19]

Section 4.4B compares the exact solution to the quenching problem provided by the standing wave mode with earlier quasi-linear work on the firehose mode.[24] Qualitative features of the exact solution are quenching in a finite time through purely wave-particle interactions and immediate decay. Similar properties characterize the quenching of flute modes and two-stream instabilities, which have been studied numerically.

Chapter 5 treats the convective evolution of the "constant-amplitude" propagating waves in the nonuniform plasma and field of the idealized model for the solar wind. Section 5.1 details the structure of the convected waves. A constant-amplitude source, which is spherically symmetric with respect to the sun, supplies aperiodic, propagating Alfvén waves. Steady state is assumed so

that wave amplitudes do not depend on time and have only a weak radial dependence as the waves propagate in and are convected by the nonuniform, expanding plasma. The plasma parameters, density and pressure, also depend only on r. A WKB phase dependence, specified in Eq. (5.2) - (5.6), is chosen for the wave components of field and velocity. To obtain consistent equations, we must allow for a small skewness δ between the wave part of the magnetic field and the wave part of the fluid velocity. In the uniform plasma theory of Chapter 4 these components are exactly parallel or antiparallel. Solutions to the convective evolution problem have been obtained in two ways.

Section 5.2 describes the derivation of a solution by the use of energy conservation. In this section the Alfvén velocity and the relation between velocity and field, characteristic of the propagating waves, are taken from the uniform plasma theory. The Alfvén velocity V_A is assumed to be small compared to the bulk velocity u_0. The total energy conservation relation for waves and plasma, Eq. (5.14), reduces to Eq. (5.20) for the spherically symmetric and steady state configuration. The energy flux vector $\underset{\sim}{S}$ is evaluated in Appendix C for a Chew-Goldberger-Low plasma. Its radial component, required in Eq. (5.20), is obtained in Appendix D for the wave configuration of the idealized model. There results the energy relation, Eq. (5.25), which contains as unknowns the wave amplitude b and the plasma radial velocity u_0. A second equation is provided by the radial component of the Chew-Goldberger-Low momentum equation,

which is exhibited in Eq. (5.26). Elimination of u_0 between these equations leads to the differential equation (5.34). Its solution is sketched in Appendix H. The result is given by Eq. (5.36).

The convective evolution analysis is carried out in Sec. 5.3 by using the detailed wave equations. No assumptions are made regarding the velocity V_A appearing in Eq. (5.3), the wave component of the fluid velocity u_T, or the relative size of V_A and u_0. For the wave ansatz, the nonradial part of the Chew-Goldberger-Low momentum equation is given by Eq. (5.37). Similarly, the wave part the Chew-Goldberger-Low Maxwell equation is displayed in Eq. (5.38). These vector differential equations are solved, giving the usual Alfvén velocity for V_A, the expected relation between the fluid velocity u_T and the wave part of the magnetic field, the phase angle δ, and Eq. (5.52). The latter is equivalent to Eq. (5.36), the result of the energetic analysis, when $V_A \ll u_0$.

Section 5.4A shows that, for solar wind parameters, the two solutions are identical. Properties of the solution are discussed in Sec. 5.4B. With no wave present the Chew-Goldberger-Low model predicts that the expanding solar wind plasma becomes Alfvén unstable at sufficient distance from the sun, called the Alfvén critical instability radius, r_{cr}. The presence of the wave prevents this unstable condition from arising. If the wave amplitude is nonzero anywhere, V_A can never pass through zero or become imaginary according to Eq. (5.36). The dependence of V_A

and wave amplitude b on radius is sketched in Fig. 10 for various choices of wave amplitude.

If the wave amplitude is small within the Alfvén critical instability radius r_{cr}, where the generalized Alfvén velocity V_A vanishes in the absence of waves, it must increase dramatically at r_{cr} in order to keep the plasma stable. Figure 10(a)-(d) demonstrates this effect. If the growth of wave amplitude is too rapid, the assumptions used to derive the analytic solution break down. This and other limitations on the validity of the theory receive attention in Sec. 5.4C. The necessary conditions are summarized by the inequalities (5.63), (5.64), (5.68), and (5.72); when these hold the analysis is valid. They are satisfied for measured values of the solar wind parameters at 1 AU.

Section 5.4D compares the theoretical predictions of convective evolution with the observed properties of the solar wind. The Earth is well beyond the Alfvén critical radius given by simple Chew-Goldberger-Low theory, and the solution of the idealized model yields a considerably smaller Alfvén velocity at 1 AU than is observed. This discrepancy may arise from effects such as electron heat conduction, high frequency electron waves, and the spiral geometry of the solar wind.

The possibility of extending the analytic solution to more general geometries is considered in Sec. 5.4E. The convective evolution of waves may be useful in intergalactic space, where Alfvén waves have been proposed as an important particle accelerating mechanism.[31,32]

CHAPTER 2

OBSERVED PROPERTIES OF THE SOLAR WIND

2.1 Introduction

The solar wind is an extremely complex system. Great effort has been spent in experimental observations of its properties, particularly during the past decade. Considerably more will be necessary before a thorough understanding of all its aspects exists.

No attempt will be made to survey everything that is known about the solar wind. Further details can be found in a number of excellent reviews.[2-6]

The convective evolution of Alfvén waves will be analyzed in a model which is a very simplified abstraction of the physical solar wind. In this chapter known properties of the solar wind which are believed to be relevant to the convective evolution problem are outlined. The discussion will by no means be exhaustive, and the original literature should be consulted for more extensive descriptions.

Section 2.2 deals with the gross characteristics of the solar wind. Large-scale static structures of the plasma and magnetic field are discussed.

Section 2.3 describes microscale phenomena which possess Alfvén wave characteristics and which are the subject of the theoretical investigations of this dissertation.

2.2 Gross Features of the Solar Wind

The solar wind seems to be a ubiquitous element of the solar system. It expands essentially radially from the sun at

velocities which are supersonic long before 1 AU is reached. At the orbit of Earth its bulk velocity is roughly 400 km/sec, but varies between 300 km/sec and 800 km/sec. This streaming velocity is independent of distance from the sun to a good approximation.

Due to the very high electrical conductivity of this coronal plasma, it drags along magnetic field lines from the sun as it convects outward. Since the bulk plasma kinetic energy density exceeds the magnetic field energy density by nearly a factor of 100, the solar wind controls the field line motion, and the field has negligible influence on the streaming motion. The field defines a local reference frame for plasma kinetic properties such as pressure and temperature.

The sun's rotation, in conjunction with the purely radial bulk velocity of the solar wind, causes the interplanetary magnetic field lines to have an Archimedes spiral shape in the ecliptic plane. This pattern rotates with the sun and has a period of about 27 days. A simple model[7] gives the theoretical static magnetic field as

$$B_r(r, \theta, \phi) = B(r_0, \theta, \phi^*)(r_0/r)^2 , \tag{2.1}$$

$$B_\theta = 0 , \tag{2.2}$$

$$B_\phi(r, \theta, \phi) = B(r_0, \theta, \phi^*)(r_0/r)(r_0\Omega/u_0)\sin\theta , \tag{2.3}$$

where

$$\phi^* \equiv \phi + r\Omega/u_0 . \tag{2.4}$$

Throughout this paper r, θ, and ϕ are the usual spherical

coordinates, r_0 is a reference radius, u_0 is the solar wind bulk velocity, which is assumed constant here, and Ω denotes the sun's angular velocity of rotation.

The spiral field lines are nearly radial within a few solar radii of the sun. At 1 AU the azimuthal velocity of the field lines is about 440 km/sec, roughly equal to the solar wind bulk velocity there. Consequently the average field direction makes an angle of 45° with the radial direction. At times when the bulk velocity is quite high, the average field direction is slightly more radial, as the above model indicates should happen.

Since $B_r \approx B_\phi$ at 1 AU, Eqs. (2.1) and (2.3) show that within $\frac{1}{2}$ AU the magnitude of the total field, $|\underset{\sim}{B}|$, falls roughly as r^{-2}. At distances larger than 1 AU it decreases more gradually. A typical field strength at 1 AU is 3 to 8 gamma.

The solar wind can be divided along the spiral field lines into sectors as indicated in Fig. 1. In alternate sectors the average field points predominantly toward or away from the sun as shown. Although four sectors appear in Fig. 1, sometimes only two sectors are observed.[5]

The bulk velocity also shows a sector structure.[8-10] Slow streams of expanding plasma alternate with fast streams. The fast streams are generally hotter and have lower density than the low velocity streams. The magnetic field is characteristically the same in fast and slow streams, except at the leading edges of high velocity streams, where both magnetic field and plasma density are high. Temperatures are also high

in such regions as are the levels of magnetic field activity. This phenomenon is probably related to the collision of the faster moving streams with the adjacent low velocity ones. The strength of high frequency field components tends to be higher in the faster streams.

The dominant ion species in the solar wind is the proton, accounting for all but a few percent of the plasma ions.[11] A typical ion temperature is a few electron volts at 1 AU, giving a proton gyroradius of about 100 km. Electron temperatures are estimated to be approximately 13 ev at the Earth. Measured anisotropies, $T_\parallel/T_\perp$, where parallel and perpendicular refer to the local magnetic field, range in the vicinity of 2 for ions and from 1.1 to 1.2 for electrons at 1 AU.[4] The ion anisotropies were observed by Vela 3, whose velocity distribution sample time was approximately one minute. More refined experiments have produced the same kind of results. The sampling period for recent Vela 4 measurements of thermal anisotropies was 4 seconds.[33] The solar magnetic field seldom varies over such short time scales, and thus the above numbers represent instantaneous thermal anisotropies.

The properties of the solar wind outlined here must not be considered inviolable. For example, the magnetic field in an "outward" sector will occasionally point toward the sun for a brief interval.

2.3 Low Frequency Modes in the Solar Wind

The gross properties described above are considerably complicated by a great variety of physical processes with char-

acteristic scale lengths smaller than 1 AU. For the purposes of the theoretical work to follow, we concentrate on long-wavelength, low-frequency perturbations of the background plasma and magnetic field, especially those which reveal Alfvén mode characteristics.

At this time there exists a rather heated debate between investigators on opposite coasts. The East Coast observers, Ness, Burlaga, Ogilivie, and Sari, tend to emphasize the dominance of tangential discontinuities in the solar wind.[12-16] The West Coast observers, Belcher, Coleman, Davis, Jones, and Smith, picture Alfvén waves as a dominant feature of the low-frequency solar wind wave structure.[17-21] Believing that a satisfactory resolution of this argument must await more complete data, we limit our participation to a few comments without choosing either side.

Both sets of observers are agreed that perturbations with Alfvén wave properties are observed at least 25% of the time. Since this phenomenon is most thoroughly discussed by Belcher and Davis,[17-19] we concentrate on their findings in outlining the experimental evidence for Alfvén waves in the solar wind.

Figure 2 depicts solar wind data obtained by Mariner 5.[19] It shows the magnetic field $\underset{\sim}{B}$, plasma velocity $\underset{\sim}{u}$, field magnitude B, and plasma number density n. The vector quantities are resolved into three mutually orthogonal components: parallel to the radial direction (R); parallel to the azimuthal direction (T); and normal to the ecliptic plane (N). The strong correlation between the components of $\underset{\sim}{B}$ and the

components of $\underset{\sim}{u}$ appears quite clearly. The relative constancy of $|\underset{\sim}{B}|$ and n is also evident.

Figure 3 is an expansion of the field data of three ten-minute intervals of Fig. 2. Here again the constancy of $|\underset{\sim}{B}|$, despite the marked variations in field components, is clear. Further evidence of this characteristic is strikingly shown in Fig. 4, which depicts magnetometer data for a 1 hour period.

Belcher and Davis argue convincingly that such characteristics indicate the presence of Alfvén perturbations. The waves are generally nonsinusoidal and aperiodic, as is evident from Fig. 3. A spectral decomposition indicates that the field components fluctuate with characteristic times from 10^4 sec to 3 sec. The local average field direction $\hat{B}_0$ is also the direction of minimum fluctuation. The magnetic field has an observed power anisotropy of 5:4:1 in an orthogonal coordinate system whose unit vectors are $\hat{B}_0 \times \hat{r}$, $\hat{B}_0 \times (\hat{B}_0 \times \hat{r})$, and $\hat{B}_0$, respectively. The propagation direction indicated by treating these phenomena as Alfvén waves is almost always away from the sun.

The data indicate that the fluctuations are most purely Alfvénic in the high velocity solar wind streams and on their trailing edges. These perturbations have largest amplitudes in the compression regions at the leading edges of the high velocity streams, but here the mode structure is more complex. The energy in the fluctuations there is comparable to the energy in the total field.

In the low velocity streams the Alfvén structures tend to be less pure, i.e., they are combined with non-Alfvénic phenomena, such as tangential discontinuities,[34] and the amplitudes are reduced.

Magneto-acoustic modes may occur, but were not identified by Belcher and Davis. If present, they have an average power less than a tenth of the power in Alfvén modes. These investigators estimate that Alfvén waves propagating outward from the sun dominate the microscale structure at least 50 percent of the time. They speculate on a variety of possible sources for Alfvénic perturbations and conclude that they are probably remnants of waves or turbulence structures generated at or near the sun which have been convected outward by the solar wind.

This sketchy story of the experimentally determined properties of the solar wind will be used in the next chapter to construct a simple model for use in analyzing the convective evolution of Alfvén waves.

CHAPTER 3

IDEALIZED MODEL OF THE SOLAR WIND

3.1 Geometry of the Solar Wind Model

The spiral nature of the average magnetic field configuration is an important feature of the structure of the solar wind. However, its inclusion introduces formidable mathematical difficulties in an analytic study of the convective evolution of large amplitude waves.

Within 0.1 AU the average field is believed to be nearly radial, due to the slow solar rotation and the rapid radial plasma flow. A logical simplification is to eliminate the spiral nature of the magnetic lines of force entirely and assume that they are radial everywhere. This model corresponds physically to a non-rotating sun, the magnetic field swept out by the streaming solar wind being purely radial in this case.

The interplanetary magnetic sectors contribute additional complications to the theoretical model. Within each magnetic field sector the Alfvén waves find themselves in a background field which is entirely away from or entirely toward the sun. For the purposes of studying wave evolution inside such a sector, it suffices to assume that the field points outward in every such sector. Since azimuthal variations in the static field introduce an unnecessary complication, the field is chosen to be spherically symmetric for the theoretical analysis.

Whereas the fast and slow streaming sectors and consequent collision regions are vital to a great many solar wind processes,

including Alfvén waves, we seek primarily a theory of Alfvén waves convecting in a freely expanding plasma. Since there is no evidence of a preferred direction for the emission of solar wind plasma, when solar rotation effects are negligible, we are led to consider a spherically symmetric expanding plasma.

Thus we consider an idealized solar wind model which consists of a background magnetic field corresponding to a magnetic monopole:

$$\underset{\sim}{B}(r, \theta, \phi) = B_0(r)\,\hat{r}\,, \tag{3.1}$$

where B_0 has an inverse square relation with r:

$$B_0(r) = B_{00}(r_0/r)^2\,. \tag{3.2}$$

Here, B_{00} denotes the radial background field at the reference radius r_0. It can be negative or positive, corresponding, respectively, to an inward or outward directed field throughout interplanetary space.

Likewise, in the absence of Alfvén perturbations, the plasma fluid velocity $\underset{\sim}{u}$ is taken to be spherically symmetric:

$$\underset{\sim}{u}(r, \theta, \phi) = u_0(r)\,\hat{r}\,. \tag{3.3}$$

The r dependence of u_0 will be derived later.

Similarly, we assume that the other plasma parameters, density and pressure, depend only on r. Gravitational effects are ignored in the analysis.

The WKB method of studying a wave which propagates in a nonuniform, time dependent medium assumes as a first approximation that the wave behaves as if it were in a locally uniform and

constant environment. Providing the space and time variations of the background are sufficiently small over characteristic wavelengths and wave periods, they affect the wave only by producing gradual changes in wave parameters such as its amplitude, phase, and frequency. The fundamental character of the wave is unchanged.

A wave in the idealized model and a wave in a more complicated geometry find themselves in a plasma whose properties, in a frame of reference moving with the plasma, are changing slowly in time. The wave responds in either case to the varying characteristics of the supporting medium. Whether the variations are caused by a slowly moving piston, an inverse square law expansion, or a complex convection process is relatively unimportant to the wave, providing the variations occur over distances large compared to a wavelength. In the solar wind problem, the largest wavelengths are 10^6 km, whereas gross plasma properties evolve over distances like 1 AU or 10^8 km.

Applying this philosophy to the convective evolution of Alfvén waves in the solar wind, we hypothesize that the wave parameters vary slowly as a consequence of the gradual changes in the idealized medium in which it propagates. Knowing this dependence of wave parameters on the properties of the medium in the idealized model, we hope to use the actual solar wind configuration, i.e. the variations of density, pressure, and the spiral background field of the interplanetary medium, to predict the true wave behavior.

Although it cannot provide the exact behavior of Alfvén waves in the physical solar wind, the solution of convective evolution in the idealized model should yield the correct qualitative features. Once the propagation properties are understood in the simple geometry, propogation in the actual spiral geometry can be predicted by an appropriate transformation of the static plasma characteristics. Quantitatively, the model may serve as a lowest order solution in a spherical harmonic expansion of the actual field geometry.

Of course, the overwhelming argument in favor of the idealized model lies in the simplicity which permits the analytic results that are derived in subsequent chapters.

Because distances characteristic of the model are so much larger than the wavelengths of interest, the waves find themselves in a locally uniform plasma and field. Although slowly time-varying in the plasma frame, these properties are constant over the time and space scales characteristic of the waves. Thus to obtain insight into the waves to be studied in the idealized, spherically symmetric model, we will first consider large amplitude Alfvén waves in a uniform plasma immersed in a uniform magnetic field. The properties of the background medium will be assumed stationary, except as they are influenced by the waves themselves. This preliminary study is the subject of Chapter 4. Waves analyzed there are much like the experimentally observed Alfvén perturbations. They are introduced into the idealized model for the convective evolution investigations of Chapter 5.

3.2 Plasma Equations for the Solar Wind Model

Even with the limited complications of the idealized model, the analytic details of the behavior of waves in an adiabatically expanding plasma are rather formidable. Thus the equations describing the interactions of plasma and fields should be as simple as possible, and we are led to consider fluid models. We assume that the plasma consists of a single ion species; it is a relatively simple matter to generalize the result to multiple species, at least in the collisionless limit. Since we wish to consider unstable Alfvén waves, the model equations must include the possibility of pressure anisotropy. The simplest choice is the Chew-Goldberger-Low or "double adiabatic" model.[1] These equations can be obtained from Maxwell's equations and velocity moments of the Vlasov equation, assuming that the ion gyroradius is small compared to the length scales to be studied, that the ion gyrofrequency is larger than the frequencies of interest, and that the divergence of the heat flux tensor $\underset{\approx}{Q}$ vanishes.

The Alfvén waves observed in the solar wind have wavelengths greater than 10^3 km, which is large compared to the 100 km typical of the ion gyroradius.[19] This also implies that Alfvén wave frequencies are smaller than ion gyrofrequencies, because the Alfvén velocity and the ion thermal velocities are comparable in the solar wind. In Chapter 4, the analysis of Alfvén waves in a uniform plasma is carried out in the more general "guiding-center" theory, which includes the possibility of heat flow.[22,23] In the guiding-center solution, the heat

flow tensor vanishes identically. Thus its neglect is justified in retrospect, and the Chew-Goldberger-Low model is a fortunate choice in the case of Alfvén waves in a uniform plasma and field.

Dropping $\nabla \cdot \underset{\approx}{Q}$ in the idealized model is not justified, because of the plasma's nonuniformity, and constitutes probably the most serious defect of the model. Electron heat conduction is expected to be an efficient means of communicating temperatures at the sun to great distances.[35] The transfer of these high temperatures to the ions would modify the predictions of the double adiabatic model, which are that $\rho T_{\parallel}$ and $p_{\parallel}$ are proportional to r^{-2} and that $\rho T_{\perp}$ and $p_{\perp}$ fall as r^{-4}, in the absence of waves. These latter relations are obtained in Sec. 5.4B.

The pressure tensor which appears in the double adiabatic model includes ion and electron contributions. Since $\nabla \cdot \underset{\approx}{Q}$ is appreciable for electrons, the electron pressures do not obey the Chew-Goldberger-Low equations and represent an unknown in the convective evolution problem. Multiple fluid theories have attempted to predict electron thermal properties, but none have succeeded in simulating the known characteristics of the solar wind.[35,36]

In order to maintain the simplicity of the double adiabatic model, heat flow due to electrons is arbitrarily assumed to be zero in the analysis which follows. With this hypothesis, electron temperatures and pressures follow from the Chew-Goldberg-Low equations.

The observed electron pressure difference $p_{\parallel} - p_{\perp}$ is only a tenth of the electron pressure, whereas for ions it is one to four times the ion perpendicular pressure. Since electron and ion pressures at 1 AU are comparable, electron contributions are negligible when computing the total pressure difference $p_{\parallel} - p_{\perp}$. Both the Alfvén wave dispersion relation, Eq. (4.16), and the solution of the convective evolution problem, Eq. (5.36), depend on the pressures only through this difference. Thus, when details of the actual electron temperature behavior are included in the theory, the answer may still depend mainly on the ion pressure tensor.

One possible improvement in the present approach might be the inclusion of an ad hoc heat flow term in the Chew-Goldberger-Low model. This would preserve the basic simplicity, which permits a relatively simple solution, while serving as a better approximation to the physical world. Alternatively, the analysis could be carried out in the guiding-center formalism used in Chapter 4, which includes the possibility of heat conduction.

Wave-wave interactions, the effect of Coulomb collisions, and resonant-particle interactions with Alfvén waves are omitted in this study. Some of these, such as collisional effects, can be readily incorporated into the fluid theory, but their inclusion would complicate an already formidable analysis and prevent a closed form solution. Finite gyroradius corrections have been omitted for similar reasons. Eviatar and Schulz studied

the influence of some of these effects on ion pressure anisotropy in the solar wind.[37] They concluded that the ion-cyclotron instability and Coulomb collisons could account for the smallness of the observed anisotropy. The results derived in Chapter 5 show that Alfvén waves of the type experimentally observed can also limit the anisotropy.

Sagdeev and Galeev have studied three-wave interactions using the magnetohydrodynamic theory, in which $p_{\parallel} = p_{\perp}$.[38] They conclude that a large amplitude circularly polarized Alfvén wave propagating parallel to a uniform magnetic field can decay into another Alfvén wave and a sound wave. Although the type of Alfvén wave observed experimentally has not been studied explicitly with respect to this type of instability, there is every reason to suspect that it, too, should be vulnerable to a similar decay process. Nevertheless, the observed presence of extensive Alfvén modes in the solar wind indicates the presence of some effective barrier against such three-wave interactions. No attempt is made to include them in the ensuing chapters.

CHAPTER 4

EXACT NONLINEAR EVOLUTION OF LARGE AMPLITUDE ALFVÉN WAVES IN A UNIFORM PLASMA

4.1 Introduction

In anticipation of the labor involved in studying the evolution of large amplitude waves in the solar wind, which is both nonuniform and convecting, it is necessary to find a mode with a mathematically simple description, at least in a uniform plasma.

As this preliminary stage in studying the convective evolution problem, two classes of Alfvén waves have been discovered which in a uniform plasma immersed in a uniform magnetic field are exact solutions of the Chew-Goldberger-Low model[1] and the guiding-center equations.[22,23] The first is a wave propagating parallel to the uniform magnetic field. It is characterized by a wave magnetic field component perpendicular to the uniform field whose magnitude is constant in space and time, but whose orientation is arbitrary. There is experimental evidence that this mode is important in the solar wind,[19] and Chapter 5 treats its theoretical behavior in a convecting plasma modeled after the solar wind. The second class of Alfvén waves is a circularly polarized standing wave oriented parallel to the uniform magnetic field. When an excess of pressure parallel to the magnetic field makes such a wave unstable, it is known as the "firehose" or "garden-hose" instability. By use of elementary analytical methods, the nonlinear quenching of this unstable wave

can be solved exactly in either model, thus providing perhaps the first simple and complete solution of the nonlinear growth of a plasma wave, rigorous within the limitations of the guiding-center equations.

In what follows we consider Alfvén waves in an infinite, uniform plasma in a uniform magnetic field $\underset{\sim}{B}_0$. The velocity distribution is in general anisotropic.

The firehose mode has already been studied in such a plasma by quasilinear techniques.[24,39,40] The Vlasov equation carried to second order in the perturbation shows that the unstable waves, initially growing due to an excess of pressure parallel to $\underset{\sim}{B}_0$, react back on the particle distribution, causing the parallel pressure to decrease and the perpendicular pressure to increase as long as any waves are growing; the growth rate is made smaller by the relative decrease of parallel pressure, and wave growth is thus self-quenched. An explicit examination of this process has not appeared in the literature.

The Chew-Goldberger-Low model is chosen for the simplicity inherent in a fluid description and because to lowest order it predicts the same nonlinear behavior of Alfvén waves as the Vlasov equation. In Appendix A the earlier quasilinear results are generalized to arbitrary $\underline{k}$ by carrying the Chew-Goldberger-Low equations to second order in the wave perturbation. (Of course, finite ion-gyroradius effects must be appended to the Chew-Goldberger-Low equations to correctly predict growth rates for small wavelengths.) This calculation verifies that, at least to

second order, the Chew-Goldberger-Low model agrees with the more complete kinetic description. It was thus deemed a reasonable model for this investigation despite the approximations implicit in it.

The Alfvén modes that exactly solve the Chew-Goldberger-Low model also satisfy without approximation the more widely recognized guiding-center equations. Moreover, the guiding-center solution has the property that the heat-flow tensor, which is arbitrarily dropped in deriving the Chew-Goldberger-Low equations, vanishes, providing further justification for the suitability of the Chew-Goldberger-Low equations to this study.

Section 4.2 treats exact Alfvén wave solutions in the Chew-Goldberger-Low model. In Sec. 4.2A a magnetic perturbation perpendicular to the uniform field $\underset{\sim}{B}_0$ of constant, but arbitrarily large, amplitude is shown to be an exact solution of the Chew-Goldberger-Low model provided the usual Alfvén wave stability criterion, Eq. (4.19), is satisfied. Such waves propagate without distortion parallel to $\underset{\sim}{B}_0$ at the generalized Alfvén velocity, given by Eq. (4.16). Figure 5 illustrates examples of this wave. The constant-amplitude Alfvén wave in the Chew-Goldberger-Low model has been briefly treated as an example of a "simple wave" of classical fluid theory.[41]

In Sec. 4.2B a circularly polarized Alfvén wave with $\underset{\sim}{k}$ parallel to $\underset{\sim}{B}_0$ is studied. This mode reduces the Chew-Goldberger-Low model to Eqs. (4.12), (4.13), (4.20), and (4.23) through (4.27), which are derived without any approximations.

The mode does not propagate. The magnetic field has a helical structure consisting of $\underset{\sim}{B}_0$ and a component perpendicular to $\underset{\sim}{B}_0$ of signed amplitude $\check{b}(t)$, as shown in Fig. 6. The time evolution of $\check{b}(t)$ is easily obtained from the energy Eq. (4.24): $\check{b}(t)$ can be viewed as the displacement of a classical particle moving in the potential $\mathcal{J}(\check{b})$, which is sketched in Fig. 7 for various initial plasma conditions. If the stability criterion (4.19) holds, $\check{b}(t)$ oscillates between positive and negative values with an amplitude-dependent frequency, which approaches the Alfvén frequency in the small-amplitude limit.

If the Alfvén stability criterion (4.19) is not satisfied, three special cases can occur, depending on the particular boundary conditions assumed for the plasma. The usual initial condition assumed for plasma instability studies corresponds to Fig. 7(c), in which $p_{\parallel}(0) > p_{\perp}(0) + B_0^2/4\pi$, and the initial perturbation amplitude $\check{b}$ and its time derivative $\check{b}'$ are small and positive. The amplitude grows exponentially at first, then more slowly; it reaches a maximum value in a finite time and immediately decreases, ultimately decreasing to zero exponentially. This demonstrates that wave quenching occurs in a finite time and is followed by immediate decay. If the initial conditions correspond to the situation in Fig. 7(d), the wave amplitude oscillates (nonsinusoidally), never passing through zero. If the initial conditions correspond to Fig. 7(b), the wave amplitude oscillates nonsinusoidally and passes through zero twice each period.

Section 4.3 shows that identical results are obtained from the guiding-center equations.

In Sec. 4.4 the exact results of Secs. 4.2 and 4.3 are discussed. It is noted that the constant-amplitude wave may be an important low-frequency phenomenon in the solar wind. The circularly polarized firehose mode is related to the quasilinear theory of the Alfvén instability.[24,39,40] Qualitative features of the nonlinear evolution of the circularly polarized firehose mode are compared with characteristics of other unstable waves.

4.2 Parallel Alfvén Waves in the Chew-Goldberger-Low Model

The Chew-Goldberger-Low equations or double adiabatic equations are[1,23]

$$d\rho/dt = -\rho\nabla\cdot\underset{\sim}{u}\,, \tag{4.1}$$

$$\rho d\underset{\sim}{u}/dt = -\nabla\cdot\underset{\approx}{p} + (\nabla\times\underset{\sim}{B})\times\underset{\sim}{B}/4\pi\,, \tag{4.2}$$

$$\partial\underset{\sim}{B}/\partial t = \nabla\times(\underset{\sim}{u}\times\underset{\sim}{B})\,, \tag{4.3}$$

$$d(p_{\perp}\rho^{-1}B^{-1})/dt = 0\,, \tag{4.4}$$

$$d(p_{\parallel}B^2\rho^{-3})/dt = 0\,, \tag{4.5}$$

$$\nabla\cdot\underset{\sim}{B} = 0\,, \tag{4.6}$$

$$\begin{aligned}\underset{\approx}{p} &= p_{\perp}(\underset{\approx}{I} - \hat{\hat{B}}\hat{\hat{B}}) + p_{\parallel}\hat{\hat{B}}\hat{\hat{B}}\,,\\ &= p_{\perp}\underset{\approx}{I} + p_{\Delta}\hat{\hat{B}}\hat{\hat{B}}\,,\end{aligned} \tag{4.7}$$

$$p_{\Delta} \equiv p_{\parallel} - p_{\perp}\,. \tag{4.8}$$

The usual notation for the convective derivative,

$$d/dt \equiv (\partial/\partial t + \underset{\sim}{u}\cdot\nabla),$$

has been used. In these equations B denotes the magnitude of the total magnetic field $\underset{\sim}{B}$.

We assume that the unperturbed state consists of a uniform plasma in a uniform and constant magnetic field $\underset{\sim}{B}_0$. Choose a Cartesian coordinate system with z axis parallel to $\underset{\sim}{B}_0$.

All plasma waves discussed in Secs. 4.2 and 4.3 are assumed to have the following space-time dependence:[42]

$$\underset{\sim}{u} = \underset{\sim}{u}(z,t), \tag{4.9a}$$

$$\underset{\sim}{B} = \underset{\sim}{B}_0 + \underset{\sim}{b}(z,t), \tag{4.9b}$$

$$\underset{\sim}{u}\cdot\underset{\sim}{B}_0 = 0, \tag{4.9c}$$

$$\underset{\sim}{b}\cdot\underset{\sim}{B}_0 = 0, \tag{4.9d}$$

$$b \equiv |\underset{\sim}{b}(z,t)| = b(t), \tag{4.9e}$$

$$p_\perp = p_\perp(t), \tag{4.9f}$$

$$p_\parallel = p_\parallel(t), \tag{4.9g}$$

$$\rho = \text{constant}. \tag{4.9h}$$

Note that the only spatial dependence is through the variable z, hence the name parallel Alfvén waves.

Without any approximation, use of properties (4.9) reduces the Chew-Goldberger-Low Eqs. (4.1) through (4.8) to the simple system

$$\partial\underset{\sim}{b}/\partial t = B_0\,\partial\underset{\sim}{u}/\partial z, \tag{4.10}$$

$$\rho\partial\underset{\sim}{u}/\partial t = -(B_0/B^2)(p_\Delta - B^2/4\pi)\partial\underset{\sim}{b}/\partial z, \tag{4.11}$$

$$p_\perp(t)/p_\perp(0) = B(t)/B(0), \tag{4.12}$$

$$p_\parallel(t)/p_\parallel(0) = B^2(0)/B^2(t). \tag{4.13}$$

Equations (4.10) and (4.11) can be combined to give a wave equation for $\underset{\sim}{b}$:

$$\partial^2\underset{\sim}{b}/\partial t^2 = -\rho^{-1}(B_0/B)^2(p_\Delta - B^2/4\pi)\partial^2\underset{\sim}{b}/\partial z^2. \tag{4.14}$$

Equation (4.14) can be treated by a separation of variables technique, but, due to its nonlinearity, particular solutions cannot be superposed to give more general ones. Guided by solutions of the linearized plasma equations, we investigate two classes of solutions of Eqs. (4.10) through (4.14).

A. Constant-Amplitude Propagating Solutions in the Chew-Goldberger-Low Model

Assume $b(t)$ is constant in time. Equations (4.12) and (4.13) imply that $p_\parallel$ and $p_\perp$ are also constant. With $\underset{\sim}{b} = b\,\hat{b}(z,t)$, Eq. (4.14) reduces to

$$\partial^2\hat{b}/\partial t^2 = V_A^2\,\partial^2\hat{b}/\partial z^2, \tag{4.15}$$

where the generalized Alfven velocity V_A is given by

$$V_A^2 = \rho^{-1}(B_0/B)^2[(B^2/4\pi) - p_\Delta] \tag{4.16}$$

and is also constant.

The general solution of the simple wave Eq. (4.15) is

$$\hat{b} = \hat{x}\cos\theta(z - V_A t) + \hat{y}\sin\theta(z - V_A t), \tag{4.17}$$

where $\underset{\sim}{b}$ has been chosen perpendicular to $\underset{\sim}{B}_0$ in accordance with Eq. (4.9d), and $\theta(\cdot)$ is any twice differentiable real function.

For example, if $\theta(x) \propto \tanh(kx)$, then for $|z - V_A t| \gg k^{-1}$ the direction of $\underset{\sim}{b}$ is nearly constant, whereas when $|z - V_A t| \lesssim k^{-1}$, $\underset{\sim}{b}$ rotates. The total magnetic field is essentially uniform where $|z - V_A t| \gg k^{-1}$ and is slanted with respect to the $\underset{\sim}{B}_0$ direction in this region. The field lines twist in the vicinity of $z = V_A t$ so that the total field $\underset{\sim}{B}$ always makes the same angle with $\underset{\sim}{B}_0$. The approximate shapes of the field lines for $\theta(x) = \pi \tanh(kx)$, $\theta(x) = \pi/2 \tanh(kx)$, and $\theta(x) = (7\pi/2)\exp[-(kx)^2]$ are shown in Fig. 5(a), (b), and (c), respectively. In the Chew-Goldberger-Low model, the field structures shown propagate without distortion at velocity V_A parallel to $\underset{\sim}{B}_0$. The propagating interface at $z = V_A t$, where the interesting field behavior occurs, has been likened to a shock front moving through a uniform plasma. The helical structure of Fig. 6 results if $\theta(x) = kx$.

The fluid velocity $\underset{\sim}{u}$ is obtained from Eq. (4.10):

$$u(x,t) = -(V_A/B_0)\underset{\sim}{b}(z,t). \tag{4.18}$$

Since $\underset{\sim}{u}$ must be real, V_A must be real, i.e.,

$$p_{\parallel} < p_{\perp} + B^2/4\pi, \tag{4.19}$$

which is the well-known stability criterion for Alfvén waves.

In summary, Eqs. (4.16) through (4.18) and (4.9a) through (4.9h) constitute an exact solution of the full nonlinear Chew-Goldberger-Low equations when the stability criterion (4.19) is satisfied. The solution is a wave of arbitrary but constant

amplitude, propagating without distortion at the Alfvén velocity $|V_A|$, parallel or antiparallel to $\underset{\sim}{B}_0$. The total field $\underset{\sim}{B}$ always makes the same angle with $\underset{\sim}{B}_0$ and has the same orientation throughout each plane z = constant.

B. Standing Wave Solutions with Time-Varying-Amplitudes in the Chew-Goldberger-Low Model

We next consider solutions of Eqs. (4.10) through (4.14) in which the wave amplitude can vary with time.

Since Eq. (4.9) assumes that the wave amplitude is independent of z, we write

$$\underset{\sim}{b}(z,t) = \mathfrak{b}(t)\,\hat{b}(z), \tag{4.20}$$

where $\mathfrak{b}(t)$ represents an amplitude that may assume positive or negative values. Substitution of this trial solution into Eq. (4.14) gives

$$(d^2\mathfrak{b}/dt^2)\hat{b} = -\rho^{-1}(B_0/B)^2(p_\Delta - B^2/4\pi)\mathfrak{b}\; d^2\hat{b}/dz^2.$$

Separating this equation into parts dependent on z and t, respectively, we find

$$d^2\hat{b}/dz^2 = -k^2\hat{b} \tag{4.21}$$

and

$$d^2\mathfrak{b}/dt^2 = k^2\,\rho^{-1}(B_0/B)^2(p_\Delta - B^2/4\pi)\mathfrak{b}\,. \tag{4.22}$$

In order that $\hat{b}$ have finite components, the constant k must be real, and Eq. (4.21) gives:

$$\hat{b}(z) = \hat{x}\cos(kz + \delta) + \hat{y}\sin(kz + \delta). \tag{4.23}$$

Thus the magnetic field has a helical structure with axis parallel to $\underset{\sim}{B}_0$ as shown in Fig. 6. In what follows we assume the wavelength large compared with the ion gyroradius to preserve the validity of the Chew-Goldberger-Low model.

An energy-like equation for $\eth(t)$ can be obtained by multiplying Eq. (4.22) by $\eth'$, using Eqs. (4.12) and (4.13) to carry out the resulting elementary integrations. Thus we find

$$\tfrac{1}{2}(\eth')^2 + \bar{\phi}(\eth) = K, \tag{4.24}$$

where K is a constant and

$$\bar{\phi}(\eth) \equiv \tfrac{1}{2} k^2 B_0^2 \rho^{-1}\{p_{\parallel}(0)[B(0)/B]^2 + 2p_{\perp}(0)[B/B(0)] + B^2/4\pi\}. \tag{4.25}$$

The dependence of $\bar{\phi}$ on $\eth$ is through B:

$$B = (B_0^2 + \eth^2)^{\frac{1}{2}}. \tag{4.26}$$

From Eqs. (4.10), (4.11), (4.20), and (4.23) we find

$$\underset{\sim}{u}(z,t) = (kB_0)^{-1}\eth'[\hat{x}\sin(kz + \delta) - \hat{y}\cos(kz + \delta)]. \tag{4.27}$$

Equations (4.12) and (4.13) specify $p_{\perp}(t)$ and $p_{\parallel}(t)$.

If Eq. (4.18) is multiplied by $\rho(kB_0)^{-2}$, and Eqs. (4.12), (4.13), and (4.27) are used to simplify the result, we obtain

$$\tfrac{1}{2}\rho u^2(t) + \tfrac{1}{2}p_{\parallel}(t) + p_{\perp}(t) + B^2(t)/8\pi = K'. \tag{4.28}$$

This is the energy equation for the combined system of plasma and wave with the obvious physical interpretations: $\frac{1}{2}\rho u^2$ represents the plasma translational energy density, $\frac{1}{2}p_{\parallel}$ is the thermal energy density parallel to $\underset{\sim}{B}$, $p_{\perp}$ is the thermal energy density perpendicular to $\underset{\sim}{B}$, and $B^2/8\pi$ is the total energy density in the field.

Viewing Eq. (4.24) as an equation in $\eth(t)$, we see that it describes the motion of a particle with displacement $\eth$, velocity $\eth'$, and total energy K moving in the potential $\bar{\phi}(\eth)$. The time development of $\eth(t)$ follows easily from this interpretation of Eq. (4.24).

First we consider the properties of $\bar{\phi}(\eth)$. From Eq. (4.25), one obtains

$$\partial\bar{\phi}/\partial\eth \propto \eth\{[B_0^2/4\pi] + p_{\perp}(0)B_0^2[B(0)B]^{-1} - p_{\parallel}(0)B_0^2 B^2(0)B^{-4}\}. \tag{4.29}$$

One extremum occurs at $\eth = 0$, because $\bar{\phi}$ is even in $\eth$. When multiplied by B^4 the curly brace in Eq. (4.29) is a monotonically increasing function of $|\eth|$. Thus the brace is positive for all $\eth \neq 0$, if it is nonnegative at $\eth = 0$, i.e., if

$$(B_0^2/4\pi) + p_{\perp}(0)[B_0/B(0)] - p_{\parallel}(0)[B(0)/B_0]^2$$

$$= (B_0^2/4\pi) + (p_{\perp})_{\eth=0} - (p_{\parallel})_{\eth=0} > 0. \tag{4.30}$$

Equation (4.30) is the Alfvén stability criterion; when it holds, $\bar{\phi}(\eth)$ has only the extremum at $\eth = 0$ and must have the form sketched in Fig. 7(a). In the Alfvén unstable case, when Eq. (4.30) does not hold, the curly brace is zero for exactly one value of $|\eth| > 0$, and $\bar{\phi}(\eth)$ must have the form sketched in Fig. 7(b).

Evolution of the circularly polarized Alfven wave in the stable and unstable cases is governed by the energy constant K, which is determined by the initial conditions.

Case 1. Stable Plasma

When Eq. (4.30) holds, $\mathcal{P}(0)$ is the minimum value of $\mathcal{P}(\mathcal{b})$. Thus K cannot be less than $\mathcal{P}(0)$, since this would imply an imaginary velocity $\mathcal{b}'$.

A quiescent, stable plasma with $\mathcal{b} = 0$ corresponds to $K = \mathcal{P}(0)$.

Assume $K > \mathcal{P}(0)$, and let $-\mathcal{b}_1 = \mathcal{b}_2 > 0$ be the real roots of the equation $\mathcal{P}(\mathcal{b}) = K$, which is a quartic in B. In view of Eq. (4.24) and Fig. 7(a), $\mathcal{b}$ oscillates between the turning points $\mathcal{b}_1$ and $\mathcal{b}_2$. Figure 6 shows the magnetic field behavior for this wave. One complete cycle, observed from a fixed spatial reference, is demonstrated by the sequence (a)(b)···(f)(g)(f)···(a).

When $|\mathcal{b}_{1,2}| \ll B_0$, Eq. (4.24) can be expanded in $\mathcal{b}$ to give

$$\tfrac{1}{2}(\mathcal{b}')^2 + \tfrac{1}{2}\rho^{-1}k^2[(B_0^2/4\pi) + p_{\perp}(0) - p_{\parallel}(0)]\mathcal{b}^2 = \Delta, \quad (4.31)$$

where Δ is a positive constant. Equation (4.31) is that of a simple harmonic oscillator with its frequency ω given by

$$\omega^2 = \rho^{-1}k^2[(B_0^2/4\pi) + p_{\perp}(0) - p_{\parallel}(0)]. \quad (4.32)$$

Thus for small amplitude waves we recover the Alfvén dispersion relation. This solution is a standing wave; it can be viewed as

a linear combination of two circularly polarized Alfvén waves, special types of the constant-amplitude solution considered in Sec. 4.2A, propagating in opposite directions.

For more severe perturbations the frequency of oscillation is amplitude-dependent, the period τ being simply the transit time of the "magnetic" particle oscillating in the potential $\mathcal{P}(\mathcal{b})$:

$$\tau = 2\int_{\mathcal{b}_1}^{\mathcal{b}_2} \frac{d\mathcal{b}}{\mathcal{b}'} = 4\int_0^{\mathcal{b}_2} \frac{d\mathcal{b}}{[2[K - \mathcal{P}(\mathcal{b})]]^{\frac{1}{2}}}. \quad (4.33)$$

Although this solution is a standing wave, $\mathcal{b}$ does not oscillate sinusoidally, so this mode cannot be viewed as a superposition of circularly polarized parallel propagating Alfvén waves.

Case 2. Unstable Plasma

Assume that Eq. (4.30) does not hold, i.e., assume

$$(p_{\parallel})_{\mathcal{b}=0} > (p_{\perp})_{\mathcal{b}=0} + B_0^2/4\pi. \quad (4.34)$$

The plasma is unstable with respect to small-amplitude Alfvén waves, and the magnetic potential $\mathcal{P}$ has the form sketched in Fig. 7(b)-(d). The evolution of the circularly polarized Alfvén wave depends on the value of K relative to $\mathcal{P}(0)$.

(a) Assume $K > \mathcal{P}(0)$, which corresponds to Fig. 7(b). Let $\mathcal{P}(\mathcal{b}_1) = \mathcal{P}(\mathcal{b}_2) = K$, where $-\mathcal{b}_1 = \mathcal{b}_2 > 0$ as before.

As in Case 1 for large-amplitude waves, $\mathcal{b}$ oscillates between the values $\mathcal{b}_1$ and $\mathcal{b}_2$ with period τ given by Eq.

(4.33). The oscillation is nonsinusoidal to the extent that ϕ is nonparabolic. The development of the magnetic field in time can be seen in Fig. 6: a complete cycle consists of the sequence (a)···(f)(g)(f)···(a); ζb passes through zero twice each period.

(b) Assume $K \approx \bar{\phi}(0)$, which corresponds to Fig. 7(c).

The case $K = \bar{\phi}(0)$ is the situation usually considered in instability studies: the plasma is unstable, but initially unperturbed. If a small-amplitude circularly polarized Alfvén wave perturbation is introduced with $\zeta b(0) > 0$ and $\zeta b'(0) > 0$, ζb initially grows exponentially, then more slowly until its growth stops at ζb_2, the positive root of $\bar{\phi}(\zeta b) = K$. Immediately the mode decays, with ζb ultimately falling exponentially to zero.

The time τ required for the amplitude to reach saturation and decay to its initial amplitude $\zeta b(0)$ is

$$\tau = 2 \int_{\zeta b(0)}^{\zeta b_2} \frac{d\zeta b}{\zeta b'} . \qquad (4.35)$$

The exponential rate for growth and decay is the usual firehose growth rate. The duration of exponential growth will be arbitrarily long as $\zeta b(0)$ is made arbitrarily small, although in practice $\zeta b(0)$ cannot be made much less than the inherent random fluctuations in $\underset{\sim}{B}$.

The growth-decay behavior is demonstrated in Fig. 6 by the sequence (c)(b)(a)(b)(c), with ultimate decay to the uniform magnetic field pictured in Fig. 6(d).

When $K = \bar{\phi}(0)$ the exact equations predict pure decay, or growth-saturation-decay, but the mode is not periodic. When K is near $\bar{\phi}(0)$, but not equal to it, any circularly polarized wave oscillates between solutions of $\bar{\phi}(\zeta b) = K$. The perturbation amplitude spends most of its time near zero amplitude, since $\zeta b'$ is small there. The period increases markedly as K approaches $\bar{\phi}(0)$.

(c) Assume $\bar{\phi}_{min} < K < \bar{\phi}(0)$, where $\bar{\phi}_{min}$ denotes the minimum value of $\bar{\phi}(\zeta b)$, corresponding to Fig. 7(d).

Let $\bar{\phi}(\zeta b_1) = \bar{\phi}(\zeta b_2) = K$, where $0 < \zeta b_1 < \zeta b_2$, and choose the coordinate system so that $\zeta b_1 < \zeta b(0) < \zeta b_2$. Figure 7(d) shows that ζb oscillates between the limits ζb_1 and ζb_2, never passing through zero. The field behavior for a full cycle is illustrated in Fig. 6 by the sequence (a)(b)(c)(b)(a).

4.3 Parallel Alfvén Waves in the Guiding-Center Model

The results obtained in Sec. 4.2 in the Chew-Goldberger-Low model also follow from the guiding-center equations, which, because the heat-flow tensor is not arbitrarily neglected, constitute a more realistic approximation to an actual plasma. We work with the equations obtained by Kulsrud from the Vlasov equation in the small gyroradius limit.[23] This is a kinetic description, and thus the particle distribution function F_0 must be specified. We take F_0 to be bi-Maxwellian:

$$F_0(w,q,t) = C\, p_\perp^{-1}\, p_\parallel^{-\frac{1}{2}} \exp[-\rho w/p_\perp - \rho(q - u_\parallel)^2/2p_\parallel] , \qquad (4.36)$$

where

$$w \equiv \frac{1}{2}(\underset{\sim}{v} - \underset{\sim}{u})_{\perp}^{2} \tag{4.37}$$

and

$$q \equiv v_{\parallel} . \tag{4.38}$$

Parallel and perpendicular refer to the total magnetic field.

Using Eq. (4.36) and the characteristics (4.9) of the waves of interest, we show in Appendix B that Kulsrud's guiding-center equations reduce to

$$E_{\parallel} = 0, \tag{4.39}$$

$$\partial \underset{\sim}{b}/\partial t = B_0 \, \partial \underset{\sim}{u}/\partial z, \tag{4.40}$$

$$\rho \partial \underset{\sim}{u}/\partial t = -(B_0/B^2)(p_{\Delta} - B^2/4\pi)\partial \underset{\sim}{b}/\partial z, \tag{4.41}$$

$$p_{\perp}(t)/p_{\perp}(0) = B(t)/B(0), \tag{4.42}$$

$$p_{\parallel}(t)/p_{\parallel}(0) = B^2(0)/B^2(t), \tag{4.43}$$

$$2\dot{B}/B = \rho(p_{\Delta} - B^2/4\pi)^{-1} \, \partial u^2/\partial t, \tag{4.44}$$

$$(\underset{\sim}{u} \cdot \underset{\sim}{b})\dot{B} = 0. \tag{4.45}$$

Equations (4.40) through (4.43) are identical to those obtained from the Chew-Goldberger-Low model, Eqs. (4.10) through (4.13). Equation (4.39) disposes of the parallel electric field, which appears in the guiding-center theory, but not in the Chew-Goldberger-Low model.

A. Constant-Amplitude Propagating Solutions in the Guiding-Center System

The solutions of the Chew-Goldberger-Low system considered in Sec. 4.2A have the property that $|\underset{\sim}{B}|$ and $|\underset{\sim}{u}|$ remain constant in time. Thus both sides of Eq. (4.44) vanish, Eq. (4.45) is satisfied, and the guiding-center equations reduce to those derived from the Chew-Goldberger-Low model and lead to the same solutions as obtained in Sec. 4.2A.

B. Time-Varying-Amplitude Standing-Wave Solutions in the Guiding-Center System

The time-varying-amplitude Alfvén modes considered in Sec. 4.2B satisfy Eq. (4.44) in view of Eq. (4.27) and a simple manipulation of Eq. (4.22). Equation (4.45) is likewise satisfied because Eqs. (4.23) and (4.27) show that $\underset{\sim}{b}$ and $\underset{\sim}{u}$ are orthogonal.

The guiding-center equations have thus been simplified to the Chew-Goldberger-Low results, Eqs. (4.10) through (4.13), and lead to the same time-varying-amplitude solutions obtained in Sec. 4.2B.

Note that, since the solutions obtained from the guiding-center equations have a bi-Maxwellian velocity distribution, the heat-flow tensor $\underset{\approx}{Q}$ vanishes. This justifies, in retrospect, the use of the Chew-Goldberger-Low model, which arbitrarily assumes that $\nabla \cdot \underset{\approx}{Q} = 0$.[1,23]

4.4 Discussion of the Uniform-Plasma Solutions

A. Significance of the Constant-Amplitude Propagating Alfvén Wave

It has been known for many years that in a uniform magnetofluid-dynamic plasma a transverse magnetic perturbation of arbitrary orientation and constant amplitude (or special cases of this type of wave) propagates at the Alfvén velocity parallel to a uniform magnetic field without distortion, i.e., there is no coupling to particles or waves in the absence of other perturbations.[38,43-45] Sections 4.2A and 4.3A show that this conclusion holds even for an anisotropic plasma in the Chew-Goldberger-Low and guiding-center models. Examples are pictured in Fig. 5.

The constant-amplitude propagating Alfvén wave may be important in the solar wind. Mariner V data[18,19] show the high correlation or anticorrelation between magnetic field and fluid velocity which characterizes Alfvén waves [see Eq. (4.18)]. Although the individual field components fluctuate in a seemingly random fashion, the total field magnitude is relatively constant over large regions of the solar wind. The wave propagates at the Alfvén velocity, always away from the sun. Furthermore, the amplitude of the magnetic fluctuation is comparable to the total field, so that explanation of the phenomenon requires a large-amplitude theory. Subsequent analysis of the data may show that the random fluctuations in the observed field can be duplicated by the constant-amplitude Alfvén wave with suitable choice of the

arbitrary function θ. The constant-amplitude Alfvén wave is characterized by a constant magnetic field component B_0 in the direction of propagation; it has not been established whether the solar wind has this property.[46]

The simple picture of a constant-amplitude wave propagating parallel to the uniform field without distorion may no longer be valid if other waves are present. It has been shown, for example, that a large-amplitude circularly polarized Alfvén wave in a magnetofluid-dynamic plasma ($p_{\parallel} = p_{\perp}$) can couple to another Alfvén wave and an ion sound wave if the waves satisfy certain three-wave resonance conditions.[38]

This wave is used in Chapter 5 for the study of the convective evolution of large-amplitude Alfvén waves in the solar wind. Although it retains the important property of being locally constant in amplitude, its amplitude varies slowly with distance from the sun as it propagates through the nonuniform and rapidly convecting plasma. Its importance in the solar wind receives further attention in Chapter 5.

Barnes and Suffolk have investigated the large-amplitude propagating Alfvén wave using a relativistic kinetic theory.[47]

B. The Variable-Amplitude Circularly Polarized Alfvén Mode

Energy conservation prevents the indefinite growth of a linearly unstable plasma wave. Nonlinear effects, such as wave-particle and wave-wave interactions, ultimately limit the amplitude of modes that increase exponentially with time in linear theory.

This mode quenching problem rarely yields analytic solutions in closed form, and insight regarding wave-saturation processes is acquired with difficulty. Except in special cases, even the qualitative properties are unknown. For example, does the plasma approach the saturated state of maximum wave energy asymptotically as $t \to \infty$, or does saturation occur in a finite time? If the latter holds, does the quenched state represent a stable configuration, or will further evolution occur?

Earlier quasilinear studies[24,39,40] of the firehose mode produced equations accurate to second order in the wave amplitudes of the form

$$d\langle P_\perp\rangle/dt = (\langle P_\parallel\rangle/B_0^2)\int d^3k\, \gamma(\underset{\sim}{k},t)\psi(\underset{\sim}{k},t), \tag{4.46}$$

$$d\langle P_\parallel\rangle/dt = [(4\langle P_\parallel\rangle - 2\langle P_\perp\rangle)/B_0^2]\int d^3k\, \gamma(\underset{\sim}{k},t)\psi(\underset{\sim}{k},t), \tag{4.47}$$

$$d\psi(\underset{\sim}{k},t)/dt = 2\gamma(\underset{\sim}{k},t)\,\psi(\underset{\sim}{k},t), \tag{4.48}$$

$$\gamma^2(\underset{\sim}{k},t) = \rho^{-1}(\underset{\sim}{k}\cdot\hat{\underset{\sim}{B}}_0)^2(\langle P_\parallel\rangle - \langle P_\perp\rangle - B_0^2/4\pi), \tag{4.49}$$

$$\psi(\underset{\sim}{k},t)\,\delta(\underset{\sim}{k}+\underset{\sim}{k}') \equiv \langle \delta\underset{\sim}{B}(\underset{\sim}{k},t)\cdot\delta\underset{\sim}{B}(\underset{\sim}{k}',t)\rangle. \tag{4.50}$$

Here $\delta\underset{\sim}{B}$ is the perturbation in the magnetic field, parallel and perpendicular refer to the direction of $\underset{\sim}{B}_0$, and finite gyroradius effects have been dropped. The brackets denote ensemble and spatial averaging in the derivation of Davidson and Völk. Equations (4.46) through (4.50) are obtained in Appendix A from the Chew-Goldberger-Low model.

The quasilinear equations have the advantage of treating an arbitrary distribution of linearly polarized Alfvén waves. They imply the existence of a quenching point: the plasma is initially unstable if $\langle P_\parallel\rangle(0) > \langle P_\perp\rangle(0) + B_0^2/4\pi$, but, as the waves grow, $\langle P_\perp\rangle$ increases and $\langle P_\parallel\rangle$ decreases until $\gamma(\underset{\sim}{k},t) = 0$, and no waves are unstable.

However, Eqs. (4.46) through (4.50) have not been solved in even the simplest cases. The qualitative properties of the quenching process obtained so simply in Sec. 4.2B for the circularly polarized mode--namely, that quenching occurs in a finite time and is followed immediately by decay--are obscured by the complexity of Eqs. (4.46) through (4.50). Indeed these gross features may have been lost by the approximations used in deriving them from the more fundamental equations. The quasilinear theory cannot provide quantitative information concerning the quenching process, since, as Davidson and Völk note, higher-order nonlinear effects become important as $\gamma \to 0$. In deriving the quasilinear equations one treats $\gamma^2(\underset{\sim}{k},t)$ as a zero-order quantity, an assumption which clearly breaks down at the quenching point.

Qualitative features of the quenching of the circularly polarized Alfvén wave are shared by other wave saturation processes:

1. Numerical studies of the flute mode in the low-density regime show exponential growth at small amplitudes, then saturation followed by decay.[25] The energy in the mode oscillates,

much like the Alfvén wave of Case 2(b), Sec. 4.2B, when K is slightly less than $\bar{\phi}(0)$.

2. Investigation of the nonlinear evolution of a single-wavelength longitudinal flute mode with frequency near a harmonic of the gyrofrequency in a loss-cone plasma indicates saturation in a finite time followed by decay.[26] The analysis is invalid beyond the decay regime, so that oscillatory behavior cannot be revealed. The mode considered is a symmetric standing wave, and the analysis involves a pseudopotential, both characteristics having analogues in the theory of Sec. 4.2B.

3. In a plasma consisting of two cold streams, a dynamical theory of the two-stream instability shows that "the electric field does not grow and level off at some value E_{max} where $\gamma = 0$, but, rather, because of the dynamics, overshoots this point and then oscillates back to its initial state."[27]

4. The bump-on-the-tail limit of the two-stream instability has similar properties: wave saturation occurs in a finite time and is followed by gentle oscillations of the wave energy, with period comparable to particle-trapping times.[28-30]

The pure circularly polarized Alfvén wave discussed here may never occur in the physical world. The requirement of a large uniform plasma in a uniform magnetic field subject to no other perturbation makes its experimental realization nearly impossible. It is hoped that the advantage of having an exact solution in a simple form to an otherwise intractable class of problems will make this study beneficial. The characteristics

of the simple wave-quenching process may serve a useful purpose if only pointing the way to important characteristics of more complete and more complex plasma instability problems.

Berezin and Sagdeev have studied the variable amplitude circularly polarized Alfven mode in a generalized double adiabatic model which includes finite gyroradius effects.[48] The resulting analysis is more complicated, but the evolution of the mode remains essentially the same as found in Sec. 4.2B.

CHAPTER 5

CONVECTIVE EVOLUTION OF ALFVÉN WAVES IN THE IDEALIZED SOLAR WIND MODEL

5.1 The Wave Structure

The convective evolution analysis of Alfvén waves in the solar wind is based on the spherically symmetric idealized model discussed in Chapter 3. This consists of a static magnetic monopole field, in which a spherically symmetric plasma flows radially outward at supersonic and super-Alfvénic velocity u_0 along the field lines.

At some arbitrary radius a source of Alfvén waves is introduced. It is spherically symmetric, in a sense to be explained below, and emits propagating Alfvén waves of the type studied in Sec. 4.3A in the guiding-center approximation. The amplitude of these emitted waves, i.e., the component of $\underset{\sim}{B}$ perpendicular to the radial direction, is assumed to be constant in time at the source.

The locus of the source can be at the surface of the sun in the theoretical model, although the location of the actual source of the Alfvén waves observed experimentally in the vicinity of 1 AU is not known at present. Recalling the ideas of Chapter 2, the turbulence in the solar corona produces fluctuations in the magnetic field which metamorphose into Alfvén waves long before they reach 1 AU. Another possibility is that the turbulent region between the fast and slow streams of the solar wind sectors may be the dominant source of constant-

amplitude outward-propagating Alfvén waves. Whatever and wherever the actual source may be, for the analytic model it suffices to assume a constant-amplitude source at some radius r_s. This reference radius must be large compared to a wavelength so that the wave is not aware of the curvature of the model. The solution is readily extended to smaller radii. For example, one might postulate known properties of Alfvén waves at 1 AU and solve for the source required at the solar corona to produce them.

In the uniform plasma problem considered in Chapter 4, the magnetic field for the Alfvén wave propagating along the z axis can be written,

$$\underset{\sim}{B}(z,t) = B_0\hat{z} + b[\hat{x}\cos\theta(t - z/V_A) + \hat{y}\sin\theta(t - z/V_A)]. \tag{5.1}$$

In Eq. (5.1), $\theta(\cdot)$ is an arbitrary twice-differentiable function, subject to the restriction that it not change so abruptly that the gyroradius limit of the Chew-Goldberger-Low theory is exceeded.

An appropriate generalization to a spherically symmetric convecting plasma containing large-amplitude propagating Alfvén waves is the ansatz

$$\underset{\sim}{B}(\underset{\sim}{r},t) = B_0(r)\hat{r} + b(r)[\hat{\theta}\cos\theta(r,t) + \hat{\phi}\sin\theta(r,t)], \tag{5.2}$$

where r, θ, and ϕ denote the usual spherical coordinates.

We choose the WKB phase dependence appropriate to a wave propagating radially at the Alfvén velocity V_A in a plasma which is itself convecting radially at the velocity u_0:

$$\theta(r,t) \equiv \theta\left\{t - \int_{r_s}^{r} dr'[u_0(r') + V_A(r')]^{-1}\right\}. \quad (5.3)$$

The function $\theta\{\cdot\}$ must be differentiable and possess smoothness properties to be derived later; otherwise it is arbitrary, as in the uniform-plasma case.

To simplify the notation, we define

$$\hat{b}(\theta) \equiv \hat{\theta}\cos\theta + \hat{\phi}\sin\theta, \quad (5.4)$$

i.e., $\hat{b}(\theta)$ is a unit vector perpendicular to the radial direction which makes an angle θ with the local $\hat{\theta}$ direction. This notation is somewhat unsatisfactory, since $\hat{\theta}$ and $\hat{\phi}$ are determined by the radial position $\underset{\sim}{r}$ at which θ is computed. Making this relation notationally explicit, e.g. $\hat{b}[\theta(\underset{\sim}{r},t),\underset{\sim}{r}]$, would unnecessarily complicate the equations. The meaning of $\hat{b}(\theta)$ should always be clear from the context.

Using this notation, the ansatz (5.2) can be written

$$\underset{\sim}{B}(\underset{\sim}{r},t) = B_0(r)\hat{r} + b(r)\,\hat{b}(\theta), \quad (5.5)$$

with $\theta(r,t)$ defined by Eq. (5.3).

Since a steady-state solution is sought, the wave amplitude b at any radius is independent of time. However, the waves are no longer "constant-amplitude" as they are in a uniform plasma. The slow variation of wave amplitude with radius as the wave propagates in the expanding plasma is the objective of this investigation.

With the introduction of ansatz (5.2) or (5.5), the topology of spherical systems causes the idealized model to become ill-posed and destroys its spherical symmetry. Suppose that for some spherical surface $r = r_0$ and some time t_0, $\theta(r_0,t_0) = 2\pi q$, where q is any integer. On this surface the wave components of $\underset{\sim}{B}$ given by Eq. (5.5) would be in the $\hat{\theta}$ direction everywhere as shown in Fig. 8. The loss of spherical symmetry is clear, and the evident field singularity at the pole is physically and mathematically nonsensical.

Figure 8 shows that in the vicinity of the equatorial plane the ansatz, Eq. (5.5), is consistent and represents a locally spherically symmetric wave. Providing the analysis is restricted to waves propagating radially in equatorial latitudes such that $|\theta - \pi/2| \ll 1$, Eq. (5.5) is mathematically consistent. This allows the analysis to be carried out locally as if the entire system possesses spherical symmetry, even though the model breaks down at polar latitudes, and the wave introduces a preferred direction. The restriction of the analysis to a small solid angle is adequate, since the large amplitude Alfvén waves reside principally in the narrow, high-velocity spirals at the boundaries between high and low density sectors.[18,19]

The ansatz represented by Eq. (5.5) is sufficiently general to fit the seemingly random phase of the aperiodic large-

amplitude Alfvén waves observed by the interplanetary spacecraft, with suitable choice of the arbitrary phase function $\theta(\cdot)$. The wave is expected to propagate away from the sun[49] in the convecting plasma without modification of the shape function $\theta(\cdot)$, but the magnetic field changes as the amplitudes of its radial and perpendicular components vary slowly.

In analogy with the large-amplitude propagating Alfvén wave in a homogeneous plasma, we assume that the bulk plasma velocity $\underset{\sim}{u}$ has the form

$$\underset{\sim}{u}(\underset{\sim}{r},t) = u_0 \hat{r} + u_T \hat{b}(\theta + \delta), \tag{5.6}$$

where δ and u_T are slowly varying functions of r, and the time dependence of $\underset{\sim}{u}(\underset{\sim}{r},t)$ occurs through the phase function $\theta(\underset{\sim}{r},t)$.

In Eq. (5.6), $\delta(r)$ is a small phase angle which is arbitrarily introduced to allow for the small difference in direction between the wave components of $\underset{\sim}{B}$ and $\underset{\sim}{u}$ which results from the nonuniform plasma and field. In the case of a uniform plasma and field, Eq. (4.8) shows that these components are parallel (antiparallel) when the direction of propagation is antiparallel (parallel) to the uniform field direction. For the nonuniform solar wind model considered in this chapter, the ansatz, Eqs. (5.5) and (5.6), is overspecified if we assume that $\delta(r)$ is identically zero, as it is in the uniform case. That is, the equations that result when Eqs. (5.5) and (5.6) are substituted in the Chew-Goldberger-Low equations are inconsistent,

and no solution exists if $\delta \equiv 0$. We assume throughout that $\delta(r)$ is small:

$$|\delta(r)| \ll 1, \tag{5.7}$$

and we verify in Sec. 5.4C that this holds for Alfvén waves in the solar wind at 1 AU.

As in the uniform situation, the pressures and density do not vary in time at a particular position. Due to the nonuniformity of the solar wind model, each depends on r:

$$\rho = \rho(r), \tag{5.8}$$

$$p_{\parallel} = p_{\parallel}(r), \tag{5.9}$$

$$p_{\perp} = p_{\perp}(r). \tag{5.10}$$

We carry out the analysis of large-amplitude Alfvén waves propagating in the idealized model in two ways. In Sec. 5.2 we solve the problem by using energy and momentum conservation equations for the radial direction. In Sec. 5.3 the solution is obtained by using the wave parts of the Chew-Goldberger-Low momentum and Maxwell equations, without reference to energy conservation.

Section 5.4 compares the results of the two methods, specifies ranges of validity of the analyses, and discusses consequences and applications of the solutions.

5.2 Solution of the Convective Evolution Problem from an Energetic Viewpoint

In order to apply energetic considerations to Alfvén waves propagating in the expanding solar wind plasma, certain properties of the waves must be known. In this section we assume the following properties derived for propagating Alfvén waves in Secs. 4.2 and 4.3:

$$u_T(r) = - V_A(r)\, b(r)/B_0(r), \tag{5.11}$$

and

$$V_A^2(r) = \rho^{-1}(r)\, B_0^2(r)[(1/4\pi) - p_\Delta(r)/B^2(r)]. \tag{5.12}$$

Recall that $p_\Delta \equiv p_{//} - p_\perp$, Eq. (4.8). Thus we suppose that the relations obtained for waves in a uniform system hold locally in the nonuniform plasma, with each wave parameter assigned its local value.

We also assume throughout this section that the Alfvén velocity is small compared to the plasma bulk velocity:

$$V_A/u_0 \ll 1. \tag{5.13}$$

This assumption is discussed in more detail in Sec. 5.4. In the solar wind the ratio is $V_A/u_0 \lesssim 0.1$.

Taking a global viewpoint of the spherically symmetric system outlined in Sec. 5.1, we write the energy conservation equation

$$\frac{\partial U}{\partial t} + \nabla \cdot \underset{\sim}{S} = 0 \tag{5.14}$$

where U represents the total energy per unit volume, including contributions from plasma particles and the electromagnetic fields, and $\underset{\sim}{S}$ denotes the total energy flux vector. Equation (5.14) states that the total energy lost from a fixed volume equals the flux of energy out of that volume.

The model described in Sec. 5.1 is assumed to be in a steady-state condition, i.e., the sources of Alfvén waves and convecting plasma were turned on at $t = -\infty$, and all transient effects have disappeared at the time of observation.

Although the wave is time dependent, and its shape is quite irregular, its amplitude is constant in time at each point. Consequently the energy density U is stationary in time. Thus, in the steady-state situation being considered, Eq. (5.14) reduces to

$$\nabla \cdot \underset{\sim}{S} = 0, \tag{5.15}$$

and it suffices to compute the energy flux vector $\underset{\sim}{S}$.

Since $\underset{\sim}{S}$ must include the flux of particle energy and the flux of electromagnetic energy or Poynting flux, it has the form:

$$\underset{\sim}{S} = \sum_{e,i} \int d^3v\, \frac{1}{2} m\, v^2\, \underset{\sim}{v}\, f(\underset{\sim}{v};\, \underset{\sim}{r};\, t) + (c/4\pi)\underset{\sim}{E} \times \underset{\sim}{B}\,. \tag{5.16}$$

In Eq. (5.16), m is the particle mass, $\underset{\sim}{v}$ is its velocity, f is its distribution function, and the summation is over electrons and ions.

In Appendix C, $\underset{\sim}{S}$ is computed for a general bi-thermal particle distribution f. From the guiding-center analysis of Chapter 4 it would seem appropriate to assume that f is bi-Maxwellian in $\underset{\sim}{v}$. However, the Chew-Goldberger-Low formalism ignores the details of the particle distribution, and f is left in its most general form. In this formalism, $\underset{\sim}{S}$ becomes

$$\underset{\sim}{S} = \frac{1}{2}\rho u^2 \underset{\sim}{u} + (p_\perp + \frac{1}{2} p_{\parallel})\underset{\sim}{u} + p_\perp \underset{\sim}{u}_\perp + p_{\parallel} \underset{\sim}{u}_{\parallel}$$

$$+ \underset{\sim}{Q} + \underset{\sim}{B} \times (\underset{\sim}{u} \times \underset{\sim}{B})/4\pi. \qquad (5.17)$$

As usual, perpendicular and parallel refer to the local total magnetic field direction. In Eq. (5.17) $\underset{\sim}{Q}$ is the heat flow tensor $\underset{\approx}{Q}$ contracted over two of its three indices:

$$[\underset{\sim}{Q}]_i \equiv [\underset{\approx}{Q}]_{ijj}. \qquad (5.18)$$

Since $\nabla \cdot \underset{\approx}{Q} = 0$ is assumed in the Chew-Goldberger-Low model, the term $\underset{\sim}{Q}$ is dropped henceforth, because only the divergence of $\underset{\sim}{S}$ occurs.

Since we assume spherical symmetry, Eq. (5.15) has the form

$$r^{-2}\, \partial(r^2 S_r)/\partial r = 0, \qquad (5.19)$$

where S_r is the radial component of the energy flux vector. Equation (5.19) has the obvious solution

$$r^2 S_r = \text{constant}. \qquad (5.20)$$

The calculation of the radial component of $\underset{\sim}{S}$ requires some algebra, because parallel and perpendicular in Eq. (5.17) refer to the total field direction rather than the radial direction. For example, $\underset{\sim}{u}_{\parallel}(\underset{\sim}{r},t)$, which is a vector in the direction of $\underset{\sim}{B}(\underset{\sim}{r},t)$, is the projection of the total fluid velocity onto $\underset{\sim}{B}(\underset{\sim}{r},t)$. Appendix D contains the details for the ansatz, Eqs. (5.5) and (5.6), and shows that

$$S_r = \frac{1}{2}\rho u_0^3 + (p_\perp + \frac{3}{2} p_{\parallel})u_0 + \frac{1}{2}\rho V_A^2(3u_0 + 2V_A)(b/B_0)^2. \qquad (5.21)$$

The first term in Eq. (5.21) is the dominant term for thermal velocities small compared to the convection velocity u_0. The remaining terms determine the evolution of the wave amplitude in the convecting plasma. In keeping with inequality (5.13) we drop the term proportional to ρV_A^3 in Eq. (5.21) so that the latter becomes

$$S_r = \frac{1}{2}\rho u_0^3 + (p_\perp + \frac{3}{2} p_{\parallel})u_0 + \frac{3}{2}\rho V_A^2 u_0 (b/B_0)^2. \qquad (5.22)$$

The Chew-Goldberger-Low relations supply the additional equations which are needed to obtain the dependence of the parameters on r.

The mass conservation law, Eq. (4.1) in the steady state becomes

$$\nabla \cdot (\rho \underset{\sim}{u}) = 0, \qquad (5.23)$$

and, since the system is spherically symmetric, Eq. (5.23) integrates to give

$$r^2 \rho u_0 = \text{constant}. \tag{5.24}$$

When S_r given in Eq. (5.22) is substituted in the energy conservation law, Eq. (5.20), and the constant factor specified in Eq. (5.24) is divided out, there results the relatively simple energy equation:

$$u_0^2 + 3\frac{p_{\parallel}}{\rho} + 2\frac{p_{\perp}}{\rho} + 3 V_A^2 (b/B_0)^2 = \text{constant}. \tag{5.25}$$

The bulk solar wind velocity u_0 is approximately constant; the lowest order corrections to $u_0^2 = \text{constant}$ are of order $p_{\perp,\parallel}/\rho \sim v_{th}^2$. Although these correction terms can usually be neglected, it is not valid to absorb u_0^2 in the constant term in Eq. (5.25), since the other terms in this equation are the same order as the lowest order corrections to $u_0^2 = \text{constant}$.

Thus, in order to solve Eq. (5.25), we need an accurate expression for u_0. This can be obtained from the radial component of the Chew-Goldberger-Low momentum equation, Eq. (4.2). Appendix F proves that, for the spherically symmetric model of outward propagating Alfvén waves, the radial part of Eq. (4.2) can be written

$$\rho u_0 \, du_0/dr = -d(p_{\perp} + b^2/8\pi)/dr - B_0 \, d(p_{\Delta} B_0 B^{-2})/dr. \tag{5.26}$$

Inspection of Eq. (5.26) verifies that the variations in u_0^2 are of order v_{th}^2.

We must add to Eqs. (5.25) and (5.26) the adiabatic laws, Eqs. (4.4) and (4.5), to determine the pressures in the convecting plasma. For the steady state problem, these equations reduce to

$$\rho^{-1} B^{-1} p_{\perp} = \text{constant} \tag{5.27}$$

and

$$\rho^{-3} B^2 p_{\parallel} = \text{constant}. \tag{5.28}$$

In view of Eq. (5.24), and the fact that changes in u_0 are of order v_{th}^2/u_0^2,

$$\rho \propto r^{-2}[1 + O(v_{th}^2/u_0^2)].$$

In Eq. (5.25) we have dropped a term of order v_{th}^3. Thus, for the purpose of calculating ρ and the pressures to the order required in Eq. (5.25) and the right side of Eq. (5.26), it is unnecessary to carry along the exact r dependence of the bulk velocity u_0. It suffices to treat u_0 as constant in Eq. (5.24) to calculate ρ, and hence $p_{\perp}$ and $p_{\parallel}$, except where ρ appears with the large u_0^2 factor on the left side of Eq. (5.26).

We introduce the notation

$$\mathcal{B}(r) \equiv B(r)/B_0(r) = (1 + b^2/B_0^2)^{1/2} \tag{5.29}$$

and define

$$\rho_0 \equiv \rho(r_0) \tag{5.30a}$$

$$p_{\perp 0} \equiv p_{\perp}(r_0) \tag{5.30b}$$

$$p_{\perp 0} \equiv p_{\perp}(r_0) \tag{5.30c}$$

$$B_{00} \equiv B_0(r_0) \tag{5.30d}$$

and

$$\mathcal{B}_0 \equiv \mathcal{B}(r_0). \tag{5.30e}$$

To the accuracy required in Eq. (5.25) and the right side of Eq. (5.26), we can write

$$\rho(r) = \rho_0(r_0/r)^2, \tag{5.31}$$

$$p_{\perp}(r) = p_{\perp 0}(r_0/r)^4 \mathcal{B}/B_0, \tag{5.32}$$

and

$$p_{\parallel}(r) = p_{\parallel 0}(r_0/r)^2 (\mathcal{B}_0/\mathcal{B})^2. \tag{5.33}$$

The remaining task is to eliminate the large terms involving u_0 between Eqs. (5.25) and (5.26) and, using Eqs. (5.31) - (5.33), to obtain a differential equation for $\mathcal{B}(r)$. The algebraic steps are sketched in Appendix G. The result is

$$\left[\frac{\beta_\perp}{4}\left(\frac{r_0}{r}\right)^4 \frac{\mathcal{B}_0}{\mathcal{B}^3}(3\mathcal{B}^2 + 1) - \beta_\parallel \left(\frac{r_0}{r}\right)^2 \frac{\mathcal{B}_0^4}{\mathcal{B}^6} + \frac{r_0^4}{r^4}\right] \frac{d\mathcal{B}^2}{dr}$$

$$= \left(\beta_\perp \frac{\mathcal{B}_0}{\mathcal{B}} + 1\right) \frac{r_0^4}{r^5} (\mathcal{B}^2 - 1), \tag{5.34}$$

where

$$\beta_{\perp,\parallel} \equiv (4\pi\, p_{\perp,\parallel}/B^2)_{r=r_0}$$

$$= 4\pi\, p_{\parallel,\perp 0} B_{00}^{-2} \mathcal{B}_0^{-2}. \tag{5.35}$$

Appendix H outlines the solution of the differential equation (5.34). The result is

$$V_A(b/B_0)^2 = \text{constant}. \tag{5.36}$$

This solution will be discussed in Sec. 5.4, when the solution provided by the wave analysis has been obtained.

5.3 Solution of the Convective Evolution Problem from a Wave Viewpoint

In this section we carry out the analysis of the convective evolution of large-amplitude Alfvén waves by working directly with the detailed magnetic and velocity vectors which describe the waves.

The nonradial or wave components of the Chew-Goldberger-Low momentum equation, Eq. (4.2), and Maxwell equation, Eq. (4.3), are required. Appendix F shows that the wave part of the momentum equation for the idealized solar wind model can be written

$$\rho(\partial/\partial t + u_0 \partial/\partial r + u_0/r)[u_T \hat{b}(\theta + \delta)]$$

$$= -B_0 b\hat{b}(\theta)\partial(p_\Delta B^{-2})/\partial r$$

$$+ [(1/4\pi) - p_\Delta B^{-2}]B_0(\partial/\partial r + r^{-1})[b\hat{b}(\theta)]. \tag{5.37}$$

Appendix J demonstrates how to obtain the following form for the wave part of the Chew-Goldberger-Low Maxwell equation, Eq. (4.3), in the idealized solar wind model:

$$\partial \hat{b}(\theta)/\partial t = B_0 \partial[u_T \hat{b}(\theta + \delta)]/\partial r$$

$$- [u_0 b \hat{b}(\theta) + B_0 u_T \hat{b}(\theta + \delta)]/r$$

$$- b \hat{b}(\theta)\partial u_0/\partial r - u_0 \partial[b \hat{b}(\theta)]/\partial r . \qquad (5.38)$$

In view of the definition of $\hat{b}(\theta)$ in Eq. (5.4), it follows that

$$\partial \hat{b}(\theta)/\partial\theta = \hat{r} \times \hat{b}(\theta). \qquad (5.39)$$

Using Eq. (5.39) and the space-time dependence of the phase function $\theta(r,t)$ specified by Eq. (5.3), the differentiations in Eq. (5.37) and Eq. (5.38) can now be performed.

The wave part of the momentum equation becomes

$$\rho u_T\left[\dot{\theta} V_A(u_0 + V_A)^{-1} + u_0 \delta'\right]\hat{r} \times \hat{b}(\theta + \delta)$$

$$+ \dot{\theta}(u_0 + V_A)^{-1}\left[(1/4\pi) - p_\Delta B^{-2}\right] B_0 b \hat{r} \times \hat{b}(\theta)$$

$$= -\rho u_0(u_T' + u_T/r)\hat{b}(\theta + \delta)$$

$$+ \left\{(b' + b/r)\left[(1/4\pi) - p_\Delta B^{-2}\right] - b\, d(p_\Delta B^{-2})/dr\right\}B_0 \hat{b}(\theta), \qquad (5.40)$$

where primes denote derivatives with respect to r, and $\dot{\theta}$ is the derivative of the arbitrary function $\theta(\cdot)$ with respect to its argument (or simply the partial derivative of $\theta(r,t)$ with respect to t).

The wave part of the Chew-Goldberger-Low Maxwell equation becomes

$$\dot{\theta} V_A(u_0 + V_A)^{-1} b\hat{r} \times \hat{b}(\theta) + [\dot{\theta}(u_0 + V_A)^{-1} - \delta']B_0 u_T \hat{r} \times \hat{b}(\theta + \delta)$$

$$= B_0(u_T' - u_T/r)\hat{b}(\theta + \delta) - [(u_0' + u_0/r)b + u_0 b']\hat{b}(\theta) . \qquad (5.41)$$

The structures of Eqs. (5.40) and (5.41) are similar. Since $\hat{b}$ is orthogonal to $\hat{r}$, they are vector equations with all terms contained in the plane perpendicular to $\hat{r}$. Since δ is small, the left-hand side of each consists of vectors approximately in the $\hat{r} \times \hat{b}(\theta)$ direction; the right-hand sides are roughly in the $\hat{b}(\theta)$ direction, i.e. perpendicular to the left-hand sides. Thus both sides of the equations must almost vanish. In fact if we set the wave velocity phase lag δ equal to zero, as it is in the uniform plasma situation of Chapter 4, each side of Eqs. (5.40) and (5.41) must vanish identically, giving four scalar equations for the three unknowns V_A, u_T, and b. These four equations are incompatible, i.e., the problem is overspecified. This demonstrates the necessity of including the phase lag $\delta(r)$ in the ansatz, Eqs. (5.5) and (5.6). With the inclusion of δ, Eqs. (5.40) and (5.41) constitute four scalar equations for the four scalar unknowns V_A, u_T, b, and δ, and a consistent solution can be found. The validity of the assumptions used to derive Eqs. (5.40) and (5.41) remains to be verified.

First we show that the δ' terms in Eqs. (5.40) and (5.41) can be neglected for values of the parameters appropriate to the solar wind. In Eq. (5.41), δ' can be neglected if

$$\delta' \ll \dot{\theta}/u_0 . \tag{5.42}$$

It can be dropped from Eq. (5.40) providing

$$\delta' \ll (V_A/u_0)\, \dot{\theta}/u_0 . \tag{5.43}$$

For the solar wind problem, Eq. (5.42) holds if Eq. (5.43) is true, since $V_A < u_0$. Thus, it suffices to demonstrate the validity of Eq. (5.43).

In the solar wind $V_A \sim 50$ km/sec, $u_0 \gtrsim 400$ km/sec, $\dot{\theta} \gtrsim 10^{-3}$ rad/sec, and a characteristic length scale for variations in δ is $R \sim 1$ AU $\sim 10^8$ km.

Thus Eq. (5.43) holds for solar wind parameters if

$$\delta \ll \frac{50}{(400)^2}\, 10^{-3} \times 10^8$$

or

$$\delta \ll 30. \tag{5.44}$$

Equation (5.44) holds in view of Eq. (5.7). We demonstrate below that δ is indeed small, once a formula for δ is obtained. Thus, the δ' terms can be dropped from Eqs. (5.40) and (5.41).

Next we compare the order of a term on the left side of Eq. (5.40) with a term on its right side, for typical solar wind parameters:

$$\frac{\rho\, u_T\, \dot{\theta}\, V_A\, u_0^{-1}}{\rho\, u_0\, u_T'} \sim \frac{R\, \dot{\theta}\, V_A}{u_0^2} \gtrsim \frac{10^8 \times 10^{-3} \times 50}{(600)^2} \approx 14. \tag{5.45}$$

In estimating this ratio we have chosen observed values of the parameters which give the smallest ratio. Thus we have used the smallest observed angular frequency, $\dot{\theta} \approx 10^{-3}$ sec^{-1}, and a large value for the solar wind bulk velocity, $u_0 \approx 600$ km/sec. The ratio is much larger for more typical solar winds. A more refined estimate of the components of Eq. (5.40) is made in Sec. 5.4, where the limits of validity are discussed.

The situation is illustrated in Fig. 9, which shows the relative magnitude of the vector components of Eq. (5.40). When the component of Eq. (5.40) in the $\hat{r} \times \hat{b}(\theta)$ direction is computed, the contribution from each term on the left side is large, but the contributions from right-side terms are small, due to the combined effects of their small size and the order δ projection of the almost orthogonal unit vector $\hat{b}(\theta + \delta)$. On the other hand, if the component of Eq. (5.40) is computed in the $\hat{b}(\theta)$ direction, the important contributions include the right-side terms and the order δ projection of the large $\hat{r} \times \hat{b}(\theta + \delta)$ term on the left side.

Similar arguments apply to Eq. (5.41).

Thus we can solve Eqs. (5.40) and (5.41) by taking components in the $\hat{r} \times \hat{b}(\theta)$ direction, neglecting the right side contributions, and by taking components in the $\hat{b}(\theta)$ direction, keeping all terms.

The $\hat{r} \times \hat{b}(\theta)$ components of Eqs. (5.40) and (5.41) become, respectively,

$$\circ\, u_T\, \dot{\theta}\, V_A(u_0 + V_A)^{-1} + \dot{\theta}(u_0 + V_A)^{-1}[(1/4\pi) - p_\triangle B^{-2}]B_0 b = 0 \tag{5.46}$$

and

$$\dot{\theta}\, V_A(u_0 + V_A)^{-1}\, b + \dot{\theta}(u_0 + V_A)^{-1}\, B_0\, u_T = 0, \tag{5.47}$$

where δ^2 terms have been dropped.

Solved simultaneously, Eqs. (5.46) and (5.47) give the solutions anticipated by the uniform plasma theory of Chapter 4:

$$u_T(r) = - V_A(r)\, b(r)/B_0(r) \tag{5.48}$$

and

$$V_A^{\,2} = \rho^{-1} B_0^{\,2}[(1/4\pi) - p_\triangle B^{-2}] . \tag{5.49}$$

These properties were assumed to hold in the energetic analysis of Sec. 5.2. See Eqs. (5.11) and (5.12).

Resolving Eqs. (5.40) and (5.41) into components in the $\hat{b}(\theta)$ direction, neglecting corrections of order δ^2, we find, respectively,

$$-\rho\, u_T\, \dot{\theta}\, V_A(u_0 + V_A)^{-1}\delta = -\rho\, u_0(u_T' + u_T/r) + \left\{(b' + b/r)[(1/4\pi) - p_\triangle B^{-2}] - b\, d(p_\triangle B^{-2})/dr\right\}B_0 \tag{5.50}$$

and

$$-\dot{\theta}(u_0 + V_A)^{-1}\, B_0\, u_T\, \delta = B_0(u_T' - u_T/r) - (u_0' + u_0/r)b - u_0\, b'. \tag{5.51}$$

The simultaneous solution of Eqs. (5.50) and (5.51) for

$\delta(r)$ and $b(r)$ is straightforward, but somewhat lengthy. The procedure is outlined in Appendix K. The results are

$$V_A(b/B_0)^2 = C\, u_0(u_0 + V_A)^{-2}, \tag{5.52}$$

where C is a constant, and

$$\delta = -(2\, \dot{\theta}\, V_A\, r^2\, b^2)^{-1}\, d[rb(u_0 + V_A)]^2/dr. \tag{5.53}$$

This solution, Eqs. (5.48), (5.49), (5.52) and (5.53), is discussed in the next section, where it is compared with the predictions of the energetic analysis of Sec. 5.2.

5.4 Solutions of the Convective Evolution Problem

A. Comparison of the Results of the Two Methods

The equations of primary interest are those giving the dependence of the plasma parameters and the wave amplitude as functions of r. In the energetic analysis this is Eq. (5.36). In the detailed wave analysis of Sec. 5.3, the solution is Eq. (5.52).

The only assumptions made in deriving Eq. (5.52) were the spherical symmetry of the idealized model and the smallness of δ and δ'. No restriction places limits on the relative magnitudes of u_0 and V_A. Thus, within the approximations of the Chew-Goldberger-Low model, Eq. (5.52) should be accurate regardless of the size of V_A and u_0, providing the assumptions basic to the model and Eqs. (5.7), (5.42) and (5.43) are maintained.

Equation (5.52), alone, does not represent a self-contained solution to the convective evolution problem, because

both b and u_0 remain unknown functions of r, after V_A, ρ, $p_\perp$, and $p_{||}$ have been eliminated via Eqs. (5.48), (5.17), (5.21), and (5.22), respectively. This equation may be combined, e.g., with the parallel part of the momentum equation, Eq. (5.26), in order to obtain solutions $u_0(r)$ and $b(r)$. The complex interrelations among the parameters would necessitate a numerical solution, which has not been attempted. In any case, the problem can be solved quite satisfactorily for the purpose of modeling the solar wind. Since V_A/u_0 is small, and u_0 remains constant to order $(V_A/u_0)^2$ as noted in Sec. 5.2, $b(r)$ is the only unknown in Eq. (5.52). This represents a result of adequate accuracy for the solar wind in view of the already gross approximations included in the idealized model and the lack of precise data from space probes.

In the energetic analysis, Sec. 5.2, terms of order V_A/u_0 are consistently dropped in computing wave quantities and the solution, Eq. (5.36). It has not been possible to carry through the details of the energetic method with V_A/u_0 of arbitrary size as in Sec. 5.3. The reason for this apparent asymmetry between the energetic and wave approaches is not clear. For application to the convective evolution of Alfvén waves in the solar wind, a 10 percent inconsistency in theoretical predictions is quite acceptable. The neglect of effects such as heat flow, wave-particle and wave-wave effects mentioned in Chapter 3 are expected to contribute more serious discrepancies between the present theory and the physical world.

In the limit of large bulk velocity u_0, the factors u_0 and $u_0 + V_A$ in Eq. (5.52) are constants, and the solution obtained by wave analysis is identical to Eq. (5.36) derived from energetic considerations.

Throughout the remainder of Chapter 5 we assume that V_A/u_0 is negligibly small compared to 1, and that u_0 may be treated as a constant.

B. Properties of the Solutions

In the absence of any Alfvén wave perturbation, i.e., $b \equiv 0$, the solution of the idealized solar wind convection model is easily obtained. We find

$$\rho = \rho_0 (r_0/r)^2, \tag{5.54}$$

$$\underset{\sim}{u} = u_0 \hat{r}, \tag{5.55}$$

$$\underset{\sim}{B} = B_{00} (r_0/r)^2 \hat{r}, \tag{5.56}$$

$$p_\perp = p_{\perp 0} (r_0/r)^4, \tag{5.57}$$

and

$$p_{||} = p_{||0} (r_0/r)^2, \tag{5.58}$$

where the subscript refers to the value of the respective parameters at $r = r_0$.

From Eq. (4.16) the Alfvén velocity can be written

$$V_A = \pm (r_0/r) \left\{ \rho_0^{-1} \left[B_{00}^2/4\pi + p_{\perp 0} - p_{||0} (r/r_0)^2 \right] \right\}^{1/2}. \tag{5.59}$$

It is evident that, if $p_{||0}$ is nonzero, the Alfvén velocity becomes imaginary beyond the critical instability

radius r_{cr} given by

$$r_{cr} = r_0 \left[(B_{00}^2/4\pi + p_{\perp 0})/p_{\parallel 0} \right]^{1/2} . \qquad (5.60)$$

The plasma is unstable where $r > r_{cr}$. Far into the Alfvén unstable region V_A approaches the limiting value

$$V_A(r \to \infty) = (- p_{\parallel 0}/\rho_0)^{1/2} . \qquad (5.61)$$

The solution obtained in Secs. 5.2 and 5.3 predicts a strikingly different behavior for the convecting plasma, when Alfvén waves are present. Equations (5.36) and (5.52) show that if a wave is present, regardless of its amplitude, then the solar wind never becomes Alfvén unstable. Even an infinitesimally small wave, providing the approximations used in deriving the solution hold, renders the plasma stable everywhere by adjusting it amplitude in a way that maintains the reality of V_A. In fact, V_A can never reach zero.

In order to show explicitly the functional relation between the wave amplitude b and r, Eqs. (5.36) and (5.52) can be written

$$r^3 b^2 \left\{ 1 + \beta_\perp \left[\frac{1 + (b_0/B_{00})^2}{1 + (r/r_0)^4 (b/B_{00})^2} \right]^{1/2} - \beta_{\parallel} \frac{r^2}{r_0^2} \left[\frac{1 + (b_0/B_{00})^2}{1 + (r/r_0)^4 (b/B_{00})^2} \right]^2 \right\}^{1/2} = \text{const.} \qquad (5.62)$$

In Eq. (5.62), b_0 denotes the wave amplitude at the reference radius r_0, B_{00} is the radial field at r_0, and $\beta_{\parallel}$ and $\beta_\perp$ are defined in Eq. (5.35).

It can be seen by inspection that Eq. (5.62) is merely a polynomial in b, with coefficients depending on r. It turns out to be a polynomial of degree 8 in b^2, and hence numerical solution methods are appropriate. The resulting r dependence of V_A and b for various choices of wave amplitude at the reference radius is shown in Fig. 10 (a), (b), (c) and (d). In each case it is assumed that $p_{\parallel 0} = B_{00}^2/4\pi$ and $p_{\perp 0} = \frac{1}{2} p_{\parallel 0}$. The qualitative behavior is relatively independent of these parameters.

The wave amplitude increases most markedly in the vicinity of the critical instability point where the Alfvén velocity would vanish if the wave were not present. By Eq. (5.60), this critical instability radius is $r_{cr} = \sqrt{3/2}\ r_0$ for the particular choice of reference plasma parameters used in Fig. 10. Figure 10(a) shows an example of relatively large wave amplitude prior to the critical instability radius, and the increase necessary to maintain plasma stability is rather mild. At the other extreme, Fig. 10(d) shows an example in which the wave amplitude is initially very small. It isn't able to grow comparable to B_0 before the critical instability radius is reached. In order to stop the Alfvén velocity's plummet toward zero, b/B_0 must increase abruptly and markedly at r_{cr}.

In all cases V_A approaches zero as r increases. The ratio $(b/B_0)^2$ is proportional to r as $r \to \infty$, and Eq. (5.52) shows that V_A goes to zero as r^{-1} in this limit.

Since B_0 and ρ each vary as r^{-2} in the idealized model, Eq. (5.36) can be written in the form

$$4\pi r^2 \; V_A \; b^2/(4\pi\rho) \; = \; F,$$

where F is a constant. This expression is amenable to a physical interpretation. The quantity $4\pi r^2$ is the area of the spherical surface of radius r with center at the sun. The formula $V_A b^2/4\pi$ represents the Poynting energy flux density of the Alfvén wave as viewed in a frame moving with the local plasma bulk velocity. Thus Eq. (5.36) states that the flux F of Alfvén wave energy, viewed in a frame tied to the convecting solar wind and normalized to the local plasma density, is the same through every spherical surface centered at the sun.

This is a relatively simple conclusion when compared to the involved analyses of Secs. 5.2 and 5.3, which produced it. It suggests the existence of a general principle in operation for convecting waves in a nonuniform medium, the work of Chapter 5 providing a particular example of its application. What this more general theorem might be is unknown. Attempts to obtain Eq. (5.36) by simpler methods have failed. It is not known whether other types of convecting waves exhibit an analogous property.

C. Ranges of Validity of the Convective Evolution Analysis

The parameters in the idealized solar wind convection model are limited by restrictions which are fundamental to the validity of the Chew-Goldberger-Low equations used to describe the plasma and fields and also by requirements imposed during the analysis of the problem. These validity limits are examined below.

The fluid nature of the Chew-Goldberger-Low model requires that the average ion gyroradius r_g be small compared to distances over which plasma variables change appreciably. This places a restriction on the constant-amplitude source of propagating waves: the waves cannot be too sharply curved. In terms of the arbitrary phase function θ, this requires

$$\dot{\theta} \; \ll \; (u_0 + V_A)/r_g. \tag{5.63}$$

When inequality (5.63) is satisfied the rotation of the magnetic field and velocity vectors about $\hat{r}$ takes place over distances large compared to r_g, and the fluid model should be accurate.

Throughout most of the radial range of convective evolution, the characteristic length for amplitude changes is r. In order that such changes be small over a distance of order r_g, we require

$$r \; \gg \; r_g. \tag{5.64}$$

This also guarantees that the directional changes in the field due to the spherical geometry of the model are small over distances like r_g. Inequality (5.64) is easily satisfied in

the physical solar wind.

More severe restrictions are imposed on the parameters when effects at the critical instability radius r_{cr} are considered. Figure 10 shows clearly that as the wave amplitude is made smaller, the sudden wave growth necessary at r_{cr} to maintain plasma stability occurs over shorter length scales. Eventually, when the wave amplitude is too small inside r_{cr}, Eq. (5.52) requires that b change over distances small compared to r_g at r_{cr}, and the Chew-Goldberger-Low model breaks down.

To quantify these remarks, an estimate is obtained in Appendix L for the maximum rate of change of the quantity h, defined by

$$h(r) \equiv b(r)/B_0(r), \tag{5.65}$$

in terms of the plasma parameters h, $\beta_{\parallel}$, and $\beta_{\perp}$ at any reference radius r_0 interior to the Alfvén critical instability radius r_{cr}. Assuming $h(r_0) \ll 1$, which is the most dangerous limit with regard to producing rapid changes in h, we find

$$(\partial h/\partial r)_{max} \approx r_0^{-1}\left[1 + \beta_{\perp} - \beta_{\parallel}\right]^{-1/6} \times \left[h(r_0)(1 + \beta_{\perp})/\beta_{\parallel}\right]^{-2/3}. \tag{5.66}$$

Validity of the fluid theory requires

$$(\partial h/\partial r)^{-1} \gg r_g \tag{5.67}$$

to hold everywhere.

In terms of the wave amplitude ratio at r_0, we demand that

$$h(r_0) \gg (r_g/r_0)^{3/2}\, \beta_{\parallel}(1 + \beta_{\perp})^{-1}(1 + \beta_{\perp} - \beta_{\parallel})^{-1/4}. \tag{5.68}$$

This represents a very weak restriction on the wave amplitude when solar wind parameters are used.

Throughout the analysis of Secs. (5.2) and (5.3), it is assumed that the phase angle δ between the wave components of $\underset{\sim}{B}$ and $\underset{\sim}{u}$ is small compared to 1. An estimate of δ can be obtained from Eq. (5.53), which can be expressed in the form

$$\delta \cong -u_0^2(\dot{\theta}\, V_A)^{-1}\, \partial(\ell n\, h - \ell n\, r)/\partial r. \tag{5.69}$$

This phase lag is largest where h changes most rapidly and V_A is small, which occurs near the critical instability radius r_{cr}. The worst case occurs when h is small inside r_{cr}. Using Eq. (L.11) from Appendix L, and neglecting the $\ell n\, r$ term in Eq. (5.69), which varies slowly, we find

$$\delta_{max} \approx -\left[u_0^2(\dot{\theta}\, V_A\, r\, h^2)^{-1}\right]_{r \cong r_{cr}}. \tag{5.70}$$

In view of Eqs. (5.36) or (5.52), $V_A\, h^2$ is constant during the convective evolution. Thus we write

$$\delta_{max} \approx -u_0^2\left[\dot{\theta}\, r_{cr}\, V_A(r)\, h^2(r)\right]^{-1}. \tag{5.71}$$

The assumption that δ be small compared to 1 requires

$$h^2(r) \gg u_0^2 \left[\dot{\theta}\, r_{cr}\, V_A(r)\right]^{-1} . \tag{5.72}$$

Note that in this instance a large bulk velocity is detrimental. If u_0 is too large, the plasma convects out from the sun so rapidly that the nonradial parts of $\underset{\sim}{u}$ and $\underset{\sim}{B}$ cannot keep themselves parallel or antiparallel, as they always are in a uniform plasma and field.

In Sec. 5.3 we argue that the ratio of the left side of Eq. (5.40) to its right side is large. In view of Eqs. (5.45) and (5.48), this ratio can be written

$$L/R \approx \dot{\theta}\, V_A\, h/(u_0^2\, h'). \tag{5.73}$$

The worst case corresponds to h' large and V_A small, since both tend to make the ratio small. Thus, in view of Eq. (L.11), we have

$$L/R \gtrsim \left(\dot{\theta}\, r\, V_A\, h^2/u_0^2\right)_{r \cong r_{cr}} . \tag{5.74}$$

Since we have assumed that this ratio is large compared to 1, we again obtain restriction (5.72) on the minimum allowed wave amplitude.

The last assumption used in the analysis is that δ' is small, inequality (5.43). A more refined estimate of δ' follows from Eq. (5.69) and $d/dr \sim h'/h$. We find

$$\delta' \sim u_0^2 (h')^2 \left(\dot{\theta}\, V_A\, h^2\right)^{-1} . \tag{5.75}$$

Using Eq. (L.11) to obtain the largest value of δ', we have

$$\delta' \lesssim \left[u_0^2 (\dot{\theta}\, V_A\, h^4\, r^2)^{-1}\right]_{r \cong r_{cr}} . \tag{5.76}$$

Substitution of Eq. (5.76) into inequality (5.43) gives

$$u_0^2 (\dot{\theta}\, r\, V_A\, h^2)^{-1} \ll 1 . \tag{5.77}$$

As noted above, $V_A\, h^2$ is a constant, and inequality (5.43) holds providing inequality (5.72) is satisfied.

Summarizing these limitations, we find that the convective evolution analysis of Secs. 5.2 and 5.3 is valid when inequalities (5.63), (5.64), (5.68), and (5.72) hold.

At 1 AU the relevant parameters are typically

$$10^{-3}\ \text{Hz} \lesssim \dot{\theta} \lesssim \tfrac{1}{2}\ \text{Hz} ,$$

$$u_0 \sim 400\ \text{km/sec},$$

$$V_A \sim 50\ \text{km/sec},$$

$$r_g \sim 100\ \text{km},$$

$$r_{cr} \sim 10^8\ \text{km},$$

and

$$\beta_\perp,\ \beta_{||} \sim 1.$$

For these values the validity relations become

$$\dot{\theta} \ll 4\ \text{Hz} , \tag{5.63'}$$

$$10^8\ \text{km} \gg 10^2\ \text{km}, \tag{5.64'}$$

$$h \gg 10^{-12}, \tag{5.68'}$$

and

$$h^2 \gg 3 \times 10^{-5} \text{ Hz}/\dot{\theta}. \qquad (5.72')$$

For high frequency Alfvén perturbations, the last inequality requires $h \gg 10^{-4}$. For the lowest observed frequencies, $\dot{\theta} \sim 10^{-3}$ Hz, Eq. (5.72') requires $h^2 \gg 0.03$. Since $h \sim 1$ in the disturbed, high velocity regions where Alfvén waves predominate, these restrictions are easily satisfied in the physical solar wind.

D. Comparison of the Analytical Results with Observations

The theory of Secs. 5.2 and 5.3 is remarkable in showing that the Chew-Goldberger-Low model predicts a stable plasma in spite of the adiabatic expansion, which tends to produce the Alfvén instability condition, and in spite of the neglect of the wave-wave interactions which are usually invoked to quench such instabilities.

Due primarily to the neglect of heat flow, and secondarily to effects such as the single species analysis, the assumption of spherical symmetry, and the neglect of the spiral velocity sector structure of the solar wind, the analysis is not an accurate solution of the radial dependence of wave amplitude in the solar wind.

The outward propagating Alfvén waves are probably created by magnetic turbulence in the coronal region of the sun, which settles down within a few solar radii to the locally constant-amplitude waves observed at 1 AU.[19] The Alfvén critical instability point predicted by the Chew-Goldberger-Low model for reasonable estimates of the pressures and fields at the sun occurs much closer to the sun than 1 AU. Consequently, the convective evolution analysis predicts nearly zero Alfvén velocity at 1 AU, i.e., much smaller than the 50 km/sec observed. This theory also predicts that the wave amplitude should be much larger than observed. For example, assume that $p_{\parallel} = p_{\perp} = B_0^2/4\pi$ at two solar radii or 0.01 AU from the sun's center. The Alfvén critical instability point is then $r_{cr} \approx 0.014$ AU. When Alfvén waves are present in the solar wind, the ratio b/B_0 varies as $r^{1/2}$ beyond r_{cr}, as shown in Sec. 5.4B. Consequently, the convective evolution theory predicts $b/B_0 \sim 8$ at 1 AU. Observations indicate that this ratio is more typically unity.[19]

Equally suspicious results follow theoretically if we substitute the observed quantities at 1 AU into Eq. (5.52) and solve for them at the sun. We find $p_{\parallel}/p_{\perp} \sim 10^{-4}$ and $h \sim 0.1$ at the solar corona. Both estimates are unreasonably small in view of the powerful turbulent forces operative there, tending to isotropize pressures and field fluctuations.

This breakdown of the model over distances like 1 AU may be due to electron heat conduction effects, which are neglected in the theory. The electrons are relatively free to move along the magnetic field lines, and their large thermal velocities permit them through heat conduction to maintain temperatures at 1 AU at a much higher level than the simple adiabatic theory predicts. Consequently, the Alfvén critical instability point,

where parallel pressure exceeds the perpendicular and field pressures, is pushed out farther from the sun, or eliminated altogether. Scarf[35] notes that thermal conduction and heat transport should produce large effects even in the dilute plasma at the Earth.

Further discussion of heat flow effects, including estimates of the thermal transport involved, appears in Appendix M.

Hollweg has "semi-self-consistently" treated the effect of solar rotation on the expected proton anisotropy in the solar wind.[50] He neglects wave processes entirely and uses only the two adiabatic relations, Eqs. (4.4) and (4.5). If the protons are assumed isotropic at 10 $R_\odot$, these equations predict that the proton anisotropy at 1 AU is $p_{\parallel}/p_{\perp} \approx 75$, when the field is radial. When the spiral geometry arising from solar rotation is accounted for, $|\underset{\sim}{B}|$ increases and consequently $p_{\parallel}/p_{\perp} \approx 16$ at 1 AU. This anisotropy is still much larger than observed, but the improvement is obvious. The isotropy-producing influence of Alfvén waves, in conjunction with the spiral geometry, may provide a more satisfactory explanation for the observed proton anisotropy.

C. F. Kennel suggests that wave effects may also be important in postponing the occurrence of the Alfvén critical instability radius.[51] For example, the electrons may produce high frequency waves which affect the ion distribution; instabilities with frequencies somewhat below the ion gyrofrequency may

tend to reduce the ion pressure anisotropy and thus cause the firehose instability to occur at a larger radius than simple Chew-Goldberger-Low theory predicts.

The theory which ultimately describes the evolution of Alfvén waves in the convecting solar wind must include the effects of the slowly changing background on these waves. The expansion must locally affect the proton anisotropy regardless of how severely counter-effects limit this tendency. The wave amplitude variations also produce anisotropy changes. A complete theoretical treatment of Alfvén wave evolution must acknowledge the consequences derived in the present simplified model, together with thermal conduction and whatever other effects prove important.

E. Generalizations and Further Applications of the Convective Evolution Analysis

Although the analyses of Secs. 5.2 and 5.3 are strongly bound within the spherically symmetric model, the resulting constant of the wave evolution, Eq. (5.36) or (5.52), may have a much wider validity.

Consider a more general situation, such as the actual configuration of the solar wind, in which a plasma convects in an arbitrary, but slowly varying geometry. Suppose that it carries along Alfvén waves of the type developed in Sec. 4.2A, which propagate according to the theory of Chapter 4 relative to the moving plasma. A wave crest finds itself in a medium whose properties ρ, $p_{\parallel}$, $p_{\perp}$, $\underset{\sim}{B}_0$, and thus V_A, slowly vary in

some arbitrary fashion dictated by the geometry and the wave itself. In the idealized spherically symmetric model the wave at each point is only aware of the local environment, and its amplitude is governed by Eq. (5.52). It seems reasonable that in the more general situation the wave's development is governed by the local plasma properties, and again should obey an analogue of Eq. (5.52). What this analogue might be is difficult to say. In the idealized model, we find

$$\rho \propto (u_0 r^2)^{-1} \tag{5.78}$$

and

$$B_0 \propto r^{-2} . \tag{5.79}$$

Since $u_0 \cong$ constant for the ranges of parameters we consider, both ρ and B_0 have the same r dependence. Thus the factor B_0^2 in Eq. (5.36) can equally well be written $B_0^{2-\nu} \rho^{\nu}$, for any constant ν. For example, Eq. (5.52) can be written, including the more accurate u_0 dependence of ρ, as

$$B_0^{-1} \rho^{-1} V_A b^2 = C \left[u_0/(u_0 + V_A) \right]^2 . \tag{5.80}$$

Unfortunately, this ambiguity in the solution, i.e. whether B_0, ρ, or r^{-2} should appear in the left side of Eq. (5.36), (5.52), or (5.80), prevents its immediate application to more general solar wind geometries. In the real solar wind, ρ varies as r^{-2}, but B_0 does not, due to solar rotation and the consequent spiral field. Thus, if Eq. (5.36) is used to derive the relation between b and r, the answer depends on

whether ρ or B_0 appears as a factor in the left side.

As mentioned earlier in this chapter, the signs of u_0 and V_A are not necessarily both positive for the validity of the analysis. The treatment is aimed toward the solar wind configuration, in which the Alfvén waves are propagating outward in a plasma which is itself flowing away from the sun. The mathematical analysis is the same if the outward convecting plasma supports inward propagating waves, or vice versa.

The convective evolution of Alfvén waves may have applications outside the solar system. Kulsrud[31,32] has speculated that Alfvén waves are an important particle accelerating mechanism in interstellar space and has considered how they might be produced there. The effects of convection on such waves would form an important part of a complete theory.

5.5 Concluding Remarks

In the uniform plasma problem discussed in Chapter 4, the exact solution provides more insight into the unstable Alfvén mode's behavior than does quasilinear theory. In quasilinear analysis the growth of unstable waves produces corrections to $p_\perp$ and $p_\parallel$ which tend to lessen the instability and thus, at some point, quenches the waves' growth. The exact analysis shows quite clearly that a small-amplitude circularly-polarized wave in an unstable plasma grows exponentially for a while, then less rapidly, eventually overshooting the Alfvén stability point.[52] Finding itself in a momentarily stable plasma, it reaches a maximum amplitude and decays, ultimately exponentially with time,

toward its initial value.

The nonlinear analysis of Chapter 5, which is a large-amplitude theory like that presented in Chapter 4, similarly yields insights into the driven instability problem that may prove more useful than the information a quasilinear method could provide.

A quasilinear treatment of the convective evolution problem would solve for the linear behavior of the wave, and use the resulting linearized wave to compute higher order corrections to the distribution function and other plasma parameters. The wave could be followed in this manner from the source to the Alfvén critical radius r_{cr}, where V_A first vanishes. Just beyond this point, the Alfvén velocity is imaginary in the linear theory, the wave is unstable, and in the quasilinear theory, the resulting exponential wave growth reacts back on the plasma in a manner which makes the plasma less unstable.

The rigorous analysis of Secs. 5.2 and 5.3 shows that wave growth already occurs as the condition $V_A = 0$ is being approached. In other words, instead of waiting for the plasma to become unstable and then growing to an amplitude which renders the plasma stable, the wave grows before V_A reaches zero in a way that keeps V_A always real and Eq. (5.36) or (5.52) satisfied.

This is probably an important property of any driven instability problem in which the driving mechanism changes slowly compared to wave periods or growth rates. For example, in the

magnetosphere, when excess electrons are injected, electron cyclotron waves are believed to become unstable, grow, and cause pitch angle diffusion of other electrons, which then scatter into the loss cone and precipitate into the atmosphere. If the injection time is short and the electrons rapidly inserted, this picture is probably correct, i.e., plasma instability precedes wave growth. However, if the injection process is adiabatic on the time scale characteristic of the whistler modes, the whistler amplitude may increase slowly, maintaining an amplitude which keeps the plasma always stable.

Since rigorous solutions of driven instability problems are practically nonexistent, it is not possible to do more than speculate in this way on what properties such processes might share. Moreover, the implications of the analytical results of Chapter 5 are not fully understood at the present time.

Whatever approach is used to determine it, the effect of the expanding plasma on the waves present in it must be included in a theoretical model of the physical solar wind.

Scarf has remarked,[35] "In fact, the observed values of $(T_{\parallel}/T_{\perp})_{\pm}$ are so much smaller than predicted by strict conservation of [the adiabatic invariants] μ and ν that it is necessary to invoke some type of wave-particle interaction to account for the observed near isotropy at 1 AU."

The analytic solution (5.36) or (5.52) shows one way in which the presence of waves can produce the required isotropy.

Since $p_\perp \sim \rho B$ and $p_\parallel \sim \rho^3 B^{-2}$ are the adiabatic laws, wave growth tends to increase $p_\perp$ and decrease $p_\parallel$, thus reducing the pressure anisotropy.

The idealized models treated in this paper represent imperfect approximations to reality, but the effects derived in the simplified case must appear in a complete theoretical picture of interplanetary processes.

APPENDIX A: QUASILINEAR THEORY OF THE FIREHOSE INSTABILITY IN THE CHEW-GOLDBERGER-LOW MODEL

We outline a derivation from the Chew-Goldberger-Low equations of the quasilinear results obtained by Davidson and Völk.[24] It is not surprising that identical results follow, because the assumption of diagonal pressure tensor and neglect of the heat-flow tensor explicit in their work are used in deriving the Chew-Goldberger-Low equations. It is useful, however, to point out an important difference between the definition of the average pressures in the two analyses. Note, also, that in our analysis the ensemble averages implied by Davidson and Völk are not required: it suffices to consider only spatially averaged quantities.

We assume a uniform, infinitesimally perturbed plasma in a uniform magnetic field $\underset{\sim}{B}_0$. We view all Chew-Goldberger-Low variables as consisting of a space-average part, which may depend on time, and a fluctuating part: $\rho(\underset{\sim}{x},t) = \langle\rho\rangle(t) + \delta\rho(\underset{\sim}{x},t)$, etc. The hexagonal brackets denote spatial averaging.

Taking the space-average of the Chew-Goldberger-Low Eqs. (4.1) through (4.3), we find

$$\langle\rho\rangle(t) = \text{constant} = \rho, \tag{A.1}$$

$$\langle\underset{\sim}{u}\rangle(t) = \text{constant} = 0, \tag{A.2}$$

$$\langle\underset{\sim}{B}\rangle(t) = \text{constant} = \underset{\sim}{B}_0. \tag{A.3}$$

When the Chew-Goldberger-Low Eqs. (4.1) through (4.8) are linearized in fluctuations about these spatial averages and the

instable Alfvén wave characteristics are assumed, the usual linearly polarized firehose waves follow. To first order in the perturbation we find

$$\delta\rho = 0, \tag{A.4}$$

$$p_\perp = \langle p_\perp \rangle(t), \tag{A.5}$$

$$p_{\parallel} = \langle p_{\parallel} \rangle(t), \tag{A.6}$$

$$\delta\underset{\sim}{B}(\underset{\sim}{k},t) = \delta\underset{\sim}{B}(\underset{\sim}{k},0)\, e^{\gamma(\underset{\sim}{k},t)t}, \tag{A.7}$$

$$\delta\underset{\sim}{u}(\underset{\sim}{k},t) = -i\,\gamma(\underset{\sim}{k},t)(\underset{\sim}{k}\cdot\underset{\sim}{B}_0)^{-1}\,\delta\underset{\sim}{B}(\underset{\sim}{k},t), \tag{A.8}$$

$$\gamma(\underset{\sim}{k},t) = \pm(\underset{\sim}{k}\cdot\hat{\underset{\sim}{B}}_0)[(\langle p_\Delta \rangle(t) - B_0^{\,2}/4\pi)/\rho]^{\frac{1}{2}}. \tag{A.9}$$

We assume that the firehose instability criterion holds so that the growth rate $\gamma(\underset{\sim}{k},t)$ is real. The field fluctuation $\delta\underset{\sim}{B}$ is perpendicular to $\underset{\sim}{k}$ and $\underset{\sim}{B}_0$, a characteristic of Alfvén waves.

The average pressures are constant to first order; to calculate their second-order evolution in time it suffices to carry the two adiabatic equations (4.4) and (4.5) to second order in the perturbation and space average the result. We find

$$\partial\langle p_\perp \rangle/\partial t = (\langle p_\perp \rangle/B_0^{\,2}) \int d^3k\, \gamma(\underset{\sim}{k},t)\, \psi(\underset{\sim}{k},t), \tag{A.10}$$

$$\partial\langle p_{\parallel} \rangle/\partial t = -2(\langle p_{\parallel} \rangle/B_0^{\,2} \int d^3k\, \gamma(\underset{\sim}{k},t)\, \psi(\underset{\sim}{k},t), \tag{A.11}$$

where the magnetic field spectral density ψ is defined by

$$\psi(\underset{\sim}{k},t)\,\delta(\underset{\sim}{k}+\underset{\sim}{k}') \equiv \langle \delta\underset{\sim}{B}(\underset{\sim}{k},t)\cdot\delta\underset{\sim}{B}(\underset{\sim}{k}',t)\rangle \tag{A.12}$$

and satisfies

$$\partial\psi(\underset{\sim}{k},t)/\partial t = 2\gamma(\underset{\sim}{k},t)\,\psi(\underset{\sim}{k},t). \tag{A.13}$$

In order to compare the results (A.10) through (A.13) with those of Davidson and Völk, we note that $p_\perp$, which appears in the Chew-Goldberger-Low equations, is the pressure perpendicular to the local magnetic field $\underset{\sim}{B} = \underset{\sim}{B}_0 + \delta\underset{\sim}{B}$, whereas the quantity $P_\perp$, which is used in the earlier work, is the pressure perpendicular to $\underset{\sim}{B}_0$. Similar remarks apply to $p_{\parallel}$ and $P_{\parallel}$. Thus we have

$$\langle p_{\parallel} \rangle \equiv \langle \underset{\approx}{p} : \hat{\underset{\sim}{B}}\hat{\underset{\sim}{B}} \rangle, \tag{A.14}$$

$$\langle p_\perp \rangle \equiv \tfrac{1}{2}\langle \underset{\approx}{p} : (\underset{\approx}{I} - \hat{\underset{\sim}{B}}\hat{\underset{\sim}{B}})\rangle, \tag{A.15}$$

$$\langle P_{\parallel} \rangle \equiv \langle \underset{\approx}{p} : \hat{\underset{\sim}{B}}_0\hat{\underset{\sim}{B}}_0 \rangle, \tag{A.16}$$

$$\langle P_\perp \rangle \equiv \tfrac{1}{2}\langle \underset{\approx}{p} : (\underset{\approx}{I} - \hat{\underset{\sim}{B}}_0\hat{\underset{\sim}{B}}_0)\rangle. \tag{A.17}$$

To second order it follows that

$$\langle P_\perp \rangle = \langle p_\perp \rangle + (\langle p_\Delta \rangle/2B_0^{\,2}) \int d^3k\, \psi(\underset{\sim}{k},t), \tag{A.18}$$

$$\langle P_{\parallel} \rangle = \langle p_{\parallel} \rangle - (\langle p_\Delta \rangle/B_0^{\,2}) \int d^3k\, \psi(\underset{\sim}{k},t). \tag{A.19}$$

Note that $\langle p_\perp \rangle - \langle P_\perp \rangle$ is a second-order quantity, and similarly for $\langle p_{\parallel} \rangle - \langle P_{\parallel} \rangle$. Thus to the required accuracy, $\langle p_\Delta \rangle(t)$ in Eq. (A.9) may be replaced by $\langle P_\Delta \rangle(t)$.[53]

Taking the time derivative of (A.18) and (A.19), we have

$$\partial\langle P_\perp\rangle/\partial t = (\langle P_\parallel\rangle/B_0^2)\int d^3k\,\gamma(\underset{\sim}{k},t)\,\psi(\underset{\sim}{k},t), \tag{A.20}$$

$$\partial\langle P_\parallel\rangle/\partial t = -[(4\langle P_\parallel\rangle - 2\langle P_\perp\rangle)/B_0^2]\int d^3k\,\gamma(\underset{\sim}{k},t)\,\psi(\underset{\sim}{k},t). \tag{A.21}$$

Equations (A.9), (A.12), (A.13), (A.20), and (A.21) are identical to Eqs. (4.46) through (4.50) obtained by Davidson and Völk. Finite gyroradius effects have been ignored here and should be included in a more complete treatment.

APPENDIX B: GUIDING-CENTER EQUATIONS FOR THE PARALLEL ALFVÉN WAVE

We start with the guiding-center equations in the form obtained by Kulsrud.[23] This system, which Kulsrud terms the "Adiabatic Equations," is

$$\partial\rho/\partial t + \nabla\cdot(\rho\underset{\sim}{u}) = 0, \tag{B.1}$$

$$\rho d\underset{\sim}{u}/dt = -\nabla\cdot\underset{\approx}{p} + (\nabla\times\underset{\sim}{B})\times\underset{\sim}{B}/4\pi, \tag{B.2}$$

$$\underset{\approx}{p} = p_\parallel\hat{B}\hat{B} + p_\perp(\underset{\approx}{I} - \hat{B}\hat{B}), \tag{B.3}$$

$$p_\parallel = \sum m\int F_0(q - u_\parallel)^2\,2\pi\,dq\,dw, \tag{B.4}$$

$$p_\perp = \sum m\int F_0\,w\,2\pi\,dq\,dw, \tag{B.5}$$

$$\partial F_0/\partial t + (\underset{\sim}{\alpha} + q\hat{B})\cdot\nabla F_0 + wW\partial F_0/\partial w + Q\partial F_0/\partial q = 0, \tag{B.6}$$

$$W \equiv \hat{B}\hat{B} : \nabla\underset{\sim}{\alpha} - \nabla\cdot\underset{\sim}{\alpha} - q\nabla\cdot\hat{B}, \tag{B.7}$$

$$Q \equiv \underset{\sim}{\alpha}\cdot\partial\hat{B}/\partial t + \underset{\sim}{\alpha}\underset{\sim}{\alpha} : \nabla\hat{B} + q\underset{\sim}{\alpha}\hat{B} : \nabla\hat{B} + w\nabla\cdot\hat{B} + eE_\parallel/m, \tag{B.8}$$

$$\underset{\sim}{\alpha} \equiv \underset{\sim}{u} - \underset{\sim}{u}\cdot\hat{B}\hat{B}, \tag{B.9}$$

$$\nabla\cdot\underset{\sim}{B} = 0, \tag{B.10}$$

$$\partial\underset{\sim}{B}/\partial t = \nabla\times(\underset{\sim}{u}\times\underset{\sim}{B}), \tag{B.11}$$

$$\sum e\int F_0\,dq\,dw = 0, \tag{B.12}$$

$$\sum e\int F_0\,q\,dq\,dw = 0, \tag{B.13}$$

$$E_{||} = \sum (e/m)\, \hat{B}\cdot(\nabla\cdot\underset{\approx}{p})/(\sum N e^2/m), \tag{B.14}$$

$$w \equiv \tfrac{1}{2}(\underset{\sim}{v} - \underset{\sim}{u})_{\perp}^2, \tag{B.15}$$

$$q = v_{||}. \tag{B.16}$$

In these equations the notation of the Chew-Goldberger-Low model, Eqs. (4.1) through (4.8), has been used where applicable; the particle distribution function F_0 depends on the particle velocity $\underset{\sim}{v}$ through q and w; parallel and perpendicular refer to the direction of the local magnetic field $\underset{\sim}{B}$; $E_{||}$ is the parallel electric field component; and the summations in Eqs. (B.4) through (B.14) are over particle species.

It is convenient to simplify Eqs. (B.7) and (B.8) by using (B.9) to eliminate $\underset{\sim}{\alpha}$ in favor of the fluid velocity $\underset{\sim}{u}$. We find

$$W = \hat{\hat{B}}\hat{\hat{B}} : \nabla\underset{\sim}{u} - \nabla\cdot\underset{\sim}{u} - q\nabla\cdot\hat{B}, \tag{B.17}$$

$$Q = \underset{\sim}{u}\cdot\partial\hat{B}/\partial t + [\underset{\sim}{u}\underset{\sim}{u} + (q - \underset{\sim}{u}\cdot\hat{B})\underset{\sim}{u}\hat{B}] : \nabla\hat{B} + w\nabla\cdot\hat{B} + eE_{||}/m. \tag{B.18}$$

We consider Alfvén waves having properties (4.9) and use these characteristics to simplify (B.1) through (B.18).

Equations (B.1) and (B.10) are trivially satisfied.

Equations (B.2) and (B.3) reduce to

$$\rho\partial\underset{\sim}{u}/\partial t = -[p_{\Delta} - B^2/4\pi]\, B^{-2}\, B_0\partial\underset{\sim}{b}/\partial z. \tag{B.19}$$

Equation (B.11) becomes

$$\partial\underset{\sim}{b}/\partial t = B_0\, \partial\underset{\sim}{u}/\partial z. \tag{B.20}$$

The wave equation (4.14) is readily obtained from (B.19) and (B.20).

Equation (B.14) gives

$$E_{||} = 0. \tag{B.21}$$

Finally, Eqs. (B.17) and (B.18) simplify to

$$W = \tfrac{1}{2} B^{-2}\, \partial B^2/\partial t = \dot{B}/B \tag{B.22}$$

and

$$Q = -(\underset{\sim}{u}\cdot\underset{\sim}{b}\,\dot{B}/B^2) - \tfrac{1}{2}\rho(q - \underset{\sim}{u}\cdot\hat{B})(p_{\Delta} - B^2/4\pi)^{-1}\, \partial u^2/\partial t. \tag{B.23}$$

We assume a bi-Maxwellian distribution function:

$$F_0(w,q,t) = C\, p_{\perp}^{-1}\, p_{||}^{-\frac{1}{2}} \exp[-\rho w/p_{\perp} - \rho(q - u_{||})^2/2p_{||}]. \tag{B.24}$$

The appropriate time dependence of the normalization factor is included in Eq. (B.24). With this choice, Eqs. (B.4) and (B.5) give the appropriate pressures. The quasineutrality condition (B.12) holds for all times if it is true initially, and Eq. (B.13) requires that the fluid velocity be the same for electrons and ions, $u_{||}^{e} = u_{||}^{i}$. Equations (B.6), (B.22), (B.23), and (B.24) reduce to

$$[-\dot{p}_{\perp}/p_{\perp} - \tfrac{1}{2}\dot{p}_{||}/p_{||} + \rho w\dot{p}_{\perp}/p_{\perp}^2 + \tfrac{1}{2}\rho(q-u_{||})^2\, \dot{p}_{||}/p_{||}^2 - w(\dot{B}/B)\rho/p_{\perp}$$

$$+ [(\underset{\sim}{u}\cdot\underset{\sim}{b})\dot{B}/B^2 + \tfrac{1}{2}\rho(q - u_{||})(p_{\Delta} - B^2/4\pi)^{-1}\, \partial u^2/\partial t]\, \rho(q - u_{||})/p_{||}]F_0$$

$$= 0. \tag{B.25}$$

Since F_0 is never zero, and since $(q - u_{||})$ and w are independent variables, the coefficients of w, 1, $(q - u_{||})$, and $(q - u_{||})^2$ in the curly brace of Eq. (B.25) must vanish:

$$\dot{p}_\perp/p_\perp - \dot{B}/B = 0, \tag{B.26}$$

$$\dot{p}_\perp/p_\perp + \frac{1}{2}\dot{p}_{||}/p_{||} = 0, \tag{B.27}$$

$$(\underset{\sim}{u}\cdot\underset{\sim}{b})\dot{B} = 0, \tag{B.28}$$

$$\dot{p}_{||}/p_{||} + \rho(p_\Delta - B^2/4\pi)^{-1}\,\partial u^2/\partial t = 0. \tag{B.29}$$

Equations (B.26) and (B.27) give

$$p_\perp(t)/p_\perp(0) = B(t)/B(0) \tag{B.30}$$

and

$$p_{||}(t)/p_{||}(0) = B^2(0)/B^2(t). \tag{B.31}$$

Thus for the Alfvén modes under consideration and for a bi-Maxwellian particle distribution, the guiding-center equations reduce to Eqs. (B.19) through (B.21) and (B.28) through (B.31). Equations (4.39) through (4.43) and (4.45) are equivalent to Eqs. (B.21), (B.20), (B.19), (B.30), (B.31), and (B.28), respectively. Equation (4.44) follows from Eq. (B.29) when $\dot{p}_{||}$ is eliminated by means of Eq. (B.31).

APPENDIX C: DERIVATION OF THE ENERGY FLUX VECTOR $\underset{\sim}{S}$ IN THE CHEW-GOLDBERGER-LOW MODEL

The distribution function used in the definition of the energy flux vector $\underset{\sim}{S}$, Eq. (5.16), must describe a plasma which possesses a local fluid velocity $\underset{\sim}{u}$ and is locally anisotropic in pressure and temperature. In view of the guiding-center theory of Chapter 4, an appropriate choice would be to make f bi-Maxwellian in the particle velocities. The theory of Chapter 5 has not been carried out using the guiding-center equations, and the Chew-Goldberger-Low model used there does not require the choice of an explicit particle distribution. Thus f is simply assumed to have the properties basic to the double adiabatic model:[1]

$$\sum_{e,i} \int m\, f\, d^3v \equiv \rho(\underset{\sim}{r}, t), \tag{C.1}$$

$$\rho^{-1} \sum_{e,i} \int m\, \underset{\sim}{v}\, f\, d^3v \equiv \underset{\sim}{u}(\underset{\sim}{r}, t), \tag{C.2}$$

$$\sum_{e,i} \int m(\underset{\sim}{v} - \underset{\sim}{u})(\underset{\sim}{v} - \underset{\sim}{u})\, f\, d^3v \equiv p_\perp \underset{\approx}{I} + p_\Delta \hat{B}\hat{B}, \tag{C.3}$$

$$\sum_{e,i} \int \frac{1}{2} m\, |\underset{\sim}{v} - \underset{\sim}{u}|^2 (\underset{\sim}{v} - \underset{\sim}{u})\, f\, d^3v \equiv \underset{\sim}{Q}, \tag{C.4}$$

and

$$\nabla \cdot \underset{\sim}{Q} = 0. \tag{C.5}$$

In these equations, parallel and perpendicular notations refer to the local, total magnetic field direction; $\underset{\sim}{Q}$ is the contraction of the third rank heat flow tensor over two of its indices. The vanishing of the divergence of the heat flow tensor, basic to the Chew-Goldberger-Low model, is provided by Eq. (C.5). It is readily shown that the bi-Maxwellian distribution used in Appendix B satisfies Eqs. (C.1) to (C.5).

The particle contribution to Eq. (5.16) is written more usefully as:

$$\int \frac{1}{2} m v^2 \underset{\sim}{v} f \, d^3v = \int \frac{1}{2} m \Big[(v_{\parallel} - u_{\parallel})^2 + 2u (v_{\parallel} - u_{\parallel}) + u_{\parallel}^2 + (\underset{\sim}{v}_{\perp} - \underset{\sim}{u}_{\perp})^2 + 2\underset{\sim}{u}_{\perp} \cdot (\underset{\sim}{v}_{\perp} - \underset{\sim}{u}_{\perp}) + u_{\perp}^2 \Big] \times \Big[(\underset{\sim}{v}_{\parallel} - \underset{\sim}{u}_{\parallel}) + (\underset{\sim}{v}_{\perp} - \underset{\sim}{u}_{\perp}) + \underset{\sim}{u} \Big] f \, d^3v \, . \tag{C.6}$$

The various terms may be read off, using Eqs. (C.1) - (C.4). We find:

$$\sum_{e,i} \int \frac{1}{2} m v^2 \underset{\sim}{v} f \, d^3v = \frac{1}{2} \rho u^2 \underset{\sim}{u} + (p_{\perp} + \frac{1}{2} p_{\parallel}) \underset{\sim}{u} + p_{\perp} \underset{\sim}{u}_{\perp} + p_{\parallel} \underset{\sim}{u}_{\parallel} + \underset{\sim}{Q} \, . \tag{C.7}$$

The double adiabatic model assumes that the plasma is infinitely conducting, so the electric field satisfies

$$\underset{\sim}{E} + c^{-1} \underset{\sim}{u} \times \underset{\sim}{B} = 0. \tag{C.8}$$

Using Eqs. (5.16), (C.7), and (C.8), we write the energy flux vector $\underset{\sim}{S}$ in the Chew-Goldberger-Low model in the form

$$\underset{\sim}{S}(\underset{\sim}{r},t) = \frac{1}{2} \rho u^2 \underset{\sim}{u} + (p_{\perp} + \frac{1}{2} p_{\parallel}) \underset{\sim}{u} + p_{\perp} \underset{\sim}{u}_{\perp} + p_{\parallel} \underset{\sim}{u}_{\parallel} + \underset{\sim}{Q} + \underset{\sim}{B} \times (\underset{\sim}{u} \times \underset{\sim}{B})/4\pi. \tag{C.9}$$

APPENDIX D: CALCULATION OF THE RADIAL COMPONENT OF THE ENERGY FLUX VECTOR FOR THE IDEALIZED MODEL

We outline the calculation of the radial component S_r of the energy flux vector $\underset{\sim}{S}$ in the idealized solar wind model described in Sec. 5.1. This model consists of a spherically symmetric source of propagating Alfvén waves in a radially convecting plasma immersed in a monopole magnetic field.

Since we are only interested in taking the divergence of $\underset{\sim}{S}$, we drop the (divergenceless) heat flux vector $\underset{\sim}{Q}$ from the expression obtained for $\underset{\sim}{S}$ in Appendix C. Thus $\underset{\sim}{S}$ can be written in the form

$$\underset{\sim}{S} = \tfrac{1}{2}\rho u^2 \underset{\sim}{u} + (p_\perp + \tfrac{1}{2}p_\parallel)\underset{\sim}{u} + p_\perp \underset{\sim}{u}_\perp + p_\parallel \underset{\sim}{u}_\parallel + \underset{\sim}{B} \times (\underset{\sim}{u} \times \underset{\sim}{B})/4\pi. \tag{D.1}$$

The local magnetic field consists of the radial part $B_0 \hat{r}$ and the wave component $b\,\hat{b}(\theta)$. The plasma velocity is $\underset{\sim}{u} = u_0 \hat{r} + u_T \hat{b}(\theta + \delta)$, by Eq. (5.6). We neglect the small misalignment δ between the nonradial parts of $\underset{\sim}{B}$ and $\underset{\sim}{u}$. Because of Eq. (5.7), the consequent error in S_r, of order $\delta^2 \rho v_{th}^2 u_0$, is negligible. The geometry of field and velocity vectors is sketched in Fig. 11.

Let $\alpha \equiv \sin^{-1} b/B$ denote the angle between $\underset{\sim}{B}$ and $\hat{r}$. Recalling that $\underset{\sim}{u}_\parallel$ is the component of the total field velocity in the $\underset{\sim}{B}$ direction, we write

$$\underset{\sim}{u}_\parallel = (u_0 \cos\alpha + u_T \sin\alpha)\hat{B}. \tag{D.2}$$

Similarly we find

$$\underset{\sim}{u}_\perp = (-u_0 \sin\alpha + u_T \cos\alpha)(\hat{b}(\theta)\cos\alpha - \hat{r}\sin\alpha). \tag{D.3}$$

Using the usual expansion of the double cross product, the Poynting vector for the propagating Alfvén wave is

$$\underset{\sim}{B} \times (\underset{\sim}{u} \times \underset{\sim}{B}) = (u_0 b^2 - u_T b B_0)\hat{r} + (B^2 u_T - B_0^2 u_0 - b B_0 u_T)\hat{b}(\theta). \tag{D.4}$$

When Eqs. (D.1) - (D.4) are combined, the radial component of $\underset{\sim}{S}$ becomes

$$S_r = \tfrac{1}{2}\rho u^2 u_0 + (p_\perp + \tfrac{1}{2}p_\parallel)u_0 + p_\parallel(u_0\cos\alpha + u_T \sin\alpha)\cos\alpha + p_\perp(u_0 \sin\alpha - u_T\cos\alpha)\sin\alpha + (u_0 b^2 - u_T b B_0)/4\pi. \tag{D.5}$$

Finally, we use the properties of the propagating Alfvén waves derived for the uniform plasma case in Sec. 4.2A. These are Eqs. (5.11) and (5.12), which are assumed to hold in Sec. 5.2. With them Eq. (D.5) reduces to the following expression for the radial component of the energy flux density:

$$S_r = \tfrac{1}{2}\rho u_0^3 + (p_\perp + \tfrac{3}{2}p_\parallel)u_0 + \tfrac{1}{2}\rho V_A^2(3u_0 + 2V_A)(b/B_0)^2. \tag{D.6}$$

APPENDIX E: VECTOR CALCULUS FOR ALFVÉN WAVES IN THE IDEALIZED SOLAR WIND MODEL

We require quantities such as $\underset{\sim}{B} \cdot \nabla \underset{\sim}{B}$ and $\underset{\sim}{B} \cdot \nabla \underset{\sim}{u}$ in the analysis of the Chew-Goldberger-Low equations for convected large-amplitude Alfvén waves in the spherically symmetric solar wind model. Let $\underset{\sim}{A}$ and $\underset{\sim}{B}$ be any vectors having the forms

$$\underset{\sim}{A} = A_0 \hat{r} + a \hat{b}(\theta) \tag{E.1}$$

and

$$\underset{\sim}{B} = B_0 \hat{r} + b \hat{b}(\theta), \tag{E.2}$$

where A_0, a, B_0, b, and θ depend only on the spatial coordinates through the radius r.

Writing the vector operator in spherical coordinates we have

$$\begin{aligned} \underset{\sim}{A} \cdot \nabla \underset{\sim}{B} = {} & (\hat{r} A_0 + \hat{\theta}\, a \cos\theta + \hat{\phi}\, a \sin\theta) \\ & \cdot (\hat{r}\, \partial/\partial r + \hat{\theta}\, r^{-1} \partial/\partial\theta + \hat{\phi}(r \sin\theta)^{-1} \partial/\partial\phi) \\ & \times (\hat{r} B_0 + \hat{\theta}\, b \cos\theta + \hat{\phi}\, b \sin\theta). \end{aligned} \tag{E.3}$$

Since the assumption of spherical symmetry in Chapter 5 requires that we restrict the analysis to the vicinity of the equatorial plane, θ is approximately $\pi/2$. The differential operators in Eq. (E.3) act on both the scalars and the vectors in the last factor. Carrying out the indicated operations, we find

$$\underset{\sim}{A} \cdot \nabla \underset{\sim}{B} = A_0 \, \partial\underset{\sim}{B}/\partial r + (a B_0/r) \hat{b}(\theta) - (ab/r)\hat{r}. \tag{E.4}$$

Thus we can write

$$\underset{\sim}{B} \cdot \nabla \underset{\sim}{B} = B_0 \, \partial\underset{\sim}{B}/\partial r + (B_0 b/r) \hat{b}(\theta) - (b^2/r)\hat{r}, \tag{E.5}$$

with a similar result for $\underset{\sim}{u} \cdot \nabla \underset{\sim}{u}$. If δ is small as postulated in Eq. (5.7), then Eqs. (5.5) and (5.6) give

$$\underset{\sim}{B} \cdot \nabla \underset{\sim}{u} \cong B_0 \, \partial\underset{\sim}{u}/\partial r + (bu_0/r)\hat{b}(\theta) - (bu_T/r)\hat{r}. \tag{E.6}$$

APPENDIX F: THE MOMENTUM EQUATION FOR THE IDEALIZED MODEL OF ALFVÉN WAVES IN THE SOLAR WIND

Using the vector calculus derived in Appendix E for propagating Alfvén waves in a spherically symmetric system, we can write the Chew-Goldberger-Low momentum equation, Eq. (4.2), in the form

$$\rho(\partial \underset{\sim}{u}/\partial t + u_0\, \partial \underset{\sim}{u}/\partial r + \hat{b}(\theta + \delta)u_0\, u_T/r - \hat{r}\, u_T^2/r)$$

$$= -\nabla p_\perp - B_0\, \underset{\sim}{B}\, \partial(p_\Delta B^{-2})/\partial r - \nabla B^2/8\pi$$

$$+ [(1/4\pi) - p_\Delta B^{-2}][B_0\, \partial \underset{\sim}{B}/\partial r + \hat{b}(\theta) B_0\, b/r - \hat{r}\, b^2/r]. \qquad (F.1)$$

Equations (5.11) and (5.12) imply the result

$$-\hat{r}\, \rho\, u_T^2/r = -\hat{r}[(1/4\pi) - p_\Delta B^{-2}]b^2/r. \qquad (F.2)$$

Hence these radial terms can be eliminated from both sides of Eq. (F.1). Invoking spherical symmetry, we find that the radial component of Eq. (F.1) reduces to

$$\rho\, u_0\, du_0/dr = -dp_\perp/dr - d(p_\Delta B_0^2 B^{-2})/dr - (8\pi)^{-1}\, db^2/dr, \qquad (F.3)$$

which is equivalent to Eq. (5.26).

Equation (5.26) can also be obtained from the radial component of the total momentum conservation equation

$$\partial \underset{\sim}{g}/\partial t + \nabla \cdot \underset{\approx}{T} = 0, \qquad (F.4)$$

where $\underset{\sim}{g}$ is the total plasma momentum,

$$\underset{\sim}{g} \equiv \rho\, \underset{\sim}{u} + \underset{\sim}{E} \times \underset{\sim}{B}/(4\pi c), \qquad (F.5)$$

and $\underset{\approx}{T}$ is the total momentum flux tensor,

$$\underset{\approx}{T} \equiv \rho\, \underset{\sim}{u}\, \underset{\sim}{u} + \underset{\approx}{p} - \underset{\approx}{T}_{EM}. \qquad (F.6)$$

In Eq. (F.6), $\underset{\approx}{T}_{EM}$ is the momentum flux due to electromagnetic fields,[54]

$$\underset{\approx}{T}_{EM} \equiv [\underset{\sim}{E}\, \underset{\sim}{E} + \underset{\sim}{B}\, \underset{\sim}{B} - \tfrac{1}{2}\, \underset{\approx}{I}(E^2 + B^2)]/4\pi. \qquad (F.7)$$

The wave part of the momentum equation, Eq. (F.1), is

$$\rho(\partial/\partial t + u_0\, \partial/\partial r + u_0/r)[u_T\, \hat{b}(\theta + \delta)]$$

$$= -\hat{b}(\theta) b\, B_0\, d(p_\Delta B^{-2})/dr$$

$$+ B_0[(1/4\pi) - p_\Delta B^{-2}](\partial/\partial r + r^{-1})[b\, \hat{b}(\theta)]. \qquad (F.8)$$

APPENDIX G: DERIVATION OF A DIFFERENTIAL EQUATION FOR $\mathcal{B}(r)$ IN THE ENERGETIC SOLUTION OF THE IDEALIZED MODEL

We begin with Eqs. (5.25) and (5.26). Differentiate Eq. (5.25) with respect to r and multiply the result by $\rho/2$. Subtracting this from Eq. (5.26) to eliminate the large u_0 terms, we find

$$\rho\, d[p_\perp/\rho + (3/2)p_{||}/\rho + (3/2)V_A^2(b/B_0)^2]/dr$$

$$- d(p_\perp + b^2/8\pi)/dr - B_0\, d(p_\triangle B_0 B^{-2})/dr = 0. \qquad (G.1)$$

In obtaining Eq. (G.1) the rigorous dependence of ρ on r has been used in evaluating the large ρu_0^2 terms.

Using Eq. (5.12) to express the Alfvén velocity V_A in terms of the pressures, density and field, using Eq. (5.31) to eliminate ρ, and carrying out some of the differentiations, we can reduce Eq. (G.1) to the form

$$d\left[p_\perp + p_{||}/2 + [(1/4\pi) - p_\triangle B^{-2}/2]b^2\right]/dr$$

$$+ \left\{4p_\perp + p_{||} + [(3/4\pi) - p_\triangle B^{-2}]\, b^2\right\}/r = 0. \qquad (G.2)$$

Now we use Eqs. (4.8), (5.29), (5.32), and (5.33) to write all variables in terms of r, $\mathcal{B}(r)$, and constants. When all possible differentiations are carried out, and terms are collected, we find

$$\Big[(r_0/r)^4 p_{\perp 0} \mathcal{B}_0^{-1}(3\mathcal{B}^{-1} + \mathcal{B}^{-3})/4 - (r_0/r)^2 p_{||0} \mathcal{B}_0^{\,2} \mathcal{B}^{-6}$$

$$+ (r_0/r)^4 (B_{00}^2/4\pi)\Big]\, d\mathcal{B}^2/dr$$

$$= (p_{\perp 0} \mathcal{B}_0^{-1} \mathcal{B}^{-1} + B_{00}^2/4\pi)(\mathcal{B}^2 - 1) r_0^4/r^5. \qquad (G.3)$$

When Eq. (G.3) is multiplied by $4\pi/B_{00}^2$, and definition (5.35) is used, Eq. (5.34) is obtained.

APPENDIX H: THE SOLUTION OF DIFFERENTIAL EQUATION (5.34)

Because of the mixing of the dependent and independent variables $\mathcal{B}$ and r in Eq. (5.34), the usual integration techniques do not yield a solution without a great deal of effort. The solution itself can be written in a fairly simple form. We outline a sequence of manipulations of (5.34) which yields the required answer.

Equation (5.34) may be written:

$$\left[1 + \beta_\perp \mathcal{B}_0/\mathcal{B} - \beta_{||}(r/r_0)^2(\mathcal{B}_0/\mathcal{B})^4\right] d\mathcal{B}^2/dr$$

$$+ \left[\beta_{||}(r/r_0)^2(\mathcal{B}_0/\mathcal{B})^4 - \beta_{||}(r/r_0)^2\mathcal{B}_0{}^4\mathcal{B}^{-6} + (\beta_\perp/4)\mathcal{B}_0\mathcal{B}^{-3} - (\beta_\perp/4)\mathcal{B}_0/\mathcal{B}\right] d\mathcal{B}^2/dr$$

$$- (\mathcal{B}^2 - 1)\left[1 + \beta_\perp \mathcal{B}_0/\mathcal{B} - \beta_{||}(r/r_0)^2(\mathcal{B}_0/\mathcal{B})^4 + \beta_{||}(r/r_0)^2(\mathcal{B}_0/\mathcal{B})^4\right]/r = 0. \qquad (H.1)$$

A rearrangement and factorization of Eq. (H.1) gives

$$\left[1 + \beta_\perp \mathcal{B}_0/\mathcal{B} - \beta_{||}(r/r_0)^2(\mathcal{B}_0/\mathcal{B})^4\right] d\mathcal{B}^2/dr$$

$$+ (\mathcal{B}^2 - 1)\left\{\left[\beta_{||}(r/r_0)^2\mathcal{B}_0{}^4\mathcal{B}^{-6} - (\beta_\perp/4)\mathcal{B}_0\mathcal{B}^{-3}\right] d\mathcal{B}^2/dr - \beta_{||} r\, r_0^{-2}(\mathcal{B}_0/\mathcal{B})^4\right\}$$

$$- (\mathcal{B}^2 - 1)\left[1 + \beta_\perp \mathcal{B}_0/\mathcal{B} - \beta_{||}(r/r_0)^2(\mathcal{B}_0/\mathcal{B})^4\right]/r = 0. \qquad (H.2)$$

Next we divide Eq. (H.2) by the factor

$$(\mathcal{B}^2 - 1)\left[1 + \beta_\perp \mathcal{B}_0/\mathcal{B} - \beta_{||}(r/r_0)^2(\mathcal{B}_0/\mathcal{B})^4\right],$$

which is valid providing the solution doesn't pass through $b = 0$ or $V_A = 0$. This gives

$$-\frac{\left[(\beta_\perp/4)\mathcal{B}_0\mathcal{B}^{-3} - \beta_{||}(r/r_0)^2\mathcal{B}_0{}^4\mathcal{B}^{-6}\right] d\mathcal{B}^2/dr + \beta_{||} r\, r_0^{-2}(\mathcal{B}_0/\mathcal{B})^4}{1 + \beta_\perp \mathcal{B}_0/\mathcal{B} - \beta_{||}(r/r_0)^2(\mathcal{B}_0/\mathcal{B})^4}$$

$$+ (\mathcal{B}^2 - 1)^{-1} d\mathcal{B}^2/dr - r^{-1} = 0. \qquad (H.3)$$

The numerator of the first term is $-\frac{1}{2}$ times the r derivative of its denominator. All terms in Eq. (H.3) are now easily integrated, giving

$$\tfrac{1}{2}\ell n\left[1 + \beta_\perp \mathcal{B}_0/\mathcal{B} - \beta_{||}(r/r_0)^2(\mathcal{B}_0/\mathcal{B})^4\right] + \ell n(\mathcal{B}^2 - 1) - \ell n\, r = \text{const.} \qquad (H.4)$$

Exponentiating, we find the solution of Eq. (5.34) is

$$r^{-1}(\mathcal{B}^2 - 1)\left[1 + \beta_\perp \mathcal{B}_0/\mathcal{B} - \beta_{||}(r/r_0)^2(\mathcal{B}_0/\mathcal{B})^4\right]^{1/2} = \text{const.} \qquad (H.5)$$

Using Eqs. (5.29), (5.35), and (5.12), we can write

$$1 + \beta_\perp \mathcal{B}_0/\mathcal{B} - \beta_{||}(r/r_0)^2(\mathcal{B}_0/\mathcal{B})^4 = 4\pi V_A{}^2 \rho/B_0{}^2. \qquad (H.6)$$

In view of Eqs. (3.2) and (5.31) we have

$$\rho/B_0^2 = (\text{const.})r^2. \qquad (H.7)$$

Thus Eqs. (5.39), (H.6), and (H.7) reduce the solution (H.5) to the form

$$V_A(b/B_0)^2 = \text{const.} \qquad (H.8)$$

APPENDIX J: MAXWELL'S EQUATION FOR THE IDEALIZED MODEL

The Chew-Goldberger-Low Maxwell equation, Eq. (4.3), can be expanded as

$$\partial \underset{\sim}{B}/\partial t = \nabla \cdot \underset{\sim}{B}\,\underset{\sim}{u} - \nabla \cdot \underset{\sim}{u}\,\underset{\sim}{B}, \qquad (J.1)$$

where the divergence operator is understood to act on both vectors on its right. Carrying out the indicated differentiations and using Eq. (4.6), we find

$$\partial \underset{\sim}{B}/\partial t = \underset{\sim}{B} \cdot \nabla \underset{\sim}{u} - (\nabla \cdot \underset{\sim}{u})\underset{\sim}{B} - \underset{\sim}{u} \cdot \nabla \underset{\sim}{B}. \qquad (J.2)$$

Using the results of Appendix E to expand $\underset{\sim}{B} \cdot \nabla \underset{\sim}{u}$ and $\underset{\sim}{u} \cdot \nabla \underset{\sim}{B}$ for the ansatz, Eqs. (5.5) and (5.6), we find

$$\begin{aligned} \partial \underset{\sim}{B}/\partial t = {} & B_0\, \partial[u_T\, \hat{b}(\theta + \delta)]/\partial r \\ & - [u_0\, b\, \hat{b}(\theta) + B_0\, u_T\, \hat{b}(\theta + \delta)]/r - 2\, u_0\, \underset{\sim}{B}_0/r \\ & - b\, \hat{b}(\theta)\, \partial u_0/\partial r - u_0\, \partial \underset{\sim}{B}/\partial r . \end{aligned} \qquad (J.3)$$

The radial part of Eq. (J.3) simply gives $B_0 \sim r^{-2}$, i.e., the monopole background field of the idealized solar wind model. The wave part of the Maxwell equation is

$$\begin{aligned} b\partial\, \hat{b}(\theta)/\partial t = {} & B_0\, \partial[u_T\, \hat{b}(\theta + \delta)]/\partial r \\ & - [u_0\, b\, \hat{b}(\theta) + B_0\, u_T\, \hat{b}(\theta + \delta)]/r \\ & - b\, \hat{b}(\theta)\, \partial u_0/\partial r - u_0\, \partial[b\, \hat{b}(\theta)]/\partial r. \end{aligned} \qquad (J.4)$$

APPENDIX K: SOLUTION OF EQUATIONS (5.50) AND (5.51)

The unknown phase lag δ can be eliminated by dividing Eq. (5.50) by Eq. (5.51). This gives:

$$\rho\, V_A\, B_0^{-1} = \frac{\left\{\rho u_0 (u_T' + u_T/r) + (b' + b/r)[(1/4\pi) - p_\Delta B^{-2}]B_0 - bB_0\, d(p_\Delta B^{-2})/\partial r\right\}}{[B_0(u_T' - u_T/r) - (u_0' + u_0/r)b - u_0\, b']} \tag{K.1}$$

Using the exact mass conservation law

$$\rho\, u_0\, r^2 = \rho_0\, u_{00}\, r_0^2, \tag{K.2}$$

where ρ_0 and u_{00} are the values of ρ and u_0 at some reference radius r_0, elementary identities such as

$$u_T' + u_T/r = r^{-1}\, d(r\, u_T)/dr, \tag{K.3}$$

and Eq. (5.49) for the Alfvén velocity, we can write the numerator of Eq. (K.1) in the form

$$\left\{\quad\right\} = -r^{-1}\, \rho\, u_0\, d(ru_T - ru_0^{-1}\, V_A^2\, b/B_0)/dr. \tag{K.4}$$

Similarly, the denominator of the right-hand side of Eq. (K.1) reduces to

$$[\quad] = -\, r^{-1}\, d(r\, u_0\, b - r\, u_T\, B_0)/dr. \tag{K.5}$$

Thus Eq. (K.1) can be expressed in the simpler form

$$\rho\, V_A\, B_0^{-1} = \frac{\rho\, u_0\, d(r\, u_T - r\, u_0^{-1}\, V_A^2\, b/B_0)/dr}{d(r\, u_0\, b - r\, u_T\, B_0)/dr}. \tag{K.6}$$

Making use of Eq. (5.48) to write u_T in terms of b and V_A, we obtain

$$V_A\, u_0^{-1}\, B_0^{-1} = -d[V_A\, u_0^{-1}\, B_0^{-1}(u_0 + V_A)rb]/d[(u_0 + V_A)rb]. \tag{K.7}$$

Multiplying Eq. (K.7) by the differential in the dominator of the right-hand side, we have

$$V_A\, u_0^{-1}\, B_0^{-1}\, d[(u_0 + V_A)rb] = -\, V_A\, u_0^{-1}\, B_0^{-1}\, d[(u_0 + V_A)rb] - (u_0 + V_A)rb\, d(V_A\, u_0^{-1}\, B_0^{-1}), \tag{K.8}$$

which can be written

$$\frac{2\, d[(u_0 + V_A)rb]}{(u_0 + V_A)rb} + \frac{d[V_A\, u_0^{-1}\, B_0^{-1}]}{V_A\, u_0^{-1}\, B_0^{-1}} = 0. \tag{K.9}$$

Equation (K.9) has the obvious integral

$$\frac{(u_0 + V_A)^2\, r^2\, b^2\, V_A}{u_0\, B_0} = \text{const.}, \tag{K.10}$$

which becomes Eq. (5.52) when r^2 is replaced by B_0^{-1}.

An expression for $\delta(r)$ can be obtained from Eq. (5.51). We find, after similar manipulations,

$$\delta = -[(u_0 + V_A)/(\dot{\theta}\, V_A\, r\, b)]\, d[(u_0 + V_A)rb]/dr. \tag{K.11}$$

This can be written in the alternate form

$$\delta = -(2\,\dot{\theta}\,V_A\,r^2\,b^2)^{-1}\,d[rb(u_0 + V_A)]^2/dr\,, \qquad (K.12)$$

which gives the r dependence of δ when b is specified by Eq. (K.10).

APPENDIX L: ALFVÉN CRITICAL INSTABILITY POINT INVESTIGATIONS

The solution of the convective evolution problem, Eq. (5.36) or (5.52), can be written in the limit $V_A/u_0 \ll 1$ in the form

$$h^4\,\epsilon(r) = h_1^4\,\epsilon(r_1)(r/r_1)^2, \qquad (L.1)$$

where r_1 is an arbitrary reference radius,

$$h \equiv b(r)/B_0(r), \qquad (L.2)$$

$$h_1 \equiv h(r_1), \qquad (L.3)$$

$$\epsilon(r) \equiv 1 + \beta_\perp(r) - \beta_\parallel(r) \qquad (L.4)$$

and

$$\beta_{\perp,\parallel}(r) \equiv \left(4\pi/B^2(r)\right)p_{\perp,\parallel}(r). \qquad (L.5)$$

Differentiating Eq. (L.1) with respect to r, we solve for $h' \equiv dh/dr$ and find

$$h' = 2\,r\,r_1^{-2}\Big[h\,\beta_\parallel(r_1)(1+h_1^2)^2(1+h^2)^{-2} + h_1^4\,h^{-3}\,\epsilon(r_1)\Big] \times \Big\{\epsilon(r) + h^2(1+h^2)^{-1}\Big[4\beta_\parallel(r_1)r^2\,r_1^{-2}(1+h_1^2)^2(1+h^2)^{-2} - \beta_\perp(r_1)(1+h_1^2)^{1/2}(1+h^2)^{-1/2}\Big]\Big\}^{-1}. \qquad (L.6)$$

From Fig. 10 one sees that breakdown of the analytic theory due to fast change in amplitude of the field's wave component is only possible when $h(r) \ll 1$ inside the critical instability radius r_{cr}. Moreover, the violent change in h

occurs while h is still small. Thus, in investigating the maximum value of h', we will assume

$$h(r) \ll 1, \tag{L.7}$$

when $r \lesssim r_{cr}$.

We choose the reference radius r_1 to be at or near r_{cr} and consider $h'(r)$ for r near r_1.

Figure 10 shows that the Alfvén velocity at r_{cr} is small compared to its value, $V^* \equiv (4\pi\rho)^{-1/2} B_0$, if the plasma were isothermal there. Since we can write $V_A = (4\pi\rho)^{-1/2} B_0 \epsilon^{1/2}$, $\epsilon(r_1)$ is small:

$$\epsilon(r_1) \equiv 1 + \beta_\perp(r_1) - \beta_{||}(r_1) \ll 1 . \tag{L.8}$$

Consequently the second term in the numerator bracket of Eq. (L.6) may be neglected.

With these approximations, Eq. (L.6) reduces to the more tractable form

$$h' \cong 2 r_1^{-1} h \beta_{||}(r_1) \left\{ \epsilon(r) + h^2 \left[4\beta_{||}(r_1) - \beta_\perp(r_1) \right] \right\}^{-1} . \tag{L.9}$$

In view of Eq. (L.8), Eq. (L.9) can be written

$$h' \cong 2h \beta_{||}(r_1) r_1^{-1} \left\{ \epsilon(r) + h^2 [4+3\beta_\perp(r_1)] \right\}^{-1} , \tag{L.10}$$

which shows clearly that the denominator brace never vanishes. (Since V_A^2 is proportional to $\epsilon(r)$ and $V_A^2 > 0$ everywhere according to the solution (5.36), $\epsilon(r)$ must be positive for all values of r.)

The numerator of Eq. (L.10) is a monotonically but slowly increasing function of r for $r < r_{cr}$, the scale length for changes in h being of order r_{cr}. In the denominator brace of Eq. (L.10), $\epsilon(r)$ is the dominant term well inside the critical instability radius, since h^2 is small there. As r increases to r_1, $\epsilon(r)$ approaches zero, and the monotonically increasing h^2 term, although still small, becomes dominant in the brace. Choose r_1 to be the point where $\epsilon(r)$ equals the term $h^2[4 + 3\beta_\perp(r_1)]$. Then at r_1 the denominator brace of Eq. (L.10) is a minimum, and r_1 gives, approximately, the maximum value of h'. To avoid anomolous cases we assume $\beta_{\perp,||} \sim 1$, and, omitting factors of order 1, we find

$$h'_{max} \approx \left(r_1 \, h(r_1) \right)^{-1} , \tag{L.11}$$

where r_1 is the radius at which

$$\epsilon(r_1) \approx 4 \, h^2(r_1). \tag{L.12}$$

We require an estimate for $h^2(r_1)$ in terms of the plasma configuration at an arbitrary point interior to the critical radius.

We select a point r_0, with $r_0 < r_{cr}$, having known plasma parameters $\beta_\perp(r_0)$, $\beta_{||}(r_0)$, and $h(r_0) \ll 1$. For values of r between r_0 and r_{cr}, h remains small compared to 1, and we have

$$\epsilon(r) \cong 1 + \beta_\perp(r_0) - \beta_{||}(r_0)(r/r_0)^2 . \tag{L.13}$$

At r_1, ϵ is small as argued above, and thus r_1 is given by

$$(r_1/r_0) \cong [1 + \beta_\perp(r_0)]/\beta_{||}(r_0). \qquad (L.14)$$

Equations (L.1), (L.12), and (L.14) can now be used to estimate $h(r_1)$:

$$h(r_1) \approx \left\{ h^4(r_0)[1 + \beta_\perp(r_0) - \beta_{||}(r_0)][1 + \beta_\perp(r_0)]/\beta_{||}(r_0) \right\}^{1/6}. \qquad (L.15)$$

Substituting the last result in Eq. (L.11), we find an estimate for the maximum rate of change of h in terms of the plasma parameters at the selected radius r_0 inside the Alfvén critical instability radius:

$$h'_{max} \approx r_0^{-1} [1 + \beta_\perp(r_0) - \beta_{||}(r_0)]^{-1} \times \left\{ h(r_0)[1 + \beta_\perp(r_0)]/\beta_{||}(r_0) \right\}^{-2/3}. \qquad (L.16)$$

This result is valid only if $h(r_0) \ll 1$.

APPENDIX M: ESTIMATES OF THE SOLAR WIND HEAT FLUX DENSITY DUE TO ELECTRONS

A very crude estimate of the electron thermal flux density Q_e can be obtained by using the electron temperature at the solar corona, 10^6 °K, and at 1 AU, 10^5 °K, to estimate the electron thermal gradient at 1 AU. Spitzer's formula for the heat transport coefficient then gives[55]

$$Q_e^* \sim 2 \times 10^{13} \text{ ev cm}^{-2} \text{ sec}^{-1}. \qquad (M.1)$$

This enormously overestimates the actual heat flux, because high electron thermal conductivity severely reduces thermal gradients at 1 AU.

In the absence of Alfvén waves, the idealized theoretical model used in Chapter 5 predicts

$$T_{||} \propto p_{||}/\rho \cong \text{constant}, \qquad (M.2)$$

i.e. there is no electron heat transport.

The actual heat flow must lie somewhere in between these extremes.

Measurements of the electron velocity distribution give an estimate of the electron heat flux by taking the third moment of the distribution. The average over one year of Vela 4 data gives[33]

$$\langle Q_e \rangle \sim 4 \times 10^9 \text{ ev cm}^{-2} \text{ sec}^{-1}. \qquad (M.3)$$

By comparison, the flux density of energy in thermal motion of the electrons and ions, calculated by assuming 10 ev per ion or electron, 10 ions and electrons per cm^3, and $u_0 = 400$ km sec^{-1}, give this latter value also:

$$Q_{thermal} \sim 4 \times 10^9 \text{ ev cm}^{-2} \text{ sec}^{-1}. \qquad (M.4)$$

The energy flux density due to the bulk transport of particle kinetic energy is given by

$$Q_{bulk} \sim 2 \times 10^{11} \text{ ev cm}^{-2} \text{ sec}^{-1}.$$

Since the electron heat flow Q_e^*, obtained from the estimated sun-Earth temperature gradient, 0.01 $^oK/km$, exceeds the measured value $\langle Q_e \rangle$ by a factor of 5000, the electron temperature gradient at 1 AU must be less than its estimated value by this factor. Thus the average electron temperature gradient at 1 AU should be 2×10^{-6} $^oK/km$. This small value at 1 AU implies a swift decrease of electron temperature near the sun, probably occurring in a strongly turbulent region where the heat transport coefficient is anomolously small.

Equations (M.3) and (M.4) show that electron heat conduction is an important effect in the solar wind. However, since the energy flow due to electron heat conduction is comparable to the thermal energy transported by convection, it does not dominate other contributions to the overall energy balance.

ACKNOWLEDGMENTS

The author is indebted to Professor Allan N. Kaufman for his guidance, criticisms, and encouragement during the course of this research. Sincere appreciation is also felt for the efforts and interests of Professors A. N. Kaufman and W. B. Kunkel and Dr. J. M. Wilcox, who carefully read an early version of this manuscript and made many suggestions which are incorporated herein. A special debt is owed to Miss Georgella Perry and Mrs. Chris Graham for their expertise and patience in typing the final draft.

This work was supported by the United States Atomic Energy Commission, the National Aeronautics and Space Administration, and the United States Air Force.

FOOTNOTES AND REFERENCES

1. G. F. Chew, M. L. Goldberger, and F. E. Low, Proc. Roy. Soc. (London) A236 , 112 (1956).
2. E. N. Parker, Space Sci. Rev. 4, 666 (1965).
3. E. N. Parker, Space Sci. Rev. 9, 325 (1969).
4. A. J. Hundhausen, Space Sci. Rev. 8, 690 (1968).
5. J. M. Wilcox, Space Sci. Rev. 8, 258 (1968).
6. W. I. Axford, Space Sci. Rev. 8, 331 (1968).
7. E. N. Parker, Interplanetary Dynamical Processes (Interscience, New York, 1963), p. 138.
8. C. W. Snyder, M. Neugebauer, and U. R. Rao, J. Geophys. Res. 68, 6361 (1963).
9. M. Neugebauer and C. W. Snyder, in The Solar Wind, edited by R. J. Mackin, Jr., and M. Neugebauer (Pergamon Press, New York, 1966), p. 3.
10. J. M. Wilcox and N. F. Ness, J. Geophys. Res. 70, 5793 (1965).
11. T. E. Holzer and W. I. Axford, J. Geophys. Res. 75, 6354 (1970).
12. N. F. Ness, L. F. Burlaga, K. W. Ogilvie, and J. W. Sari, NASA-Goddard Space Flight Center preprint X-692-70-460 (1970).
13. L. F. Burlaga, Solar Phys. 4, 67 (1968).
14. L. F. Burlaga, Solar Phys. 7, 54 (1969).
15. L. F. Burlaga and N. F. Ness, Solar Phys. 9, 467 (1969).

16. L. F. Burlaga, NASA-Goddard Space Flight Center preprint X-692-70-462 (1970).
17. J. W. Belcher, P. J. Coleman, Jr., L. Davis, Jr., D. E. Jones, and E. J. Smith, "Waves and Discontinuities in the Solar Wind," Cal Tech preprint (1970).
18. J. W. Belcher, L. Davis, Jr., and E. J. Smith, J. Geophys. Res. 74, 2302 (1969).
19. J. W. Belcher and L. Davis, Jr., J. Geophys. Res. 76, 3534 (1971).
20. P. J. Coleman, Jr., Planet. Space Sci. 15, 953 (1967).
21. G. L. Siscoe, L. Davis, Jr., P. J. Coleman, Jr., E. J. Smith, and D. E. Jones, J. Geophys. Res. 73, 61 (1968).
22. H. Grad, in Magneto-Fluid and Plasma Dynamics, edited by H. Grad (American Mathematical Society, Providence, R. I., 1967), p. 162.
23. R. M. Kulsrud, in Advanced Plasma Theory, edited by M. N. Rosenbluth (Academic, New York, 1964), p. 54.
24. R. C. Davidson and H. J. Völk, Phys. Fluids 11, 2259 (1968).
25. J. A. Byers, Phys. Fluids 10, 2235 (1967).
26. R. E. Aamodt and S. E. Bodner, Phys. Fluids 12, 1471 (1969).
27. J. P. Freidberg and T. P. Armstrong, Phys. Fluids 11, 2669 (1968).
28. T. P. Armstrong and D. Montgomery, Phys. Fluids 12, 2094 (1969).
29. David Montgomery (private communication).

30. J. M. Dawson and R. Shanny, Phys. Fluids 11, 1506 (1968).

31. R. M. Kulsrud and W. P. Pearce, Astrophys. J. 156, 303 (1969).

32. R. M. Kulsrud and A. Ferrara, Princeton preprint PPL-AP43 (1970).

33. M. D. Montgomery, private communication based on "Average Thermal Properties of Solar Wind Electrons," to be published in Proceedings of the Solar Wind Conference, Asilomar, Calif. (March 21-26, 1971).

34. L. D. Landau and E. M. Lifshitz, Electrodynamics of Continuous Media (Pergamon, New York, 1960), p. 225.

35. F. L. Scarf, Space Sci. Rev. 11, 234 (1970).

36. P. A. Sturrock and R. E. Hartle, Phys. Rev. Letters 16, 628 (1966).

37. E. Eviatar and M. Schulz, Planet. Space Sci. 18, 321 (1970).

38. R. Z. Sagdeev and A. A. Galeev, Nonlinear Plasma Theory, edited by T. M. O'Neil and D. L. Book (Benjamin, New York, 1969), Chap. I.

39. V. D. Shapiro and V. I. Shevchenko, Zh. Eksp. Teor Fiz. 45, 1612 (1963) [Sov. Phys. JETP 18, 1109 (1964)].

40. A. Barnes, Phys. Fluids 11, 2644 (1968).

41. I. A. Akhiezer, R. V. Polovin, and N. L. Tsintsadze, Zh. Eksp. Teor. Fiz. 37, 756 (1959) [Sov. Phys. JETP 37 (10), 539 (1960)].

42. It is possible to find nontrivial Alfvén waves with properties (4.9a) - (4.9h) because there exist plane polarized Alfvén modes propagating parallel to $\underset{\sim}{B}_0$ with polarization

planes orthogonal to each other. The suitably phased sum of such waves is a circularly polarized Alvén mode with the property (4.9e) that the magnitude of the perturbation is constant everywhere. Equation (4.9e) greatly simplifies the Chew-Goldberger-Low and Guiding-Center equations. For propagation at an angle to $\underset{\sim}{B}_0$ there is only one Alfvén mode, and the simplifications so useful to the present work cannot occur.

43. V. C. A. Ferraro, Proc. Roy Soc. (London) A233, 310 (1956).

44. A. A. Vedenov, E. P. Velikhov, and R. Z. Sagdeev, Nucl. Fusion 1, 82 (1961).

45. A. A. Galeev and V. N. Oraevskii, Dokl. Akad. Nauk. SSSR 154, 1069 (1964)[Sov. Phys. Dokl. 9, 154 (1964)].

46. J. Belcher (private communication).

47. A. Barnes and G. C. J. Suffolk, J. Plasma Physics 5, 315 (1971).

48. Yu. A. Berezin and R. Z. Sagdeev, Dokl. Akad. Nauk. SSSR 184, 570 (1969) [Sov. Phys. Dokl. 13, 62 (1969)].

49. The analysis is equally valid for purely inward propagating waves. The great simplifications which occur for a purely outward- or purely inward-propagating wave is lost, however, if both types are simultaneously present. Inward propagating Alfvén waves are seldom observed in the solar wind, as discussed in Reference 19.

50. J. V. Hollweg, "Collisionless Solar Wind 2. Variable Electron Temperature," Cal Tech preprint (June, 1971).

51. C. F. Kennel (private communication).

52. The Alfvén stability point is where $V_A = 0$. Equations (4.12), (4.13), (4.16), and (4.29) show that this is the point where $\partial\phi/\partial\tau_b = 0$ and $\tau_b \neq 0$, i.e. the bottoms of the two wells of the magnetic potential.

53. In deriving the relations (A.4) - (A.9) from the linearized equations, we treated γ^2 as a zero order quantity. Carrying the pressure terms in γ^2 to second order is admittedly of questionable value, since other terms of this order have been ignored.

54. J. D. Jackson, Classical Electrodynamics (Wiley, New York, 1962), p. 193.

55. L. Spitzer, Jr., Physics of Fully Ionized Gases (Interscience, New York, 1962), p. 144.

56. Figures 2 - 4 represent the plasma data of H. S. Bridge, A. J. Lazarus, and C. W. Snyder and the magnetometer data of P. J. Coleman, Jr., L. Davis, Jr., and E. J. Smith. The effort of these experimenters is greatly appreciated.

FIGURE CAPTIONS

Fig. 1. Due to solar rotation and radial plasma flow outward, the average interplanetary magnetic field lines in the ecliptic plane describe the Archimedes' spirals specified by Eqs. (2.1) - (2.4). The areas in which the magnetic field is generally toward (or away from) the sun form sectors whose boundaries follow these spirals. This sketch indicates a total of four sectors, but at times only two are observed.[5]

Fig. 2. This Mariner 5 solar wind data covers a twenty-four hour period.[19,56] Magnetic field components B_R, B_T, and B_N are plotted using horizontal and vertical line segments. Plasma velocity components v_R, v_T, and v_N are plotted with diagonal lines. The units employed are magnetic field in gammas, plasma velocity in km/sec, and number density N in cm^{-3}.

The strong positive correlation between magnetic field components and plasma velocity components and the fact that the average field is toward the sun on this day clearly indicates the presence of an outward-propagating Alfvén wave.

Note that $|\underset{\sim}{B}|$ and N are relatively constant, despite the marked fluctuations in $\underset{\sim}{B}$ and $\underset{\sim}{v}$.

Fig. 3. Three ten-minute intervals of the day used in Fig. 2 show details of the Mariner 5 data.[19] The crosses denote magnetic field components B_R, B_T, B_N, and, at the bottom, $|\underset{\sim}{B}|$. The horizontal lines indicate plasma velocity components V_R, V_T, V_N, and the plasma number density N. The five minute sampling period of the velocity detector precludes the correlation of its data with the measurable high-frequency fluctuations of the magnetic field. The tendency of the averaged velocity to follow magnetic field trends is obvious.

Fig. 4. This one-hour sample of Mariner 5 data illustrates the high-frequency fluctuations of the magnetic field $\underset{\sim}{B}$.[19] The magnitude of $\underset{\sim}{B}$ remains quite constant while appreciable fluctuation in its components occur.

Fig. 5. Magnetic field lines of constant-amplitude Alfvén waves for various choices of the function $\theta(\cdot)$, which specifies the direction of the field disturbance $\underset{\sim}{b}$: (a) $\theta(x) = \pi \tanh kx$; (b) $\theta(x) = (\pi/2) \tanh kx$; (c) $\theta(x) = (7\pi/2) \exp[-(kx)^2]$. In each illustration the field lines make a 45° angle with $\underset{\sim}{B}_0$ everywhere, corresponding to $|\underset{\sim}{b}| = B_0$. In (a) and (c) the nearly uniform field at large positive values of $k(z - V_A t)$ is parallel to the field at large negative values of $k(z - V_A t)$; the exaggerated perspective makes them seem nonparallel.

In the Chew-Goldberger-Low and guiding-center

models these field configurations propagate without distortion at the generalized Alfvén velocity

$$V_A = (B_0^2/4\pi\rho)^{1/2}[1 - 4\pi(p_{\parallel} - p_{\perp})/B^2]^{1/2},$$

parallel to $\underset{\sim}{B}_0$.

Fig. 6. Temporal evolution of the time-varying-amplitude Alfvén mode. Field lines are pictured for: (a) $\mathfrak{b} \approx 6B_0$, (b) $\mathfrak{b} \approx 3B_0$, (c) $\mathfrak{b} \approx B_0$, (d) $\mathfrak{b} = 0$, (e) $\mathfrak{b} \approx -B_0$, (f) $\mathfrak{b} \approx -3B_0$, (g) $\mathfrak{b} \approx -6B_0$. The helical standing-wave structure is generated by a magnetic field component perpendicular to the uniform field $\underset{\sim}{B}_0$ having signed amplitude $\mathfrak{b}(t)$, whose time dependence readily follows from Eqs. (4.24) and (4.25). This mode is an exact solution for a stable or unstable plasma in the Chew-Goldberger-Low and guiding-center models.

Fig. 7. Sketch of the magnetic potential $\bar{\phi}(\mathfrak{b})$, Eq. (4.25), for the variable-amplitude Alfvén mode with various choices of the plasma parameters: (a) stable plasma with $K > \bar{\phi}(0)$, corresponding to Case 1; (b) unstable plasma with $K > \bar{\phi}(0)$, corresponding to Case 2(a); (c) unstable plasma with $K = \bar{\phi}(0)$, corresponding to Case 2(b); (d) unstable plasma with $\bar{\phi}_{min} < K < \bar{\phi}(0)$, corresponding to Case 2(c). In (a), $\bar{\phi}$ is sketched for the pressure anisotropy $(p_{\perp})_{\mathfrak{b}=0} = B_0^2/8\pi$, $(p_{\parallel})_{\mathfrak{b}=0} = B_0^2/4\pi$. The unstable plasma in (b) - (d) corresponds to

$(p_\perp)_{b=0} = B_0^2/4\pi$, $(p_{||})_{b=0} = 4B_0^2/\pi$. By Eq. (4.24), the time dependence of the signed amplitude b, which determines the evolution of the helical structure pictured in Fig. 6, is the displacement of a unit mass particle of energy K moving in the potential $\phi(b)$.

Fig. 8. Spherical topology causes the ansatz represented by Eq. (5.5) to be mathematically inconsistent. According to the idealized model, wave components of the magnetic field, depicted by small arrows in this sketch, point in the $\hat{\theta}$ direction at each point on the spherical surface $|\underset{\sim}{r}| = r_0$, when $\theta(r_0,t)$ is an integral multiple of 2π. The anomolous character of the wave field at the polar axis is evident. To avoid this difficulty, we restrict the analysis to the vicinity of the equatorial plane, $\theta \cong \pi/2$.

Fig. 9. Equations (5.40) and (5.41) are vector differential equations whose terms lie in the plane perpendicular to $\hat{r}$. The left side vectors are large in amplitude and nearly perpendicular to the small right side vectors. The latter can be ignored when resolving these equations into components along $\hat{r} \times \hat{b}(\theta)$. The right side terms and the large $\hat{r} \times \hat{b}(\theta + \delta)$ term on the left side must be included in computing components along $\hat{b}(\theta)$.

Fig. 10. In the idealized model of the solar wind, the convective evolution of large amplitude Alfvén waves is governed by the equation $V_A(b/B_0)^2 = \text{constant}$. Solutions of this equation are sketched here for four values of the wave amplitude. In all cases the plasma parameters at the reference radius r_0 are $p_{\perp 0} = B_{00}^2/4\pi$ and $p_{||0} = B_{00}^2/8\pi$. For these pressures the Alfvén critical instability point, where the plasma would become Alfvén unstable in the absence of the propagating wave, is $r_{cr} = (3/2)^{1/2} r_0$.

When b/B_0 is small at r_0, Cases (c) and (d), note the swift growth of wave amplitude necessary at r_{cr} to maintain the reality of V_A and hence the stability of the plasma.

Fig. 11. In the limit of infinitesimal phase lag δ, the magnetic field $\underset{\sim}{B}$, the plasma velocity $\underset{\sim}{u}$, and $\hat{r}$ are co-planar in the idealized model.

The velocity $\underset{\sim}{u}_{||}$ is computed by taking the projections of the wave and radial components of $\underset{\sim}{u}$ onto $\underset{\sim}{B}$. Since $\underset{\sim}{u}_{||} + \underset{\sim}{u}_\perp = \underset{\sim}{u}$, $\underset{\sim}{u}_\perp$ easily follows.

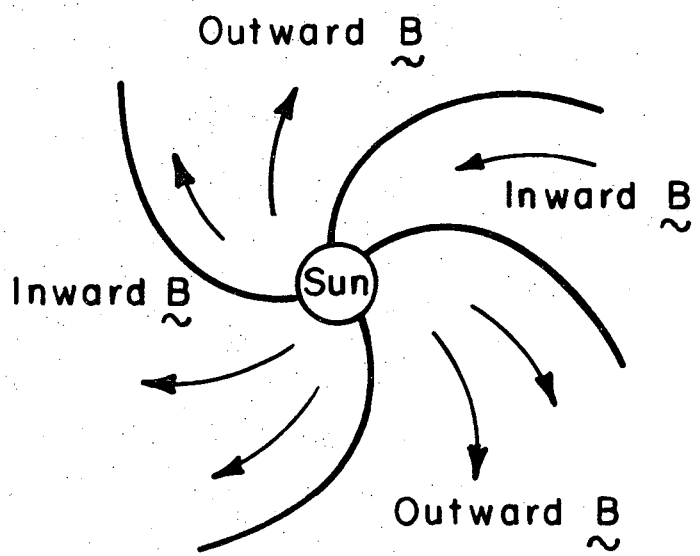

XBL718-3989

Fig. 1

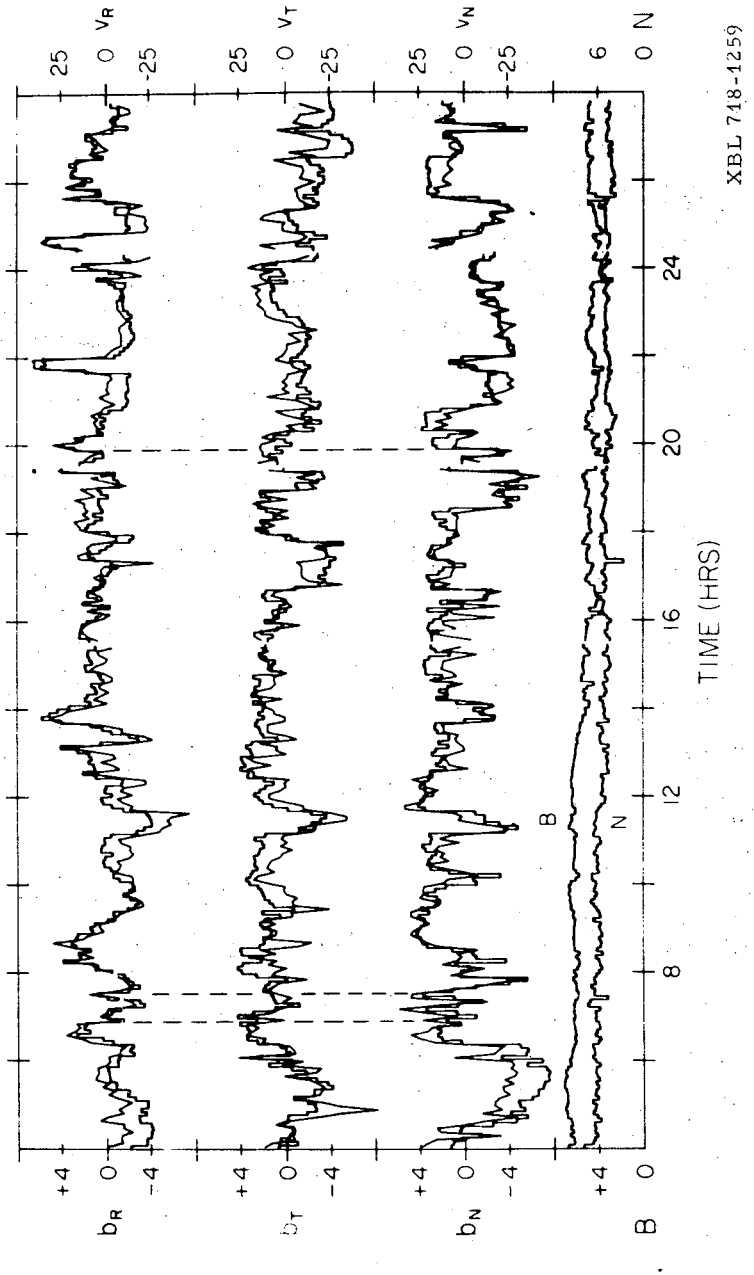

Fig. 2

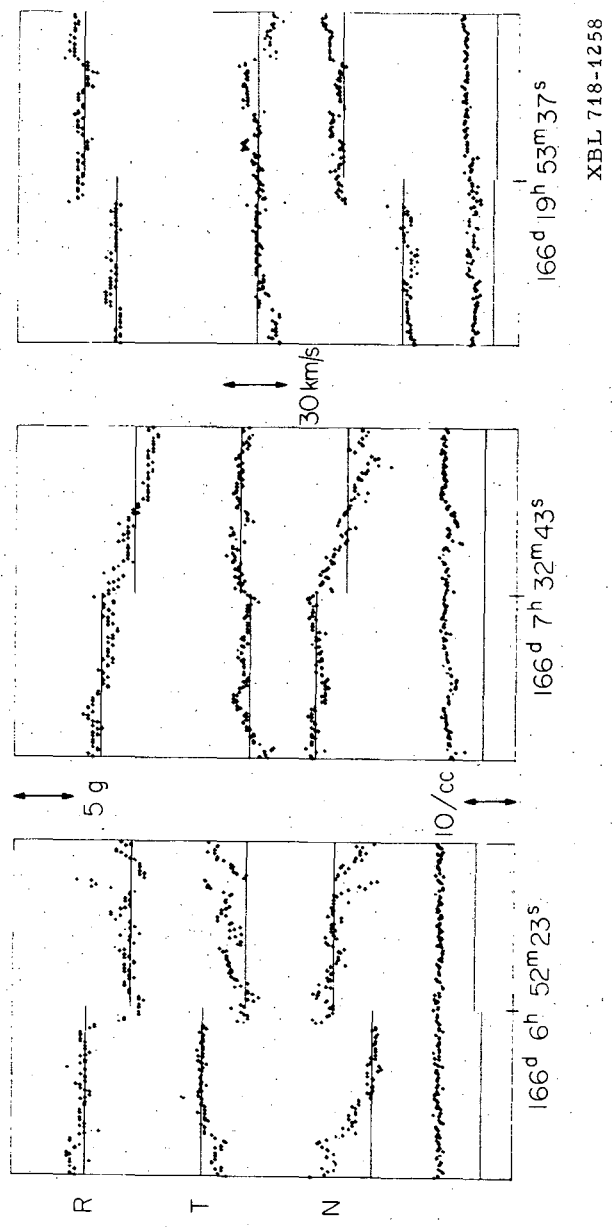

XBL 718-1258

Fig. 3

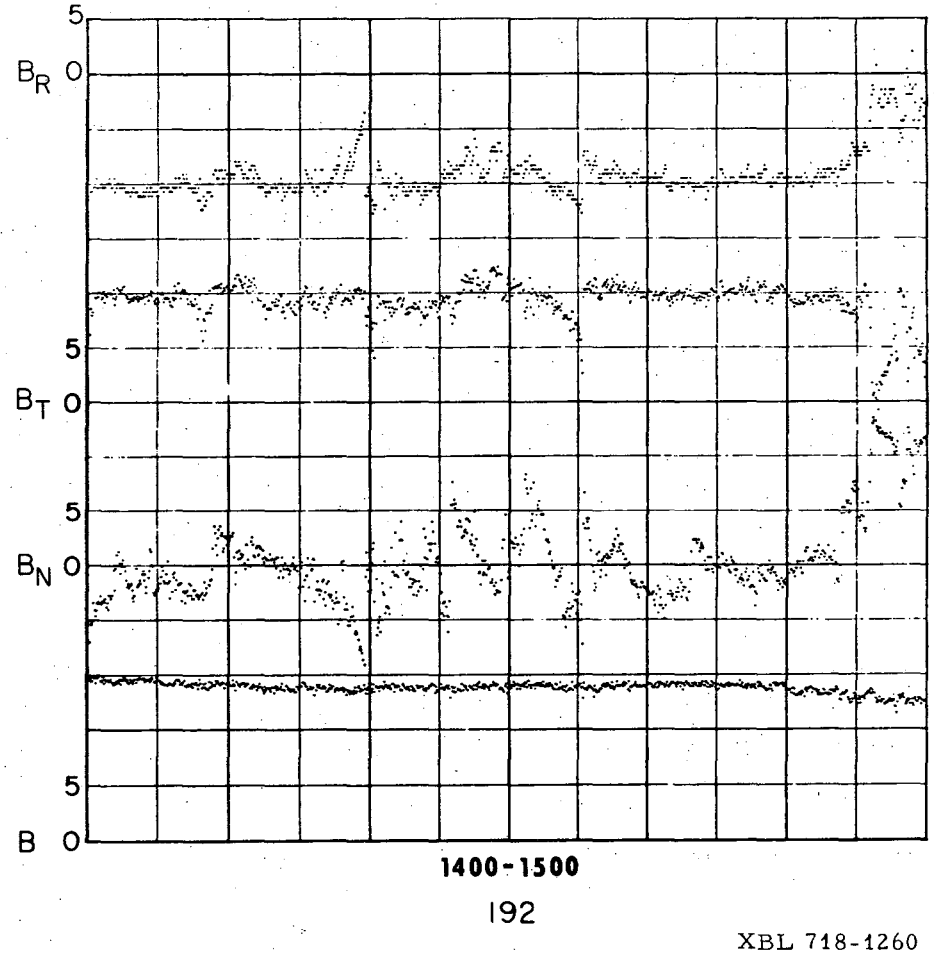

XBL 718-1260

Fig. 4

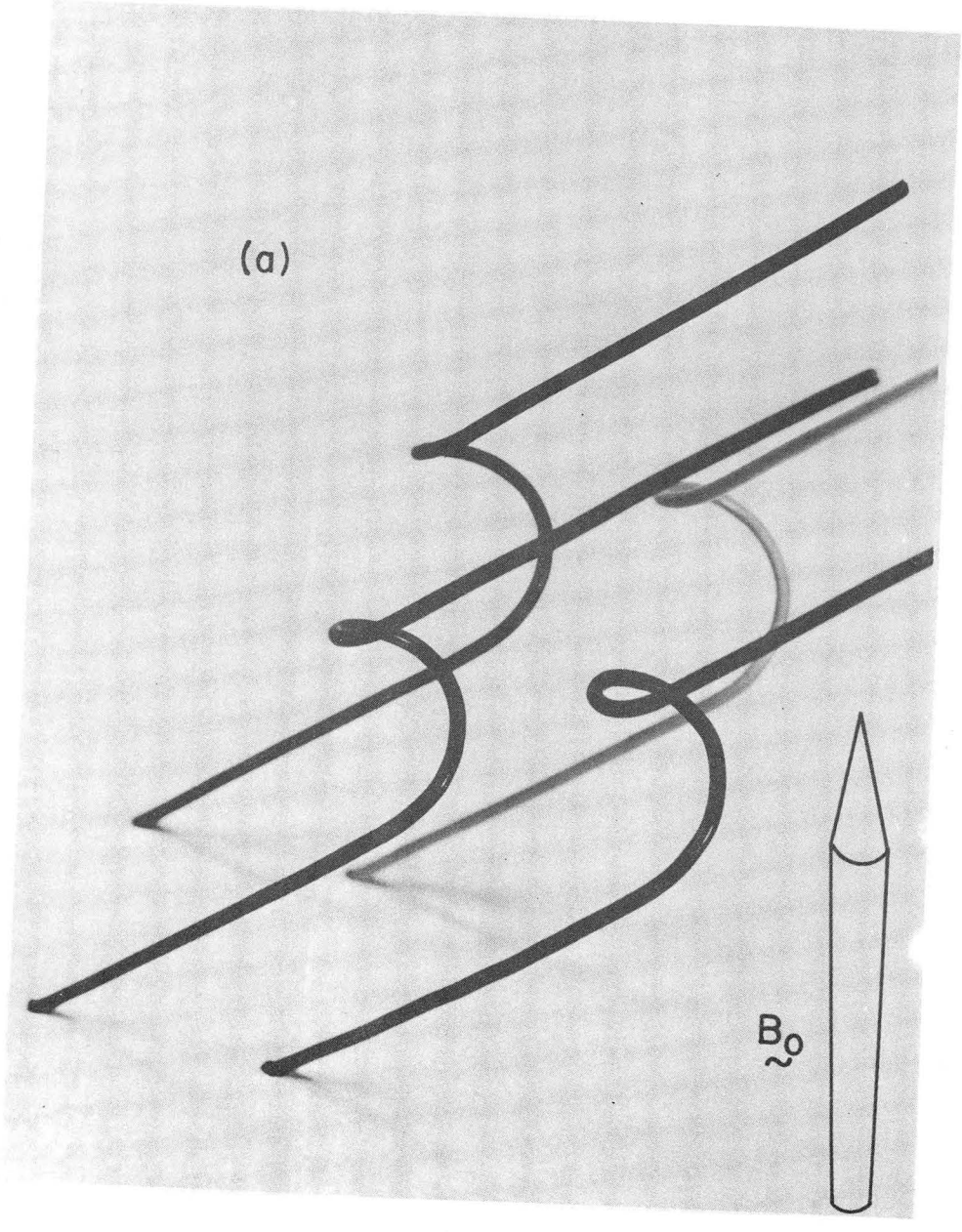

Fig. 5(a)

XBB 708-3609A

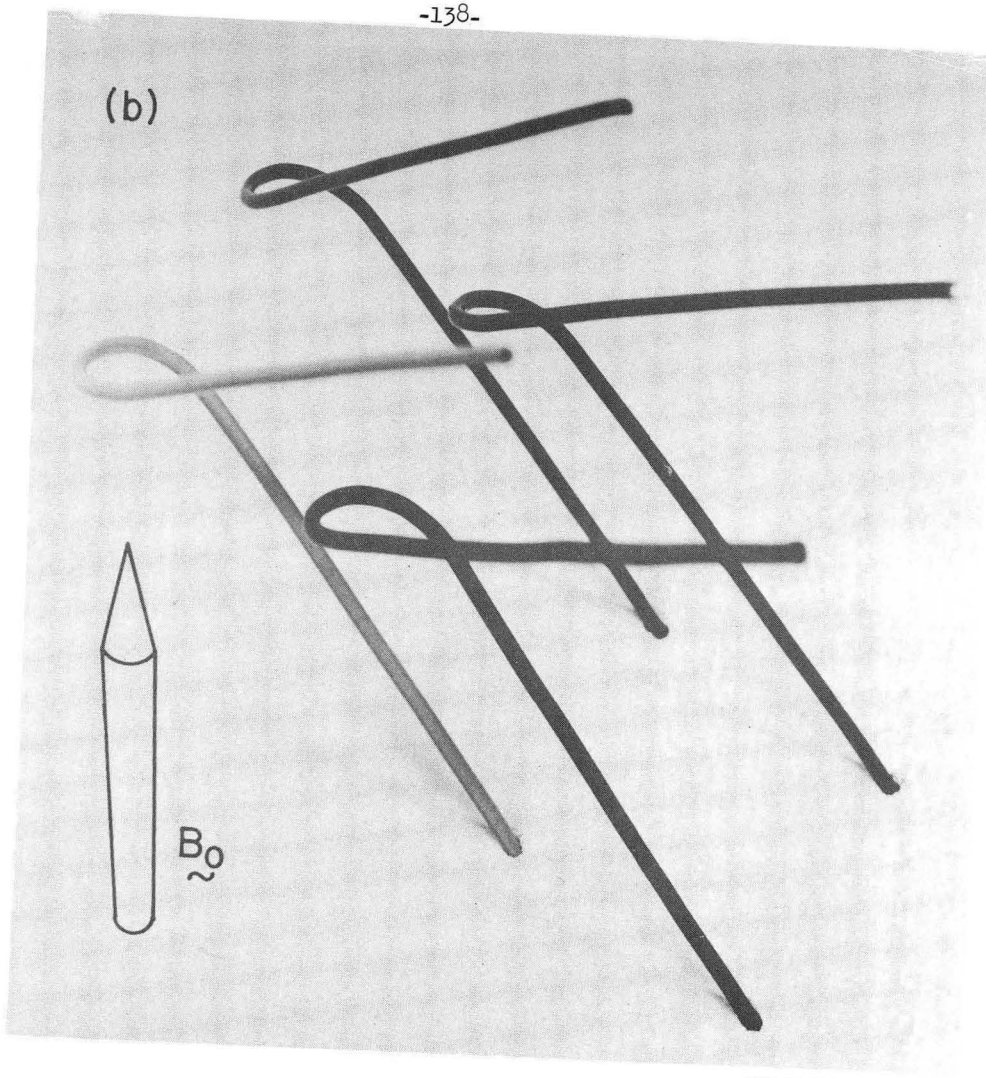

Fig. 5(b)

XBB 708-3608A

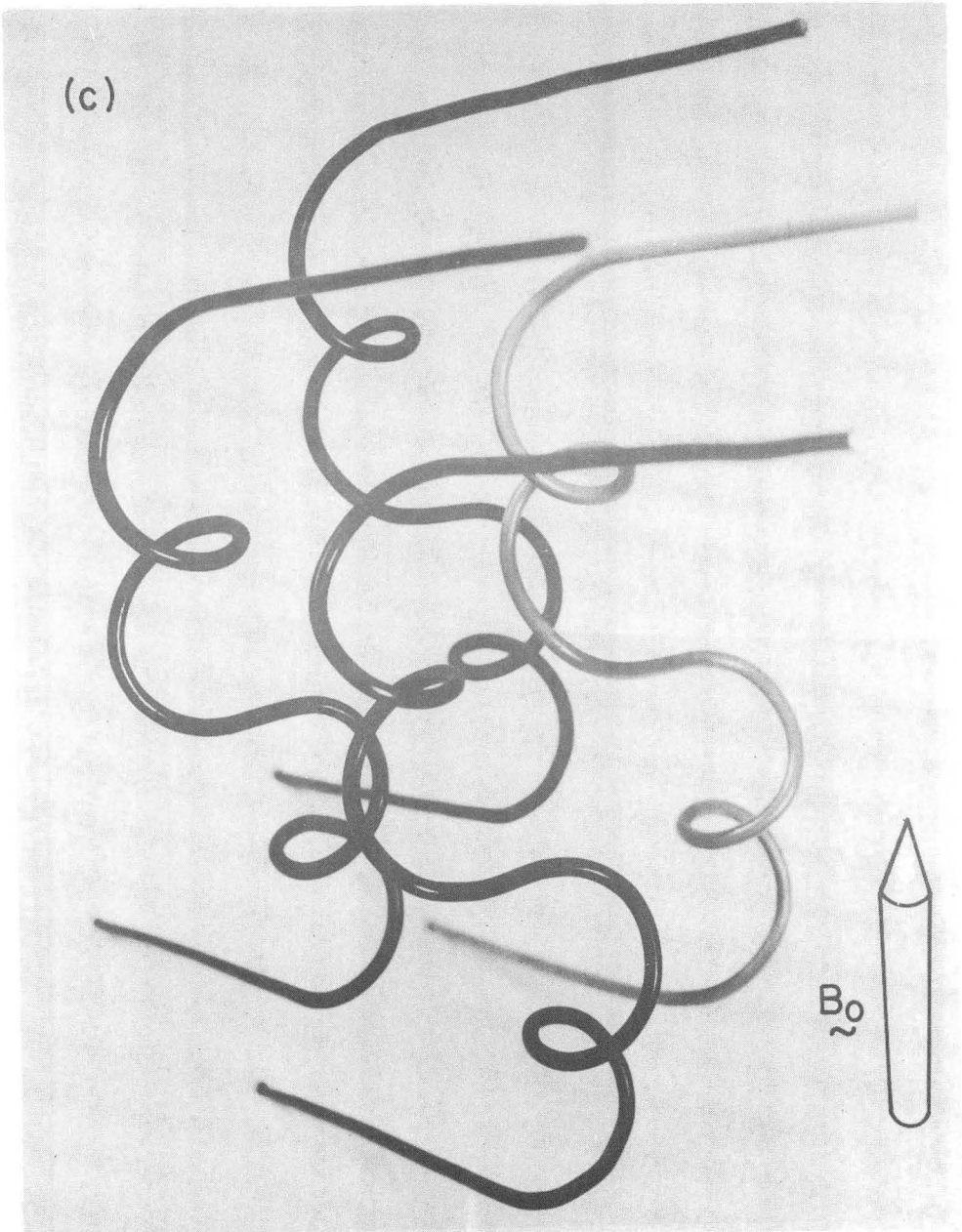

XBB 708-3607A

Fig. 5(c)

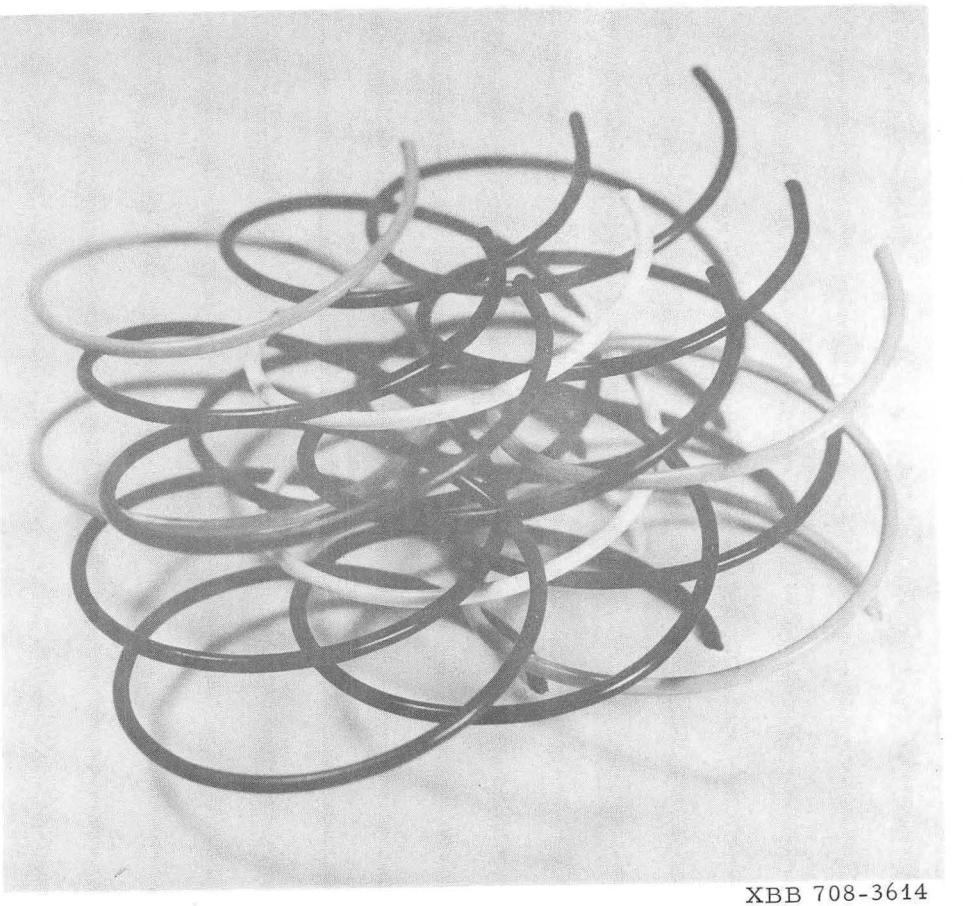

XBB 708-3614

Fig. 6(a)

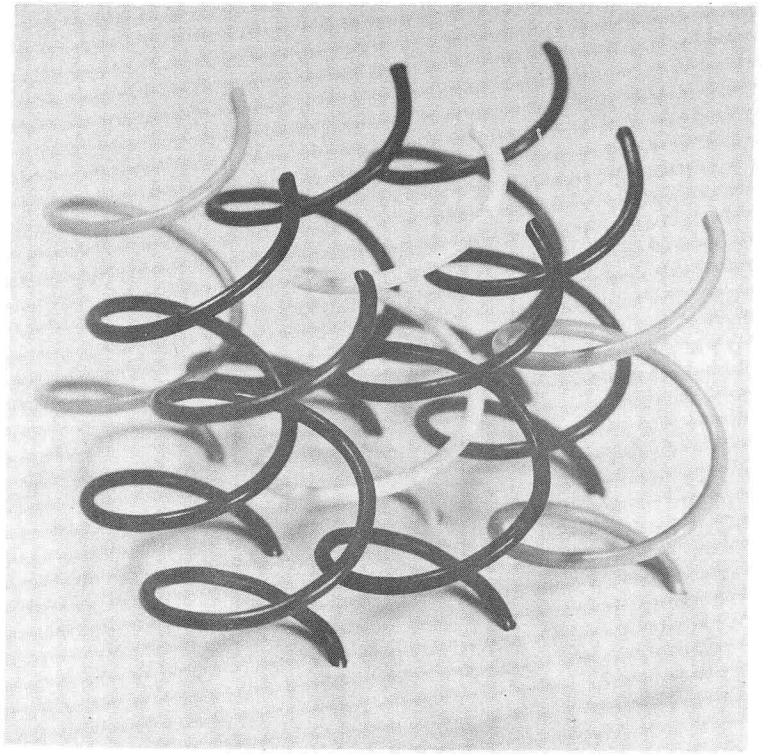

XBB 708-3616

Fig. 6(b)

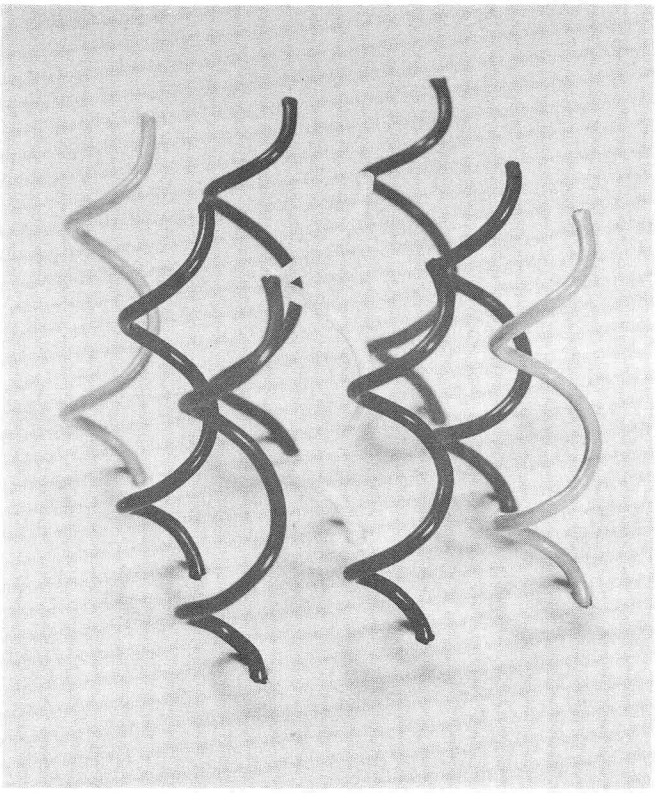

XBB 708-3611

Fig. 6(c)

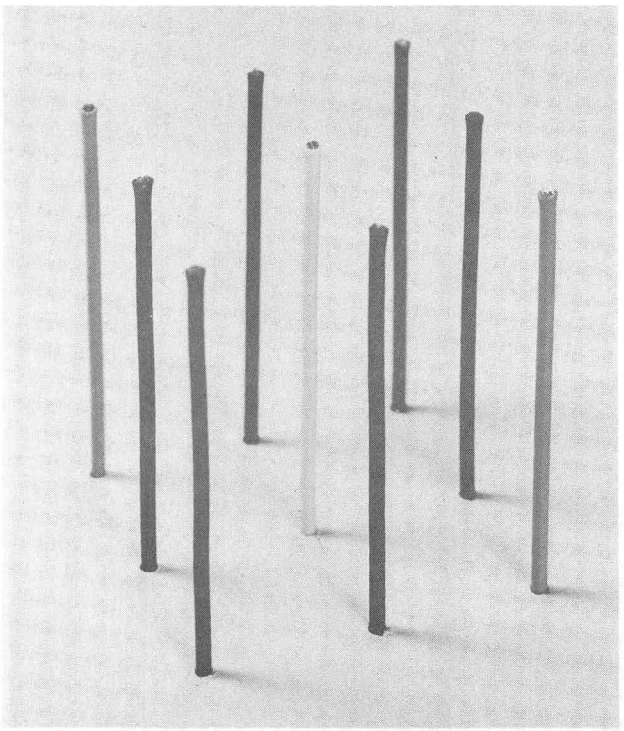

XBB 708-3610

Fig. 6(d)

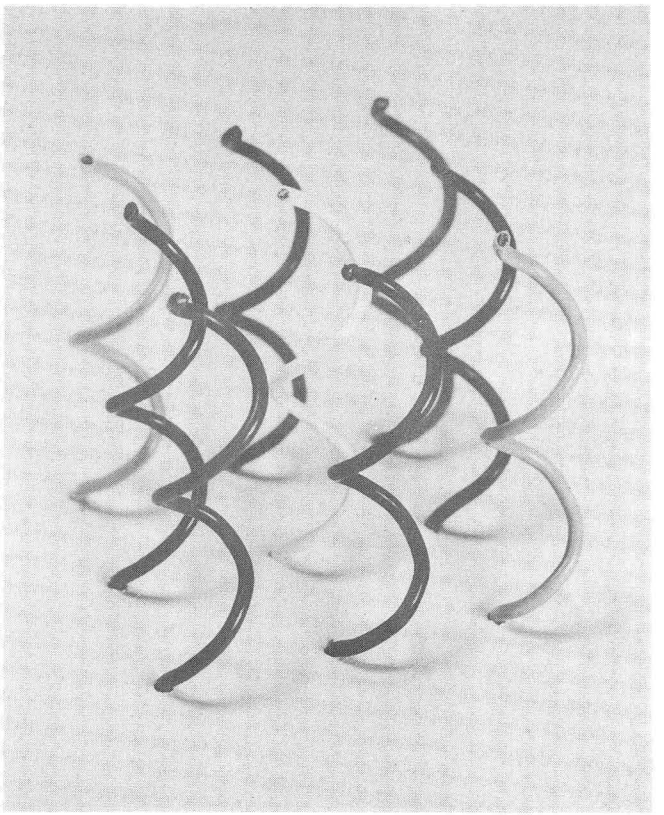

XBB 708-3612

Fig. 6(e)

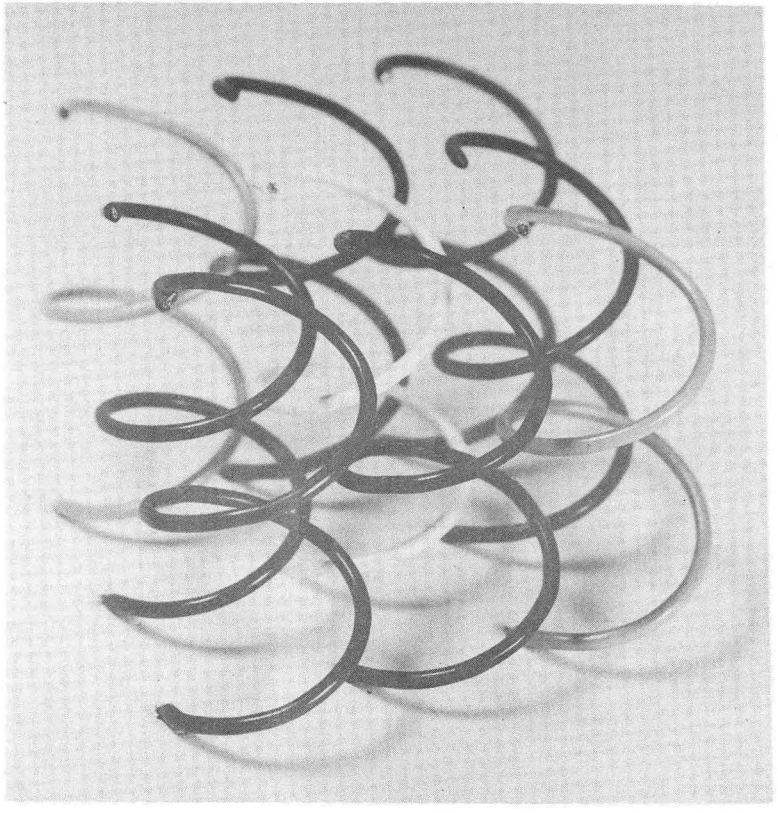

XBB 708-3615

Fig. 6(f)

XBB 708-3613

Fig. 6(g)

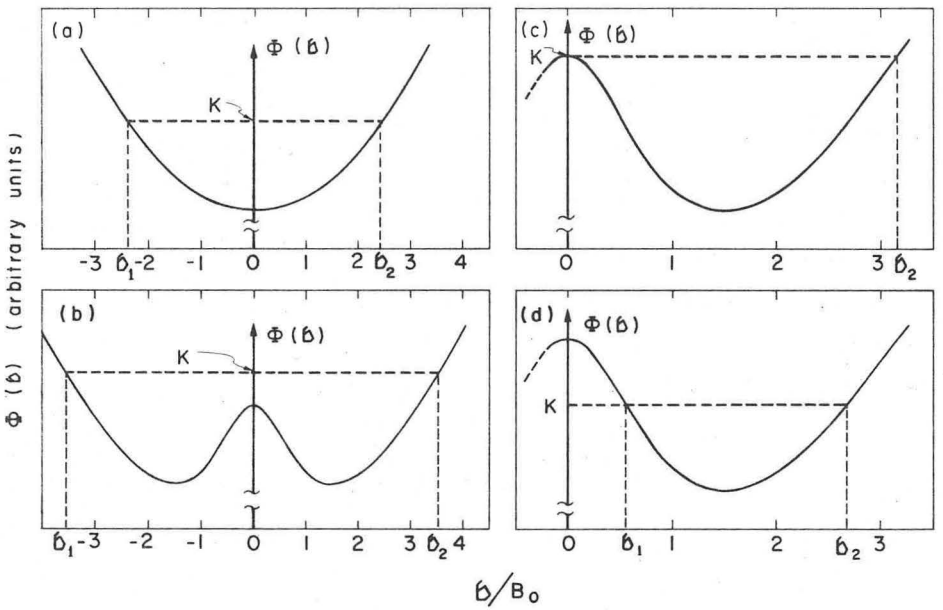

XBL708-3683

Fig. 7

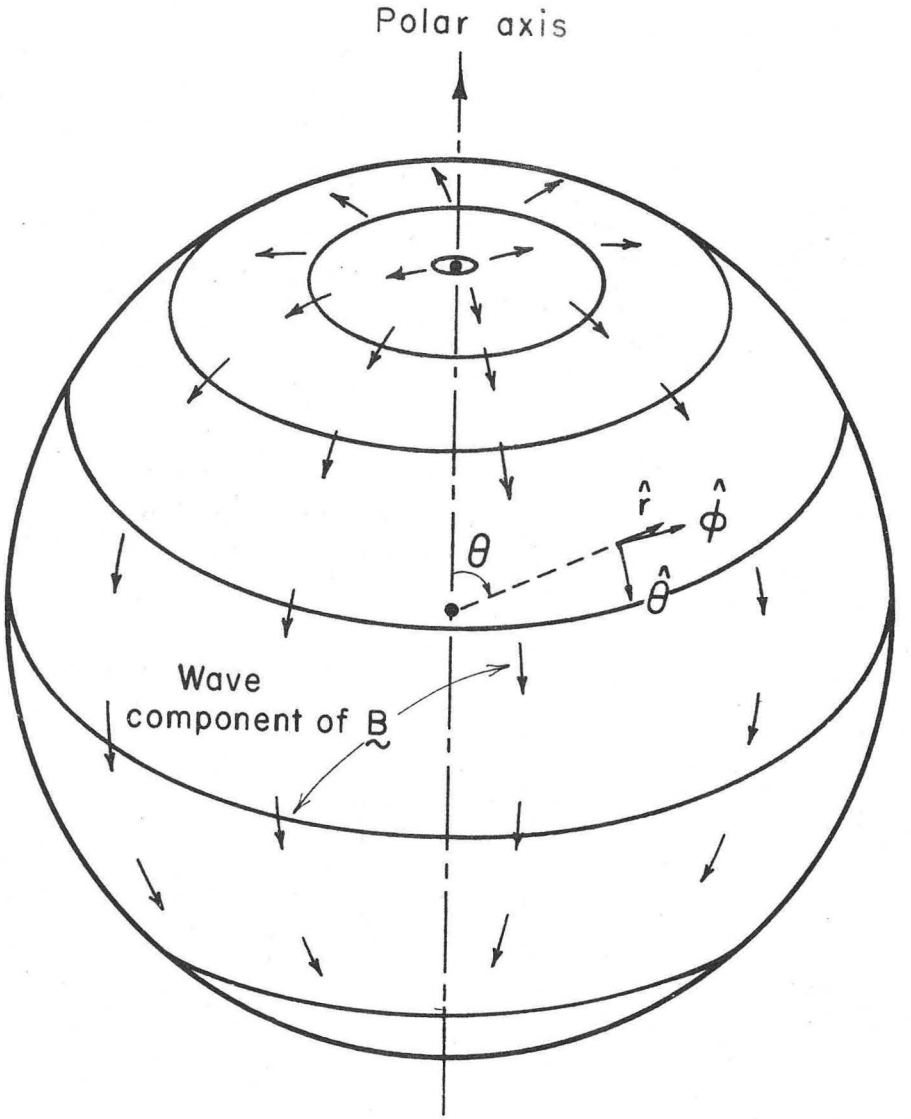

XBL718-3992

Fig. 8

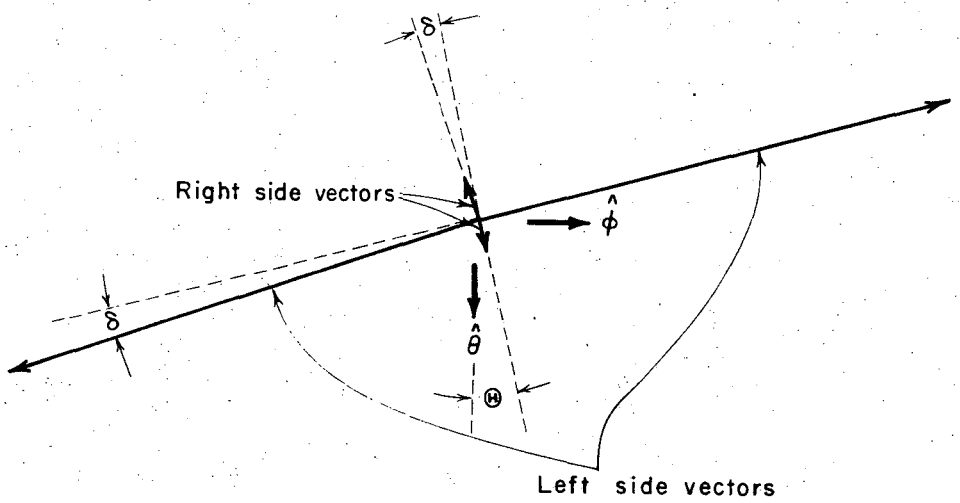

XBL718-3990

Fig. 9

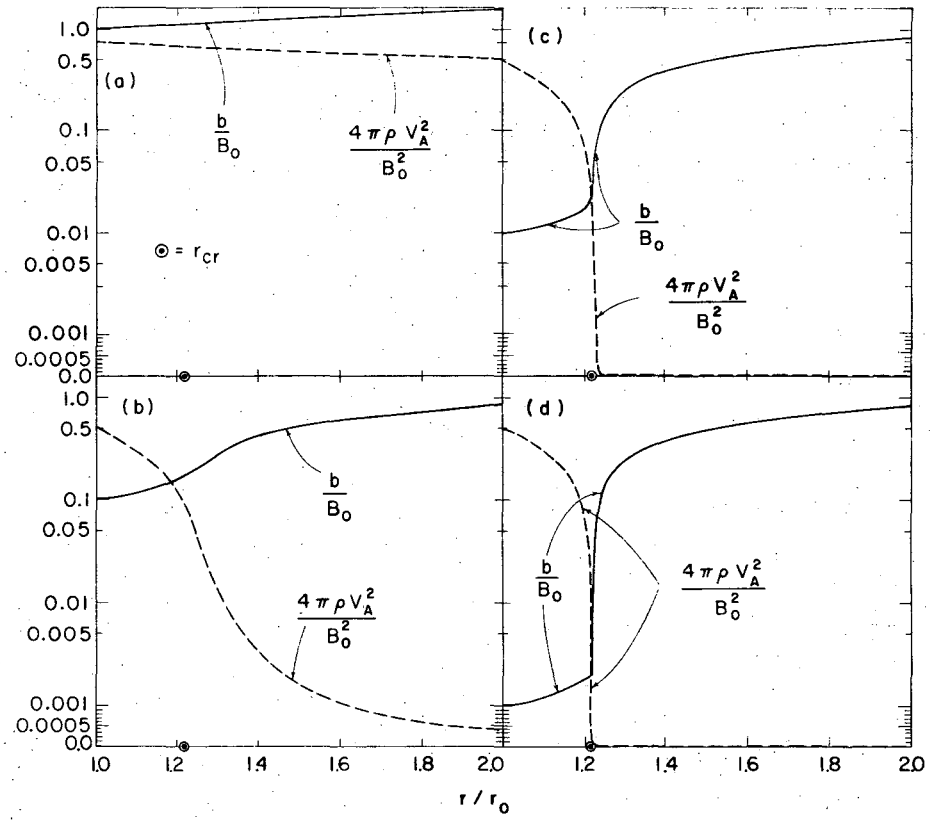

XBL718-3988

Fig. 10

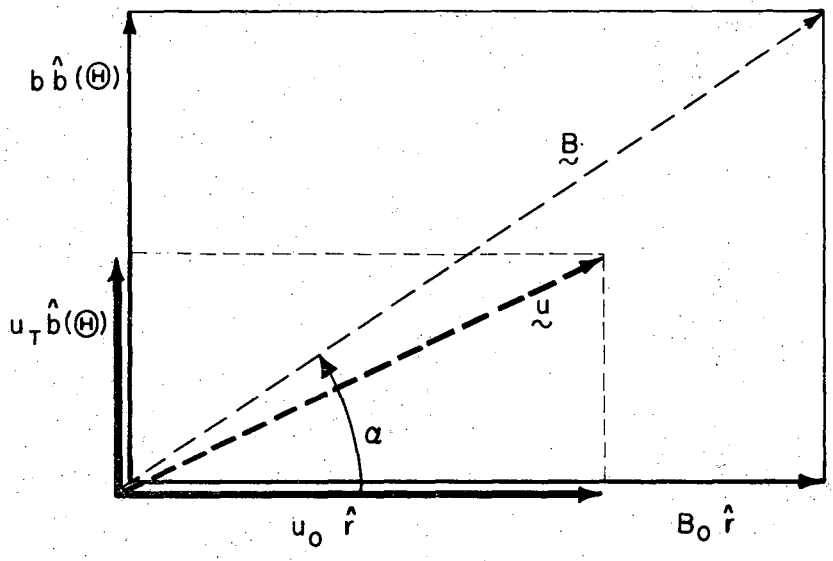

XBL718-3991

Fig. 11

TECHNICAL INFORMATION DIVISION
LAWRENCE BERKELEY LABORATORY
UNIVERSITY OF CALIFORNIA
BERKELEY, CALIFORNIA 94720